DOT/FAA/AR-02/111

Office of Aviation Research
Washington, D.C. 20591

Design, Manufacturing, and Performance of Stitched Stiffened Composite Panels With and Without Impact Damage

October 2002

Final Report

This document is available to the U.S. public through the National Technical Information Service (NTIS), Springfield, Virginia 22161.



U.S. Department of Transportation
Federal Aviation Administration

NOTICE

This document is disseminated under the sponsorship of the U.S. Department of Transportation in the interest of information exchange. The United States Government assumes no liability for the contents or use thereof. The United States Government does not endorse products or manufacturers. Trade or manufacturer's names appear herein solely because they are considered essential to the objective of this report. This document does not constitute FAA certification policy. Consult your local FAA aircraft certification office as to its use.

This report is available at the Federal Aviation Administration William J. Hughes Technical Center's Full-Text Technical Reports page: actlibrary.tc.faa.gov in Adobe Acrobat portable document format (PDF).

Technical Report Documentation Page

1. Report No.	2. Government Accession No.	3. Recipient's Catalog No.
DOT/FAA/AR-02/111		

4. Title and Subtitle	5. Report Date
DESIGN, MANUFACTURING, AND PERFORMANCE OF STITCHED STIFFENED COMPOSITE PANELS WITH AND WITHOUT IMPACT DAMAGE	October 2002
	6. Performing Organization Code

7. Author(s)	8. Performing Organization Report No.
H. Thomas Hahn, Jenn Ming Yang, Sung S. Suh, and Nanlin Han	

9. Performing Organization Name and Address	10. Work Unit No. (TRAIS)
Mechanical and Aerospace Engineering Department Materials Science and Engineering Department UCLA Los Angeles, CA 90024-1597	11. Contract or Grant No. DTFA03-98-FIA020

12. Sponsoring Agency Name and Address	13. Type of Report and Period Covered
U.S. Department of Transportation Federal Aviation Administration Office of Aviation Research Washington, DC 20591	Final Report
	14. Sponsoring Agency Code AIR-120

15. Supplementary Notes

The FAA William J. Hughes Technical Center Technical Monitor was Peter Shyprykevich.

16. Abstract

The goal of this project was to develop the knowledge base required for certification of composite structures in air transportation systems in the form of a design-manufacturing-performance relationship. Specifically, this project contributes to an improved definition of certification requirements for substantiating damage tolerance and durability of structural elements based on textile composites. Fundamental questions concerning analytical certification procedure, spectrum versus constant-amplitude fatigue, effect of low-velocity impact on strength, and effect of manufacturing defects were addressed.

Unstitched and stitched blade-stiffened panels applicable to airframe construction were investigated during Phases I and II of this project. The specific areas addressed were as follows:

- Analytical models to predict properties of unidirectional, fabric, and stitched fabric laminates
- Manufacturing processes
- Inspection methods
- Predictions of buckling and postbuckling loads
- Static compression properties
- Constant-amplitude fatigue properties
- Spectrum fatigue properties
- Effect of impact damage on static and fatigue properties

Micromechanics models indicate that in-plane elastic properties of stitched plain weave fabric laminates are fairly independent of yarn-architecture; therefore, as an approximation, unidirectional tape properties may be used to predict the plain weave fabric properties. In manufacturing, proper controls of stitching tension and inspection methods are critical in providing a good quality panel. Finite element analyses, using calculated lamina properties and simplified damage models, provide a good estimate of buckling and failure stresses of stitched panels with and without impact damage. In performance characterization, stitching improves both static and fatigue strengths where stiffener separation is a prime mode of failure. However, the stitching which is intended to prevent stiffener separation, may lead to the damage of the stiffener itself under impact. In this case, the benefit of stitching is only marginal at best. Nevertheless, the stitching improved damage tolerance of plain weave composites with up to 13% higher compressive after impact strength and its durability by factor of 1.2.

17. Key Words	18. Distribution Statement
Graphite/Epoxy/Kevlar, Micromechanics, Impact damage, Damage tolerance, Constant loading, Spectrum loading	This document is available to the public through the National Technical Information Service (NTIS) Springfield, Virginia 22161.

19. Security Classif. (of this report)	20. Security Classif. (of this page)	21. No. of Pages	22. Price
Unclassified	Unclassified	93	

ACKNOWLEDGEMENTS

The authors wish to extend their appreciation to Mr. Peter Shyprykevich, FAA project manager, for his support, guidance, and helpful comments, and to Dr. Shaw-Ming Lee of Hexcel Corporation for providing composite materials.

Thanks are also extended to the members of the Multifunctional Composites Laboratory, UCLA, for many helpful discussions, especially in Phase I.

TABLE OF CONTENTS

		Page
EXECUTIVE SUMMARY		xiii
1.	INTRODUCTION	1
1.1	Effect of Stitching on Strength and Damage Tolerance	1
1.2	Effect of Stitching on Durability	2
1.3	Resin Film Infusion Process	2
2.	DESIGN OF BLADE-STIFFENED PANELS	3
2.1	Materials	3
2.2	Geometric Design	3
2.3	Stitching	5
3.	PREDICTION OF TEXTILE LAMINATE PROPERTIES	5
3.1	Unidirectional Lamina With Yarn Undulation and Stitch Effects	6
3.1.1	Elastic Properties	6
3.1.2	Strengths	9
3.2	Multidirectional Textile Laminates for Stiffened Panel	10
4.	CRITICAL LOAD ANALYSIS OF STIFFENED PANELS	12
4.1	Finite Element Analysis	12
4.2	Damage Models	13
4.2.1	Clearly Visible Flange Damage (CVFD) Model	13
4.2.2	Clearly Visible Stiffener Damage (CVSD) Model	14
4.3	Results	14
5.	POSTBUCKLING ANALYSIS OF STIFFENED PANELS	16
5.1	Finite Element Analysis	16
5.2	Failure Criteria	17
5.3	Results	18
5.3.1	Undamaged Panel	18
5.3.2	CVFD Panel	20
5.3.3	CVSD Panel	21

6. MANUFACTURING OF STIFFENED PANELS 22

6.1 Stitching 22
6.2 Resin Film Infusion 23

7. QUALITY ASSURANCE 25

7.1 Ultraviolet Inspection of Fabrics 25
7.2 Visual Inspection of Panels 26
7.3 Dimensional Variations 28

8. PROPERTIES OF LAMINATE COUPONS 31

8.1 Experimental Procedure 32
8.2 Results 32

9. COMPRESSION BEHAVIOR OF STIFFENED PANELS 36

9.1 Impact Testing 36
9.2 Compression Testing 37
9.3 Unstitched Panels 39
9.4 Stitched Panels 40

10. FATIGUE BEHAVIOR OF STIFFENED PANELS 44

10.1 Experimental Procedure 45
10.2 Unstitched Panels 46

10.2.1 Constant-Amplitude Fatigue 46
10.2.2 Spectrum Fatigue 48

10.3 Stitched Panels 49

10.3.1 Constant-Amplitude Fatigue 49
10.3.2 Spectrum Fatigue 52

10.4 Effect of Stitching on Constant-Amplitude Fatigue 54

11. CONCLUSIONS 54

12. REFERENCES 55

APPENDICES

A—ABAQUS Input
B—Prediction of Laminate Properties

LIST OF FIGURES

Figure		Page
1	Two-Blade-Stiffened Panel Construction	4
2	A Cross-Sectional Schematic of Hexcel 282 Plain-Weave Fabric	5
3	A Schematic of Stitched Laminate (Left) and a Photo of Actual Stitch Reinforcement Isolated From Laminate (Right)	6
4	A Finite Element Model and Boundary Conditions	12
5	Finite Element Mesh for Panel With Clearly Visible Flange Damage: Damage Area = 127 mm^2, Depth = 2.54 mm	14
6	Finite Element Mesh for Panel With Clearly Visible Stiffener Damage: 0.203-mm Gap in a Stiffener	14
7	Critical Modes of Undamaged Panel	15
8	Critical Modes of CVFD Panel	15
9	Critical Modes of CVSD Panel	16
10	Load Factor Versus Strain of Undamaged Panel at Center Elements	19
11	Shear Stress Plot of Undamaged Panel at Failure	20
12	Shear Stress Plot of CVFD Panel at Failure	20
13	Load Factor Versus Strain of CVSD Panel at Center Elements	21
14	A Half Sine Wave Deformation of CVSD Panel at Failure	21
15	A Schematic of Stitching Process	22
16	Stitching Quality Dependent on Variation of Needle Thread Tension	22
17	Stitched Preform With Stiffeners	23
18	Aluminum Mold Assembly	24
19	Cure Cycle	24
20	Ultraviolet Inspection of Fabric	25
21	Ultraviolet Inspection of Cracks in CVSD Panel	26

22	Visual Inspection Areas	27
23	Coordinate Measuring Machine Measurement Points	28
24	Average Thicknesses of Unstitched Panel Versus Nominal Values	29
25	Average Dimensions of Unstitched Panel Versus Nominal Values	29
26	Key Dimensions	30
27	Average Thicknesses of Stitched Panel Versus Nominal Values	31
28	Average Dimensions of Stitched Panel Versus Nominal Values	31
29	Loading Direction Versus Stitch Direction	32
30	Tensile Failure of a Stitched Coupon	33
31	A Stress Versus Strain Plot From NASA Short Block Test	34
32	Side View of NASA Short Block With a Thin Specimen	35
33	Average Tensile Strengths and Moduli of Unstitched and Stitched Coupons	35
34	X-Ray Photographs of Drop Weight Impact Area in a Stitched Panel (a) CVFD Damage and (b) CVSD Damage	37
35	A Schematic of Test Panel Assembly	38
36	Shadow Moiré of a Stiffened Panel	38
37	Average Buckling Strengths of Unstitched Panels	39
38	Average Buckling Strengths of Stitched Panels	41
39	Comparison of Buckling Strengths Between Unstitched and Stitched Panels	42
40	Comparison of Failure Strengths Between Unstitched and Stitched Panels	43
41	Analytical Versus Experimental Buckling Strengths	44
42	Analytical Versus Experimental Failure Strengths	44
43	Constant-Amplitude Fatigue Lives of Stitched and Unstitched CVFD Panels	46
44	Advancing Crack Lines in CVFD Panel	47
45	Constant-Amplitude Fatigue Lives of Stitched and Unstitched CVSD Panels	48
46	Constant Fatigue Crack Growth Data for CVFD Panels	50

47 X-Ray Photographs of Stiffener and Skin of Specimen SP16a (a) After Impact, (b) After Two Blocks of Spectrum Fatigue, (c) After Five Blocks, and (d) After Ten Blocks 51

48 C-Scan Images of Specimen SP10b in Spectrum Fatigue (a) Fifth, (b) Eighth, and (c) Thirteenth Block 53

LIST OF TABLES

Table Page

1 Properties of Constituent Materials 3

2 Nominal Dimensions of Stiffened Panel 4

3 Parameters for Plain-Weave Fabric and Stitch Element 5

4 Calculated Properties of AS4/3501-6/Kevlar 29 Laminate, V_f = 50%, Stiffener Region 10

5 Calculated Properties of AS4/3501-6/Kevlar 29 Laminate, V_f = 50%, Skin Region 11

6 Calculated Properties of AS4/3501-6/Kevlar 29 Laminate, V_f = 50%, Flange Region 11

7 Calculated Strength Properties of AS4/3501-6/Kevlar 29 Laminate, V_f = 50%, Stiffener Region 11

8 Damage Types 13

9 Summary of Critical Modes and Critical Loads for Unstitched and Stitched Plain Weave Stiffened Panels 16

10 Modal Contributions to Initial Imperfection 17

11 Summary of Finite Element Analysis Results for Stitched Panels 19

12 Quality Rating Scheme 27

13 Overall Panel Quality 28

14 Tensile Properties of Stitched and Unstitched Coupons 33

15 Compressive Properties of Stitched Coupons Parallel to Stitch Direction 34

16	Panel Identification for Static Tests	36
17	Manufacturing Defects, Impact Damages, and Failure Modes of Unstitched Panels	40
18	Manufacturing Defects, Impact Damages, and Failure Modes of Stitched Panels	42
19	Modified Twist Spectrum	45
20	Nominal Stress Levels for Constant-Amplitude Fatigue Tests	45
21	Constant-Amplitude Fatigue Results (Unstitched CVFD Panels)	46
22	Constant-Amplitude Fatigue Results (Unstitched CVSD Panels)	47
23	Spectrum Fatigue Results (Unstitched CVFD Panels)	48
24	Spectrum Fatigue Results (Unstitched CVSD Panels)	49
25	Constant-Amplitude Fatigue Results (Stitched CVFD Panels)	49
26	Constant-Amplitude Fatigue Results (Stitched CVSD Panels)	52
27	Spectrum Fatigue Results (Stitched CVFD Panels)	52
28	Spectrum Fatigue Results (Stitched CVSD Panels)	53
29	Best-Fit Parameters for Unstitched and Stitched Panels	54

LIST OF ABBREVIATIONS AND SYMBOLS

α,β	Power-Law Coefficients
α_f	Ratio of stitching spacing to fill direction repeating segment
α_w	Ratio of stitching spacing to warp direction repeating segment
δ	Maximum imperfection shape
ϕ_i	i^{th} Critical mode shape
ϕ_v	Void volume fraction
σ_{ij}	Stress components
ω_i	i^{th} Critical mode weighting factor
Ω	Maximum off-axis angle
i	1,2,3
j	1,2,3
d_s	Diameter of stitch
E_i	Young's Modulus
E^y_i	Yarn Young's Modulus
E^s_i	Stitch Young's Modulus
Gij	Shear Modulus
G^y_{ij}	Yarn Young's Modulus
G^s_{ij}	Stitch Young's Modulus
ν_{ij}	Poisson's Ratio
ν^y_{ij}	Yarn Young's Modulus
ν^s_{ij}	Stitch Young's Modulus
cm	Centimeter
g	Gram
kg	Kilogram
kN	Kilo-Newton
m	Meter
mm	Millimeter
m^3	Cubic meter
MPa	Mega-Pascal
F_{index}	Failure index
R	Fatigue cyclic stress ratio (S_{min}/S_{max})
S	Stress
S_{max}	Maximum stress of fatigue cycle
S_{min}	Minimum stress of fatigue cycle
S^c	Compressive stress
S^t	Tensile stress
S_{12}	In-plane shear
V_f	Fiber volume fraction
V_s	Stitch volume fraction
N	Number of fatigue cycles
CMM	Coordinate Measuring Machine
CVID	Clearly visible impact damage
CVFD	Clearly visible flange damage

CVSD	Clearly visible stiffener damage
C-A	Constant amplitude fatigue loading
C-C	Compression-compression fatigue loading
CSAI	Compressive strength after impact
DUL	Design ultimate load
DLL	Design limit load
GPa	Giga-Pascal
RFI	Resin film infusion/infiltration
TWIST	Transport WIng Standard Test Spectrum

EXECUTIVE SUMMARY

The goal of this project was to develop the knowledge base required for certification of composite structures in air transportation systems in the form of design-manufacturing-performance relationship. Specifically, this project contributes to an improved definition of certification requirements for substantiating damage tolerance and durability of structural elements based on textile composites. Fundamental questions concerning analytical certification procedure, spectrum versus constant-amplitude fatigue, effect of low-velocity impact on strength, and effect of manufacturing defects were addressed.

Unstitched and stitched blade-stiffened panels applicable to airframe construction were investigated during Phases I and II of this project. The specific areas addressed were as follows:

- Analytical models to predict properties of unidirectional, fabric, and stitched fabric laminates
- Manufacturing processes
- Inspection methods
- Predictions of buckling and postbuckling loads
- Static compression properties
- Constant-amplitude fatigue properties
- Spectrum fatigue properties
- Effect of impact damage on static and fatigue properties

Micromechanics models indicate that in-plane elastic properties of stitched plain weave fabric laminates are fairly independent of yarn-architecture, therefore, as an approximation, unidirectional tape properties may be used to predict the plain weave fabric properties. In manufacturing, proper controls of stitching tension and inspection methods are critical in providing a good quality panel. Finite element analyses, using calculated lamina properties and simplified damage models, provide a good estimate of buckling and failure stresses of stitched panels with and without impact damage. In performance characterization, stitching improves both static and fatigue strengths where stiffener separation is a prime mode of failure. However, the stitching, which is intended to prevent stiffener separation, may lead to the damage of the stiffener itself under impact. In this case, the benefit of stitching is only marginal at best. Nevertheless, the stitching improved damage tolerance of plain weave composites with up to 13% higher compressive after impact strength and its durability by factor of 1.2.

1. INTRODUCTION.

Composite materials have been used in the aerospace industry over the past three decades. Still, their wider utilization is hampered by the long delay and high cost of certification testing. However, the required testing can be reduced substantially by using analytical simulations as much as possible.

The main purpose of the present research is to develop an analytical procedure to certify the damage tolerance and durability of stiffened composite panels. Stiffened panels are chosen because they are one of the widely used structural forms. The panels are fabricated by the resin film infusion process using a plain weave fabric preform. This fabrication method offers a low-cost alterative to autoclave molding of tape laminates.

Composite laminates suffer from low-damage tolerance because of their high sensitivity to out-of-plane failure, resulting from low interlaminar fracture toughness. To alleviate this shortcoming, toughened resins have been developed to reduce the initiation and growth of delamination. However, an alternate approach to improve delamination resistance is through mechanical reinforcement such as through-the-thickness stitching. Recent studies by Dow, et al. [1 and 2] have shown that stitching of conventional laminates can increase damage tolerance to the level available with toughened resin systems but at a lower cost.

The analytical substantiation procedure developed is for blade-stiffened panels fabricated of a plain weave fabric using the resin film infusion process. Both unstitched and stitched panels are included for comparison purposes. Experimental correlation includes compression strength, compression strength after impact, and constant-amplitude and spectrum fatigue after impact.

1.1 EFFECT OF STITCHING ON STRENGTH AND DAMAGE TOLERANCE.

Influence of stitching on interlaminar fracture toughness has been investigated by Dexter and Funk [3] on quasi-isotropic laminates made of unidirectional Tornel 300-6K fibers/Hercules 3501-6 resin and stitched with polyester and Kevlar yarns. Their findings indicated a 30-fold increase in Mode I fracture toughness for stitched laminates. Pelstring and Madan [4] found Mode I critical strain energy release rate to be 15 times greater than in unstitched laminates and the critical energy release rate decreased exponentially with increasing stitch spacing. Also, a good correlation was found between strain energy release rate, damage area, and compression strength after impact (CSAI). Sharma and Sankar [5 and 6] found a similar beneficial effect of stitching on interlaminar toughness and CSAI of uniweave textile composites.

The effect of stitching on static strength is controversial. Khan and Mouritz [7] reported no change in tensile strength of stitched glass fiber-reinforced plastic (GFRP) laminates, and Harris, et al. [8] reached the same conclusion for carbon fiber-reinforced plastic (CFRP) laminates. However, Dexter and Funk [3] and Su [9] measured reductions of up to 25% in tensile strength of CFRP laminates due to stitching. Various stitching patterns were used in these studies leading to different effects on tensile strength. It is noted that the stitching process introduces a surface loop of yarn between successive stitches. The loop is pressed into the surface layers of the laminate during curing and induces kinking of the in-plane fibers near the surface. Farley, et al.

[10 and 11] found that the removal of this loop (by machining) significantly increased compressive strength and CSAI.

Sharma and Sankar [5 and 6] performed compression after impact tests on stitched uniweave laminates containing implanted delaminations. Their findings indicate that stitching is very effective in retaining the CSAI as along as the stitch yarn has a minimum stiffness and strength. They concluded that the stitch density is of greater importance than the stiffness and strength of the stitch yarn. However, they also found that stitching causes approximately 10% drop in compressive strength. Dow and Smith [1] and Liu [12] examined the effects of stitching density and stitch pattern on impact damage pattern. They found that the shape of delamination area changed significantly with the stitching pattern, indicating an effective role of stitching in preventing delamination.

While these studies have provided information on the coupon-level effect of stitching, the potential of structure-level benefits still remain to be ascertained since the performance of structures is additionally influenced by their geometry and manufacturing quality.

1.2 EFFECT OF STITCHING ON DURABILITY.

Khan and Mouritz [7] investigated the effects of stitch orientation and stitch density on the S-N curve of GFRP laminates under tension fatigue. Interlaminar fracture properties were improved three times after stitching, but the ultimate tensile strength remained unchanged and fatigue resistance was reduced considerably, particularly at low fatigue stresses. Fatigue failure occurred at the stitches because of the damage incurred on the glass fibers during stitching. Moon, et al. [13] investigated postimpact fatigue response of stitched carbon/epoxy laminates to find that stitching resulted in twice the fatigue strength of the baseline unstitched laminates. In another study, comparing the effectiveness of stitching and matrix toughening under compression fatigue [14], stitching did not show any advantage in the presence of a notched hole.

Only a limited amount of data is available on constant-amplitude fatigue of stitched composites. Further, no fatigue information is available under realistic (service) loading conditions. The contradictory effects of stitching observed on fatigue behavior and static strength warrants further work to fully characterize the damage tolerance and durability of stitched composites.

1.3 RESIN FILM INFUSION PROCESS.

One of the promising manufacturing methods for stitched composites is the resin film infusion (RFI) process. In the RFI process, a textile preform is prepared to form an integral structural part. It is then placed inside a mold containing a resin film, and the composite part is cured in an autoclave. Previous studies [15] have shown that better mechanical properties resulted from the RFI process than from prepregs. For textile preforms, RFI is considered as the most cost-effective and structurally practical manufacturing process [2].

2. DESIGN OF BLADE-STIFFENED PANELS.

The design of a blade-stiffened panel consisted of three steps: material selection, design of panel geometry, and determination of stitch parameters. The overriding constraint was that the panel should be as realistic as possible, yet could be tested in the laboratory setting.

2.1 MATERIALS.

Hexcel type 282 AS4 (3k)/3501-6 carbon/epoxy was selected for study. Its typical fiber and matrix properties are shown in table 1. Hexcel Type 282 is a plain weave fabric that has the same number of warp and fill yarns at 4.92 yarns/cm. The yarn consists of 3k AS4 carbon fibers. The AS4/3501-6 is a well-characterized composite and amenable to the RFI process. The AS4 carbon fiber tows are also used as the filler material in joining stiffeners to the skin.

TABLE 1. PROPERTIES OF CONSTITUENT MATERIALS
(Manufacturer's datasheet)

	AS4 Graphite	Epoxy	Kevlar 29
E_1, GPa	228.0	3.5	69.0
E_2, GPa	40.0	3.5	2.49
G_{12}, GPa	24.0	1.30	2.01
G_{23}, GPa	14.3	1.30	0.924
ν_{12}	0.26	0.26	0.62
ν_{23}	0.25	0.26	0.31
S_1^t, MPa	3930.0	77.9	2760
S_1^c, MPa	2760	158.0	N/A
S_{12}, MPa		96.5	
ρ, g/cm3	2.34E-03	1.65E-03	1.44
ε_1^t	1.72E-02	2.22E-02	N/A
ε_1^c	1.21E-02	4.52E-02	N/A

2.2 GEOMETRIC DESIGN.

Figure 1 shows a two-blade stiffened panel. Aside from its overall dimensions, the panel geometry is characterized by skin and stiffener thicknesses, stiffener spacing and height, and flange width as listed in table 2. The skin and one half of the stiffener constitute a flange. A typical stiffener spacing investigated by Starnes Jr., et al. [16], Madan [17], and Stevens, et al. [18] ranged from 12.7 to 17.8 cm, so that a mid-range value of 15.24 cm was selected. Both the length and width of the panel are 25.4 cm each. The skin consists of 13 layers of fabric and the stiffener 12 layers. The layup sequences are as follows:

Skin: $[0/90, \pm45, 0/90, \pm45, 0/90, \pm45, 0/90, \pm45, 0/90, \pm45, 0/90, \pm45, 0/90]_T$
Stiffener: $[\pm45, 0/90, \pm45, 0/90, \pm45, 0/90]_S$
Flange: $[0/90, \pm45, 0/90, \pm45, 0/90, \pm45, 0/90, \pm45, 0/90, \pm45, 0/90, \pm45, 0/90, 0/90, \pm45, 0/90, \pm45, 0/90, \pm45]_T$

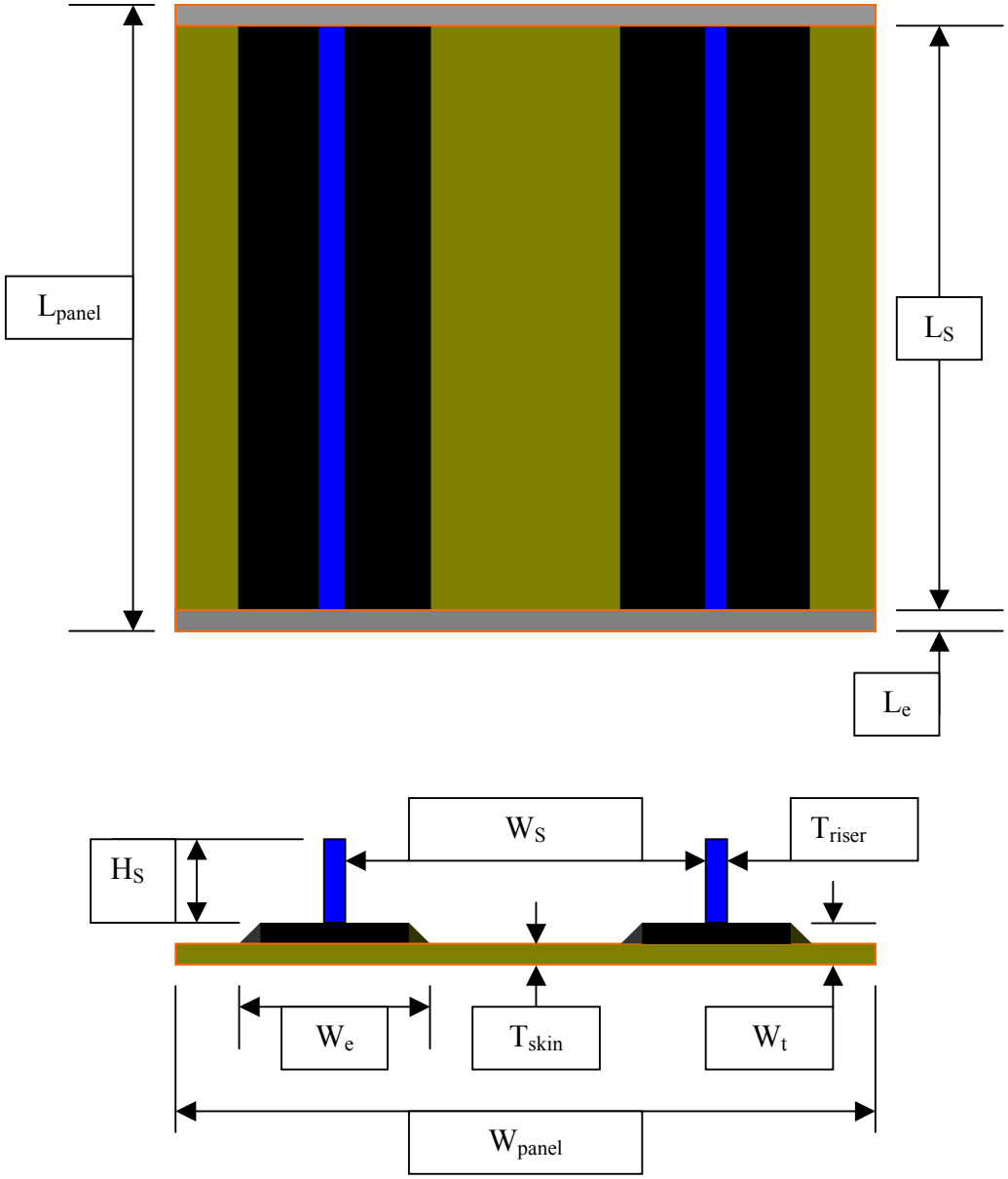


FIGURE 1. TWO-BLADE-STIFFENED PANEL CONSTRUCTION
(L_e = potting edge)

TABLE 2. NOMINAL DIMENSIONS OF STIFFENED PANEL

L_{panel}	254.0 mm	T_{skin}	2.86 mm
L_s	247.7 mm	T_{riser}	2.64 mm
L_e	3.18 mm	H_s	25.4 mm
W_{panel}	254.0 mm	W_e	76.2 mm
W_s	152.4 mm	W_t	4.18 mm

2.3 STITCHING.

A 1600-denier Kevlar 29 thread was selected for stitching together with a 400-denier Kevlar 29 thread for the bobbin. Their typical properties are shown in tables 1 and 3.

The stitch density was selected to be 9.92 stitches per cm^2, with both the pitch and the spacing kept at 3.175 mm. According to Madan [17], the selected pitch density is expected to reduce impact damage by up to 30% and any higher pitch density will reduce laminate integrity.

TABLE 3. PARAMETERS FOR PLAIN-WEAVE FABRIC AND STITCH ELEMENT
(Kevlar 29, d_s=0.965 mm)

Warp Yarn Spacing (mm)	Fill Yarn Spacing (mm)	Stitch Spacing (mm)	Stitch Pitch (mm)	Stitch Diameter (mm)
2.032	2.032	3.175	3.175	0.965

3. PREDICTION OF TEXTILE LAMINATE PROPERTIES.

Over the past three decades, a large number of micromechanics models have been proposed to predict mechanical properties of unidirectional composites from constituent properties. From these predicted lamina properties, one can effectively generate properties of a laminate with arbitrary stacking sequence using the classical lamination theory. Textile composites fibers are not straight, as shown in figure 2, and the waviness of these fibers should be accounted for. In order to incorporate the effect of the out-of-plane reinforcement, as shown in figure 3, stitching calls for further modification of micromechanics model.

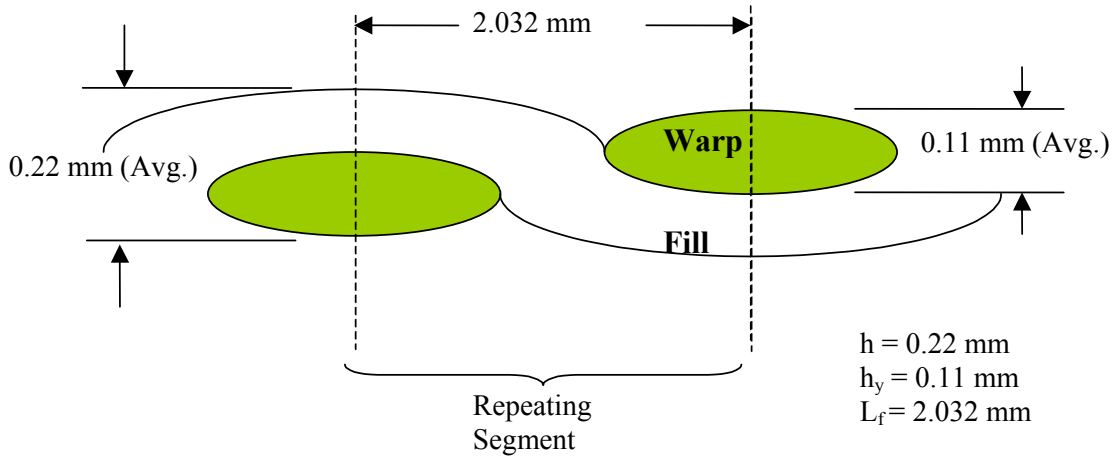


FIGURE 2. A CROSS-SECTIONAL SCHEMATIC OF HEXCEL 282 PLAIN-WEAVE FABRIC

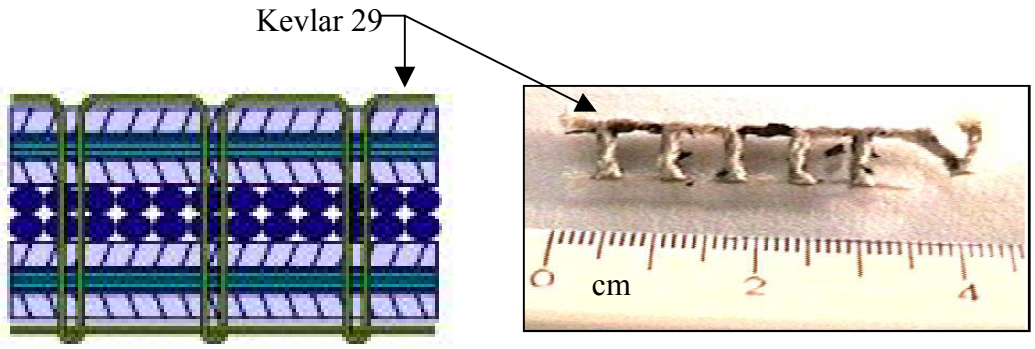


FIGURE 3. A SCHEMATIC OF STITCHED LAMINATE (LEFT) AND A PHOTO OF ACTUAL STITCH REINFORCEMENT ISOLATED FROM LAMINATE (RIGHT)

3.1 UNIDIRECTIONAL LAMINA WITH YARN UNDULATION AND STITCH EFFECTS.

3.1.1 Elastic Properties.

Elastic properties of unidirectional lamina without yarn undulation are calculated using the following equations [19]:

$$E_i = \frac{1}{V_f + \eta_i V_m}\left\{V_f E_{f,i} + \eta_i V_m E_m\right\} \tag{1}$$

$$E_2 = E_3 = \frac{4kG_{23}}{(k + mG_{23})} \tag{2}$$

$$\nu_{12} = \nu_{13} = V_f \nu_{f,12} + V_m \nu_m \tag{3}$$

$$G_{12} = G_{13} = (V_f + \eta_{12} V_m)\left[\frac{V_f}{G_{f,12}} + \frac{\eta_{12} V_m}{G_m}\right]^{-1} \tag{4}$$

$$G_{23} = (V_f + \eta_{23} V_m)\left[\frac{V_f}{G_{f,23}} + \frac{\eta_{23} V_m}{G_m}\right]^{-1} \tag{5}$$

$$\eta_{12} = \frac{1}{2}\left(1 + \frac{G_m}{G_{f,12}}\right) \tag{6}$$

$$\eta_{23} = \frac{1}{4(1-\nu_m)}\left(3 - 4\nu_m + \frac{G_m}{G_{f,23}}\right) \tag{7}$$

$$m = 1 + \frac{4k\nu_{12}^2}{E_1^2} \tag{8}$$

$$k = \frac{V_f + \eta V_m}{\frac{V_f}{k_{f,2}} + \frac{\eta V_m}{k_m}},\ \eta = \frac{1}{2(1-\nu_m)}\left(1 + \frac{G_m}{k_{f,2}}\right) \tag{9}$$

Here, subscripts f and m refer to fiber and matrix, respectively, and V_f is the fiber volume fraction. Direction indices 1 and 3 represent the fiber direction and the thickness direction, respectively, and η and k are the stress partitioning parameter and the plain strain bulk modulus, respectively.

The effect of yarn undulation is introduced using equations 10 through 18, proposed by Hahn and Pandey [20].

$$C_{11}^* = V_{wy}\left(U_1^w + V_{1w}U_2^w + V_{2w}U_3^w\right) + V_{fy}C_{22}^f + V_{im}C_{11}^m \tag{10}$$

$$C_{22}^* = V_{fy}\left(U_1^f + V_{1f}U_2^f + V_{2f}U_3^f\right) + V_{wy}C_{22}^w + V_{im}C_{22}^m \tag{11}$$

$$C_{33}^* = V_{wy}\left(U_1^w - V_{1w}U_2^w + V_{2w}U_3^w\right) + V_{fy}\left(U_1^f - V_{1f}U_2^f + V_{2f}U_3^f\right) + V_{im}C_{33}^m \tag{12}$$

$$C_{12}^* = V_{wy}\left(U_6^w - V_{1w}U_7^w\right) + V_{fy}\left(U_6^f + V_{1f}U_7^f\right) + V_{im}C_{12}^m \tag{13}$$

$$C_{13}^* = V_{wy}\left(U_4^w - V_{1w}U_3^w\right) + V_{fy}\left(U_6^f - V_{2f}U_7^f\right) + V_{im}C_{13}^m \tag{14}$$

$$C_{23}^* = V_{wy}\left(U_6^w - V_{2w}U_7^w\right) + V_{fy}\left(U_4^f - V_{1f}U_3^f\right) + V_{im}C_{23}^m \tag{15}$$

$$C_{55}^* = V_{wy}\left(U_5^w - V_{2w}U_3^w\right) + V_{fy}\left(U_8^f + V_{1f}U_9^f\right) + V_{im}C_{55}^m \tag{16}$$

$$C_{44}^* = V_{wy}\left(U_8^w + V_{1w}U_9^w\right) + V_{fy}\left(U_5^f - V_{2f}U_3^f\right) + V_{im}C_{44}^m \tag{17}$$

$$C_{66}^* = V_{wy}\left(U_8^w - V_{1w}U_9^w\right) + V_{fy}\left(U_8^f - V_{1f}U_9^f\right) + V_{im}C_{66}^m \tag{18}$$

where

$$V_{1w} = \frac{1}{L_f}\int_0^{L_f} \cos(2\theta_w)dx$$

$$V_{1f} = \frac{1}{L_w}\int_0^{L_w} \cos(2\theta_f)dx$$

$$V_{2w} = \frac{1}{L_f}\int_0^{L_f} \cos(4\theta_w)dx$$

$$V_{2f} = \frac{1}{L_w}\int_0^{L_w} \cos(4\theta_f)dx$$

$$\theta_w = \arctan\left(\frac{dh_1}{dx}\right) = \arctan\left(\left(\frac{\pi h_f}{2L_f}\right)\sin\left(\frac{\pi x}{L_f}\right)\right)$$

$$\theta_f = \arctan\left(\frac{dh_2}{dy}\right) = \arctan\left(\left(\frac{\pi h_w}{2L_w}\right)\sin\left(\frac{\pi y}{L_w}\right)\right)$$

In above equations, U's are invariants of stiffness components as defined in reference 19. The V_{1w}, V_{1f}, V_{2w} and V_{2f} are geometric efficiency factors. The subscripts *wy*, *fy* and *im* denote warp yarn, fill yarn and interyarn matrix, respectively. Angles θ_w and θ_f are the slopes of yarn undulations. The necessary dimensions of representative volume element (RVE) are the repeating segments, L's and heights, h's.

Lastly, the engineering constants are obtained from the laminate stiffness matrix:

$$A_{ij} = HQ_{ij}^* \tag{19}$$

where,

$$Q_{ij}^* = C_{ij}^* - \frac{C_{i3}^* C_{j3}^*}{C_{33}^*} \tag{20}$$

Here, H is the thickness of the laminate, and Q_{ij}^* are the effective plane-stress stiffness components of constituent plies. The relationship between the components of A_{ij} and the average engineering constants are shown below [19]. Further details are presented in reference 20 and appendix B.

$$E_1 = \frac{A_{11}A_{22} - A_{12}^2}{A_{22}H} \tag{21}$$

$$E_2 = \frac{A_{11}A_{22} - A_{12}^2}{A_{11}H} \tag{22}$$

$$G_{12} = \frac{A_{66}}{H} \tag{23}$$

$$\nu_{12} = \frac{A_{12}}{A_{22}} \tag{24}$$

For the stitched fabric laminate, the elastic moduli obtained from equations 10 through 20 are modified using the rule of mixtures as follows:

$$E^s = (1 - V_s)E^y + V_s E_s \tag{25}$$

where superscript *y* refers to yarn, subscript *s* refers to stitching yarn, and superscript *s* refers to stitched composite. The stitch volume fraction is given by

$$V_s = \frac{\pi}{4}\frac{d_s^2}{a_p a_s} \tag{26}$$

where

a_p = stitch pitch
a_s = stitch spacing
d_s = stitch diameter

The stitch parameters are given in table 3, and the calculated stitch volume fraction is 7.25%.

3.1.2 Strengths.

The following equations are used as a first-order approximation of strength:

- Longitudinal and transverse tensile strength [21]:

  For plain weave laminates, $S_1^t = S_2^t = E_1^y \varepsilon_f^t$

  For stitched plain weave laminates, $S_1^t = S_2^t = \frac{E_1^s \varepsilon_f^t}{1.3}$ (27)

- Longitudinal and transverse compressive strength [21]:

  For plain weave laminates, $S_1^c = S_2^c = E_1^y \varepsilon_f^c$

For stitched plain weave laminates, $$S_1^c = S_2^c = \frac{E_1^s \varepsilon_f^c}{1.3} \quad (28)$$

- In-plane shear strength [19]:

$$S_{12} = S_m \frac{1 + V_f\left(\frac{1}{\eta} - 1\right)}{K_{ms}}, \qquad \eta = \frac{1}{2}\left(1 + \frac{G_m}{G_{f,12}}\right) \quad (29)$$

where estimate of $K_{ms} = 2.5$ is used [22].

For stitched laminates, strengths are reduced by a stress concentration factor of 1.3. The stress concentration factor was calculated from the solution of a single inclusion model [23], assuming that one stitch is present in the representative volume element [20]. The validity of using a knockdown factor is based on a study performed using CFRP $[0/\pm45/90]_{2S}$ with an aluminum inclusion [24].

The foregoing equations were used to calculate properties for the stitched fabric. The fiber volume fraction was chosen to be 50%.

3.2 MULTIDIRECTIONAL TEXTILE LAMINATES FOR STIFFENED PANEL.

As mentioned in section 2, the stiffened panel consists of three regions with different laminate configurations: skin, stiffener and flange. For comparison purposes, the following two different types of fiber preforms were investigated: plain weave fabric and stitched plain weave fabric. The results are shown in tables 4 to 7.

It is seen that stitching decreases the in-plane modulus by 6.9%. However, the out-of-plane of modulus can increase by as much as 23.6% in the presence of stitches. There is a large decrease in tensile and composite strengths (table 7) as a result of stitching.

TABLE 4. CALCULATED PROPERTIES OF AS4/3501-6/KEVLAR 29 LAMINATE, V_f = 50%, STIFFENER REGION

	Plain Weave	Stitched Plain Weave	% Change
E_1, GPa	46.4	43.2	-6.90
E_2, GPa	46.4	43.2	-6.90
E_3, GPa	12.7	15.7	23.62
ν_{12}	0.30	0.30	0.00
G_{12}, GPa	17.2	16.6	-3.49
G_{13}, GPa	4.9	4.7	-4.08
G_{23}, GPa	2.5	2.4	-4.00

TABLE 5. CALCULATED PROPERTIES OF AS4/3501-6/KEVLAR 29 LAMINATE, V_f = 50%, SKIN REGION

	Plain Weave	Stitched Plain Weave	% Change
E_1, GPa	48.0	44.7	-6.87
E_2, GPa	48.0	44.7	-6.87
E_3, GPa	12.7	15.7	23.62
ν_{12}	0.28	0.28	0.00
G_{12}, GPa	16.8	15.7	-6.55
G_{13}, GPa	4.9	4.7	-4.08
G_{23}, GPa	2.5	2.4	-4.00

TABLE 6. CALCULATED PROPERTIES OF AS4/3501-6/KEVLAR 29 LAMINATE, V_f = 50%, FLANGE REGION

	Plain Weave	Stitched Plain Weave	% Change
E_1, GPa	47.5	44.2	-6.95
E_2, GPa	47.5	44.2	-6.95
E_3, GPa	12.7	15.7	23.62
ν_{12}	0.29	0.29	0.00
G_{12}, GPa	17.1	16.0	-6.43
G_{13}, GPa	4.9	4.7	-4.08
G_{23}, GPa	2.5	2.4	-4.00

TABLE 7. CALCULATED STRENGTH PROPERTIES OF AS4/3501-6/KEVLAR 29 LAMINATE, V_f = 50%, STIFFENER REGION

	Plain Weave	Stitched Plain Weave
$S_{t,1}$, MPa	798	572
$S_{c,1}$, MPa	-561	-402
$S_{t,2}$, MPa	798	572
$S_{c,2}$, MPa	-561	-402
S_{12}, MPa	55.9	55.9

4. CRITICAL LOAD ANALYSIS OF STIFFENED PANELS.

4.1 FINITE ELEMENT ANALYSIS.

A buckling analysis of stiffened panel was performed using PATRAN for preprocessing and ABAQUS for structural analysis and postprocessing. The calculated material properties listed in table 4 were used in the analysis. The geometry of a finite element model and its boundary conditions are shown in figure 4. The bottom nodes are simply supported, and the top nodes are allowed to displace equally in line with the loaded center node. The panel is meshed with eight-node laminate shell elements.

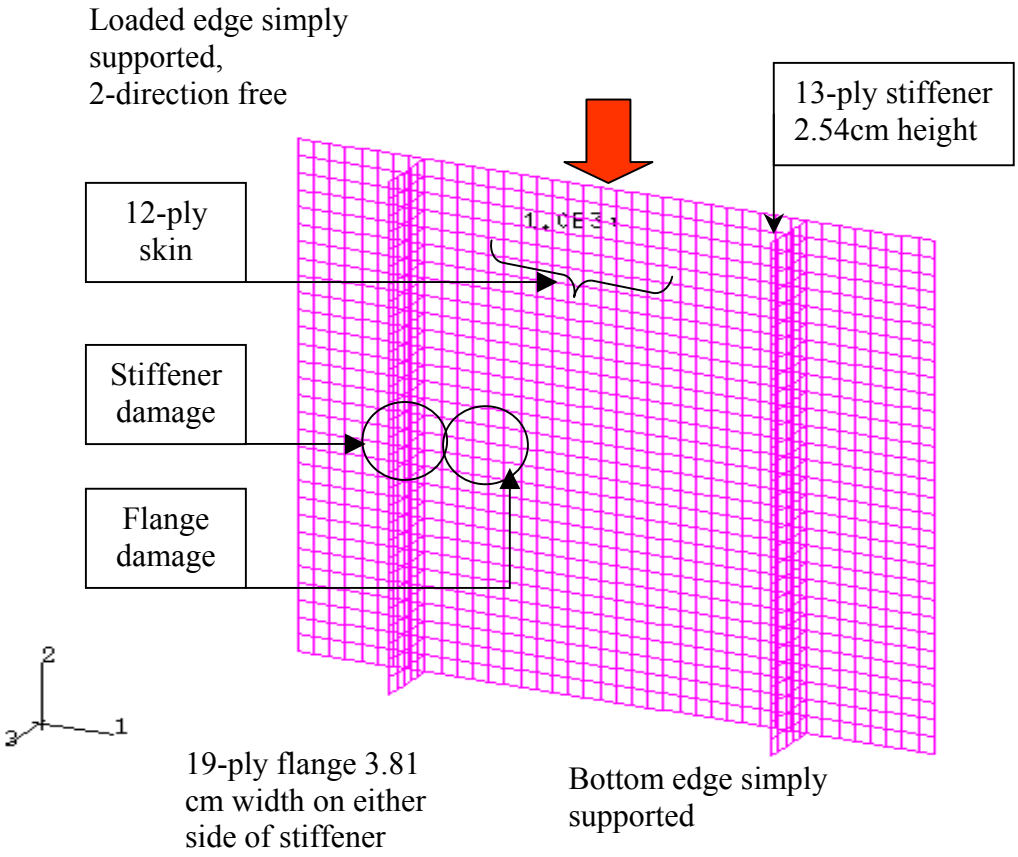


FIGURE 4. A FINITE ELEMENT MODEL AND BOUNDARY CONDITIONS

The nontrivial buckling solution is obtained from

$$\left[K_P^{NM} + \lambda_i K_Q^{NM}\right]\phi_i^M = 0 \tag{30}$$

where, K_P^{NM} and K_Q^{NM} are stiffness matrices corresponding to the base state and the loaded state, respectively, and λ_i and ϕ_i^M are the i^{th} eigenvalue and eigenvector, respectively.

The ABAQUS input listing for the buckling analysis is given in appendix A. ABAQUS calculates the critical values and stores them in an output file called *job-name*.dat[1]. The critical modes are then viewed in the ABAQUS postprocessor using the command such as draw, display, and eig = 1 (the lowest mode shape)[2].

4.2 DAMAGE MODELS.

Damages studied are classified into two main categories: nondetectable and detectable, (see table 8). All damage types are assumed to occur during in-flight operation by a foreign object such as a hail or a 1.82- to 3.64-kg bird strike. For nondetectable or barely visible impact damage (BVID), the structure is expected to carry its full design ultimate load (DUL) since it may not be detected during regular inspection intervals. For a detectable or clearly visible impact damage (CVID) over a stiffener or a flange area, the structure is expected to carry its full design limit load (DLL). The extent of impact damage depends on panel geometry, boundary conditions, impactor geometry, and impact energy.

TABLE 8. DAMAGE TYPES

Damage Classification	Description	Expected Load Capacity	Inspection
Barely visible flange damage	Dent depth less than 2.54 mm	100% design ultimate load	May remain undetected during regular intervals
Clearly visible flange damage	Broken fibers or dent depth greater than 2.54 mm	100% of design limit load	Detected during regular intervals
Clearly visible stiffener damage	Broken fibers	100% of design limit load	Detected during regular intervals

4.2.1 Clearly Visible Flange Damage (CVFD) Model.

The clearly visible flange damage is modeled with a dent depth of 2.54 mm on a flange. Since the depth value of 2.54 mm falls on the borderline between barely visible and clearly visible, it represents a best-case scenario for CVFD panel. CVFD is incorporated into a finite element model by creating a hemispherical surface with a projected area of 127 mm^2 and a depth of 2.54 mm, as shown in figure 5. The protrusion is on the stiffener side since a foreign object will have stricken from outside of an aircraft. The hemispherical shape of the damage was based on the geometry of a drop-weight indenter with a diameter of 12.7 mm that was used in impact testing. In addition, x-ray radiographs revealed that the damage spread was circular in shape with a projected area of approximately 127 mm^2. The location of the damage is at the center of an inside flange area. The CVFD finite element model consists of 2,400 elements.

[1] The job-name refers to the name that is used for the input file for postbuckling analysis, e.g. *postbuckle*.inp.
[2] A different critical modes can be viewed using eig command, e.g., for the fifth modes, set eig=5 and then draw, display.

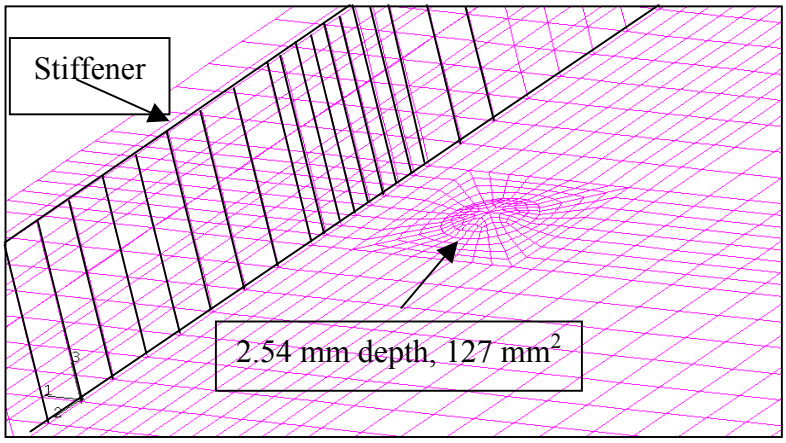


FIGURE 5. FINITE ELEMENT MESH FOR PANEL WITH CLEARLY VISIBLE FLANGE DAMAGE: DAMAGE AREA = 127 mm^2, DEPTH = 2.54 mm

4.2.2 Clearly Visible Stiffener Damage (CVSD) Model.

The clearly visible stiffener damage was modeled by a 0.203-mm-wide gap through the midline of a selected stiffener as shown in figure 6. Experimentally, broken fibers were observed in the impacted stiffener normal to the skin when the drop-weight impact energy reached 30 Joules. Under the compressive loading, the CVSD may be more severe than that of the CVFD. The finite element model consists of 1,690 elements.

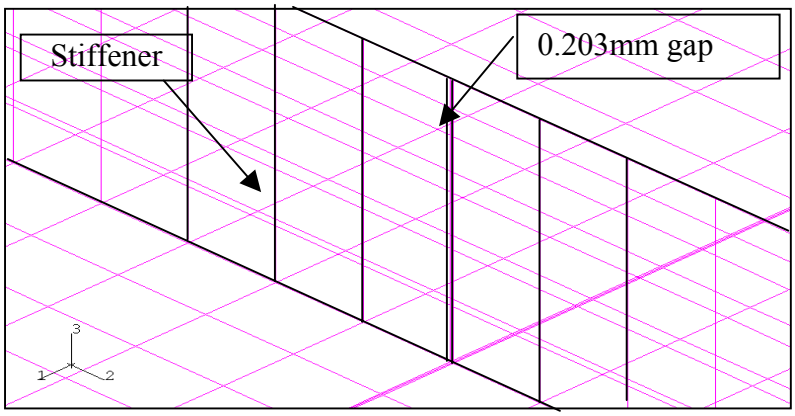
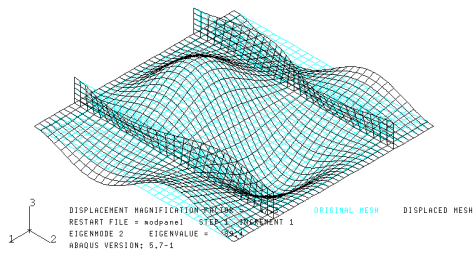


FIGURE 6. FINITE ELEMENT MESH FOR PANEL WITH CLEARLY VISIBLE STIFFENER DAMAGE: 0.203-mm GAP IN A STIFFENER

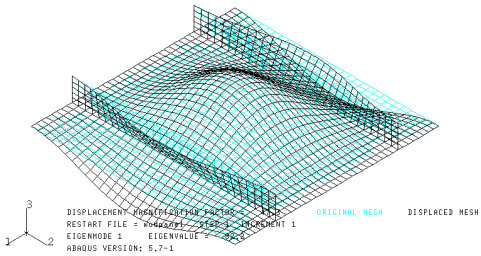
4.3 RESULTS.

For each damage type, the first five critical mode shapes were extracted. Figure 7 shows the first five modes of the undamaged panel. For the damaged panels, only the lowest two critical mode shapes are shown in figures 8 and 9 since the others were almost the same as shown in figure 7. In figure 7, the first mode resembles a full sine wave and the second mode a half sine wave. The number of waves increases for the third and fourth modes. The fifth mode is no longer

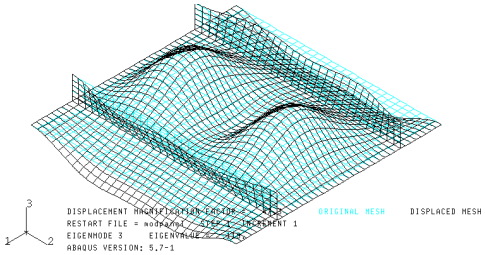
symmetric. The second critical mode of the CVSD panel shows a tearing type of deformation of the damaged stiffener. It is noted that even for the CVSD panel with a damaged stiffener, the reduction in the first critical load is only about 4.7%, as shown in table 9.



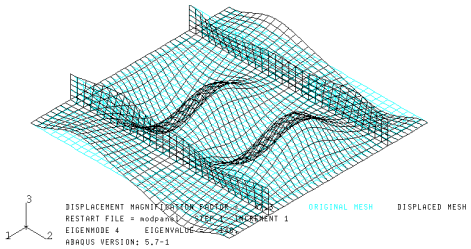
Critical Mode 1



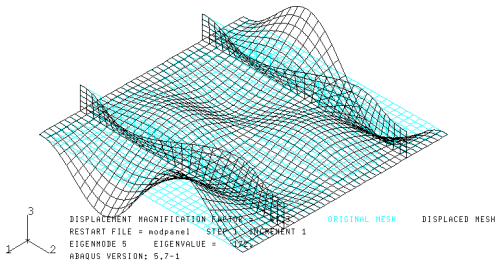
Critical Mode 2



Critical Mode 3

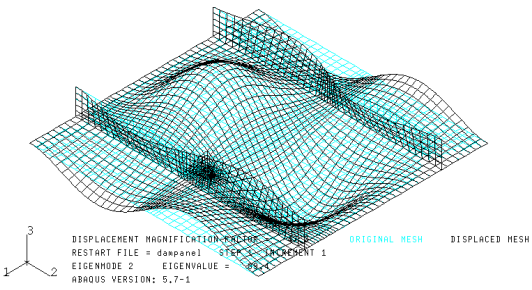


Critical Mode 4

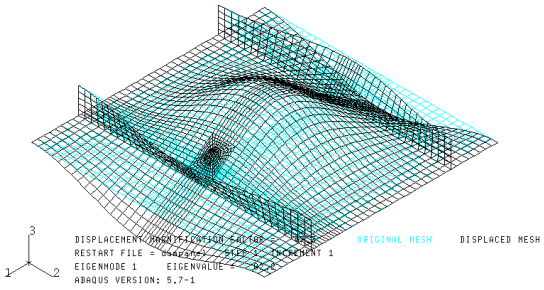


Critical Mode 5

FIGURE 7. CRITICAL MODES OF UNDAMAGED PANEL

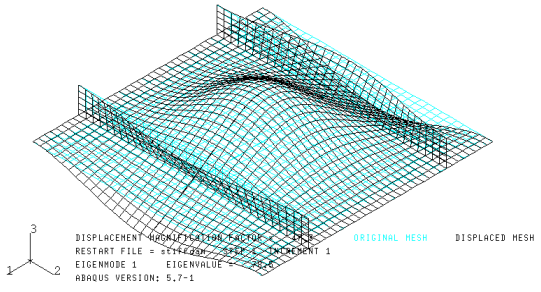


Critical Mode 1

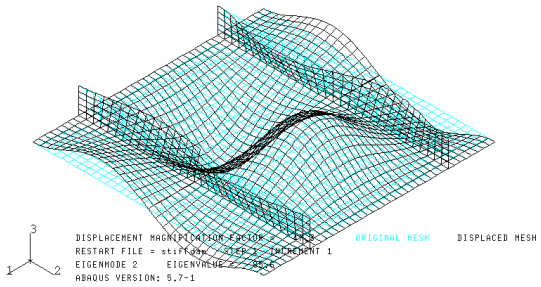


Critical Mode 2

FIGURE 8. CRITICAL MODES OF CVFD PANEL



Critical Mode 1



Critical Mode 2

FIGURE 9. CRITICAL MODES OF CVSD PANEL

TABLE 9. SUMMARY OF CRITICAL MODES AND CRITICAL LOADS FOR UNSTITCHED AND STITCHED PLAIN WEAVE STIFFENED PANELS

	Undamaged		CVFD		CVSD	
Critical Mode	PW (kN)	SPW (kN)	PW (kN)	SPW (kN)	PW (kN)	SPW (kN)
1	90.4	87.0	90.3	86.9	86.8	83.5
2	93.4	89.8	93.0	89.5	90.2	86.8
3	109.7	105.4	109.7	105.5	104.3	100.3
4	138.6	133.3	138.5	133.2	132.7	127.5
5	178.0	171.1	177.7	170.9	170.2	163.7

PW – unstitched plain weave
SPW – stitched plain weave

The lowest critical load and mode shape may be taken as the buckling load and shape, but the purpose of this analysis is to generate a perturbed mesh and an input file, *job-name*.fil[3], required for a postbuckling analysis. In the postbuckling analysis, buckling load is determined from a plot between the load and the center element strain.

5. POSTBUCKLING ANALYSIS OF STIFFENED PANELS.

5.1 FINITE ELEMENT ANALYSIS.

As mentioned in the previous section, a postbuckling analysis requires introduction of an initial imperfection to induce bifurcation. The imperfection, δ, is given by a linear combination of critical mode shapes, ϕ_i, determined from the earlier buckling analysis and weighting factors, ω_i, [25]:

$$\delta = \sum_{i=1}^{M} w_i \phi_i \tag{31}$$

[3] The file is called to create the perturbed mesh in the postbuckling analysis using command: Imperfection, file=job-name, step=1.

In the present analysis, the lowest five critical mode shapes were used with the lowest mode shape being given the highest weight, as shown in table 10. An input file for the ABAQUS analysis is described in appendix A.

TABLE 10. MODAL CONTRIBUTIONS TO INITIAL IMPERFECTION

Critical Mode	Undamaged	CVFD	CVSD
1	0.015	0.015	0.015
2	0.001	0.001	0.001
3	0.001	0.001	0.001
4	0.001	0.001	0.001
5	0.001	0.001	0.001

5.2 FAILURE CRITERIA.

There are a number of failure criteria available in the literature to account for multiaxial state of stress. Most of them are phenomenological based on macroscopic failure modes. Since it is not clear which criterion is the most appropriate for the present case, the following criteria were used for comparison purposes[4].

Maximum Stress Criterion [19]:

$$F_{index} = \max\left(\frac{\sigma_{11}^{t}}{S_1^{t}}, \frac{\sigma_{11}^{c}}{S_1^{c}}, \frac{\sigma_{22}^{t}}{S_2^{t}}, \frac{\sigma_{22}^{c}}{S_2^{c}}, \left|\frac{\sigma_{12}}{S_{12}}\right|\right) \geq 1.0 \tag{32}$$

Tsai-Wu Criterion [26]:

$$F_{index} = F_1\sigma_{11} + F_2\sigma_{22} + F_6\sigma_{12} + F_{11}\sigma_{11}^2 + F_{22}\sigma_{22}^2 + F_{66}\sigma_{12}^2 + 2F_{12}\sigma_{11}\sigma_{22}$$
$$2F_{16}\sigma_{11}\sigma_{12} + 2F_{26}\sigma_{22}\sigma_{12} \geq 1.0 \tag{33}$$

where

$$F_1 = \frac{1}{S_1^{t}} + \frac{1}{S_1^{c}}, \quad F_2 = \frac{1}{S_2^{t}} - \frac{1}{S_2^{c}}, \quad F_6 = 0, \quad F_{11} = \frac{1}{S_1^{t}S_1^{c}}, \quad F_{22} = \frac{1}{S_2^{t}S_2^{c}}$$

$$F_{66} = \left(\frac{1}{S_{12}}\right)^2, \quad F_{12} = -\frac{\sqrt{F_{11}F_{22}}}{2}, \quad F_{16} = 0, \quad F_{26} = 0$$

[4] The failure criteria shown in equation 32 to 35 are provided as subcommand of ABAQUS, i.e., contour, variable=mstrs for contour plot of maximum stress criterion.

Tsai-Hill Criterion [25]:

$$F_{index} = \frac{\sigma_{11}^2}{(S_1)^2} - \frac{\sigma_{11}\sigma_{22}}{(S_1)^2} + \frac{\sigma_{22}^2}{(S_2)^2} + \frac{\sigma_{12}^2}{(S_{12})^2} \geq 1.0 \tag{34}$$

Azzi-Tsai-Hill Criterion [25]:

$$F_{index} = \frac{\sigma_{11}^2}{(S_1)^2} - \frac{|\sigma_{11}\sigma_{22}|}{(S_1)^2} + \frac{\sigma_{22}^2}{(S_2)^2} + \frac{\sigma_{12}^2}{(S_{12})^2} \geq 1.0 \tag{35}$$

In equations 34 and 35, the values of S_1 and S_2 are taken as either tensile or compressive, depending on the signs of σ_1 and σ_2.

5.3 RESULTS.

The buckling load is taken as the load at which the load-strain relation deviates from linearity. The center element is used to monitor the strain. The final failure is assumed to occur as soon as the failure index reaches unity in any one of the plies, using unidirectional strength values listed in table 7. It is noted that no out-of-plane stresses are calculated in the analysis and, hence, no delamination can be predicted. Only the in-plane failure is assessed in the analysis.

5.3.1 Undamaged Panel.

For the undamaged panel, the analysis predicts a buckling load of 80 kN and a final failure load of 200 kN. Using the nominal cross-sectional area of 1.058E-3 m^2, this translates into the buckling and failure stresses of 75.6 and 189 MPa, respectively.

The strain plots of center elements show the bifurcation point at which the buckling load is taken, as shown in figure 10. The failure indices at final failure are shown in table 11. The maximum stress failure criterion is shown to be the least conservative and is used to predict final failure. The shear stress in angle plies exceeds the shear strength near the central region of the stiffener, as shown in figure 11. The deformed shape at buckling is similar to the first critical mode, i.e., a full sine wave and remains the same until final failure.

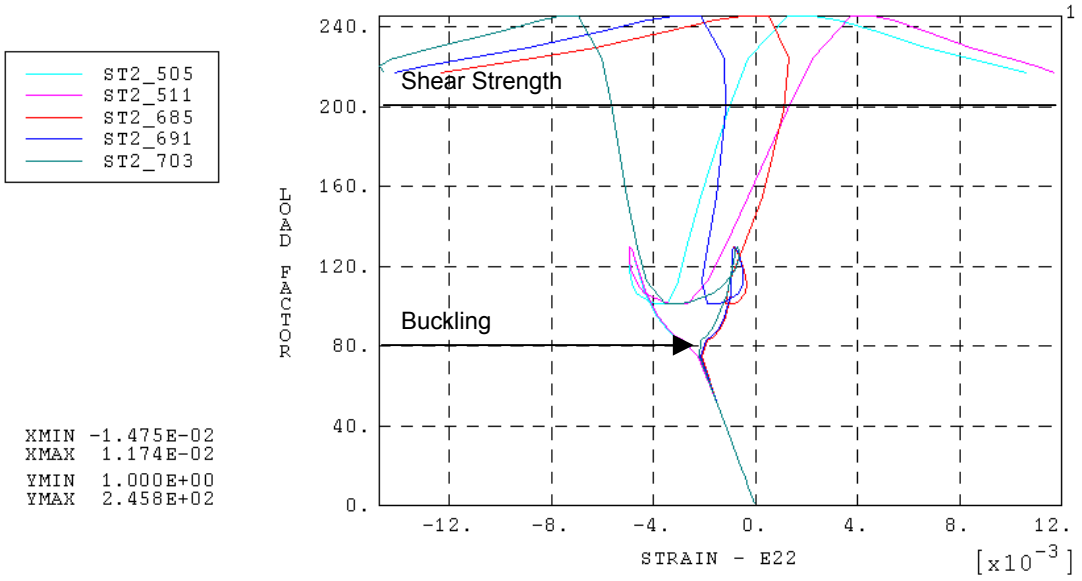


FIGURE 10. LOAD FACTOR VERSUS STRAIN OF UNDAMAGED PANEL AT CENTER ELEMENTS

TABLE 11. SUMMARY OF FINITE ELEMENT ANALYSIS RESULTS FOR STITCHED PANELS

Model		Predicted Bucking			Predicted Failure			Failure Index			
Type	Case	Load (kN)	Mode	Center Strain	Load (kN)	Mode	Center Strain	Azzi	Max. Stress	Tsai-Hill	Tsai-Wu
Und	1	80	I	2.0e-3	203	II, Shear, Stiffener	5.1e-3	1.10	1.06	1.10	1.15
	2	80	I	2.0e-3	218	II, Shear, Stiffener	5.4e-3	1.29	1.23	1.29	1.35
	3	80	I	2.0e-3	198	II, Shear, Stiffener	5.1e-3	1.10	1.05	1.10	1.16
CVFD	1	80	I	2.0e-3	204	II, Shear, Stiffener	5.0e-3	1.15	1.10	1.15	1.22
	2	80	I	2.1e-3	222	II, Shear, Stiffener	5.5e-3	1.32	1.27	1.32	1.38
	3	80	I	2.1e-3	214	II, Shear, Stiffener	5.3e-3	1.24	1.19	1.24	1.30
CVSD	1	59	I	1.3e-3	122	I, Comp, Damage	5.0e-3	1.08	1.01	1.17	1.12
	2	59	I	1.3e-3	119	I, Comp, Damage	5.0e-3	1.01	0.934	1.01	1.04
	3	59	I	1.3e-3	126	I, Comp, Damage	5.0e-3	1.15	1.07	1.23	1.19

I – deformation shape resembling first critical mode
II – deformation shape resembling second critical mode
Shear – shear strength limit
Comp – loading direction compressive strength limit
Stiffener – center region of stiffener
Damage – around the damaged area

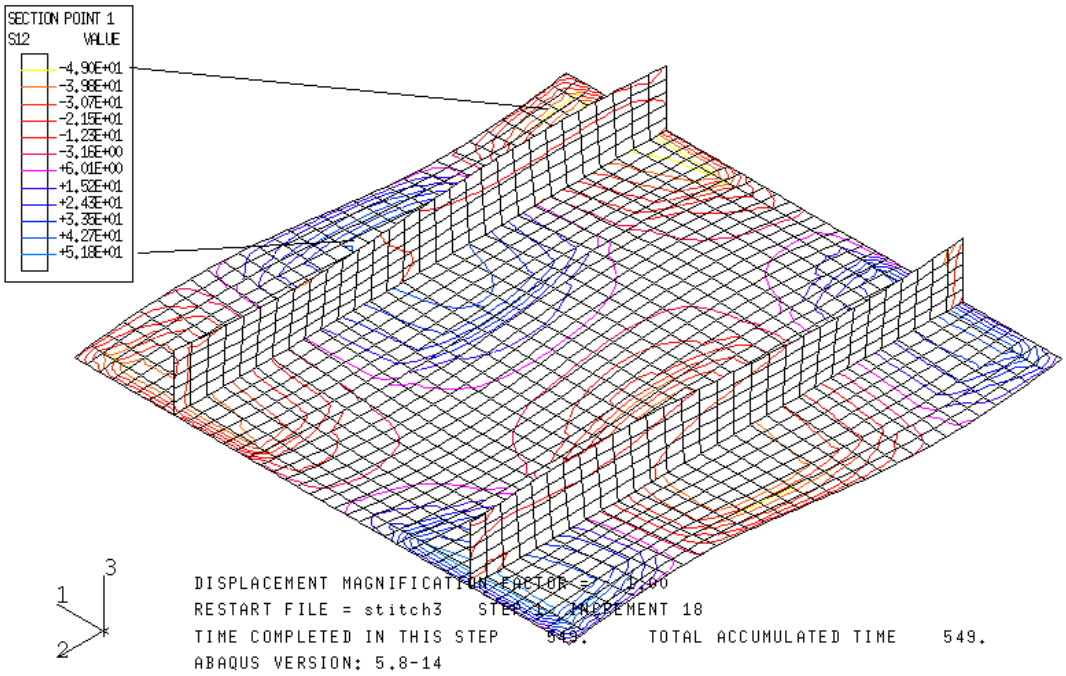


FIGURE 11. SHEAR STRESS PLOT OF UNDAMAGED PANEL AT FAILURE

5.3.2 CVFD Panel.

The load factor versus strain plots showed the buckling and failure loads to be slightly less than 80 kN (75.6 MPa) and about 204 kN (190 MPa), respectively. These values are quite close to those for the undamaged panel. As in the undamaged case, the deformation mode is a full sine wave until final failure. The failure is due to the shear stress in angle plies exceeding the strength limit near the center region of a stiffener that is close to the damage as shown in figure 12.

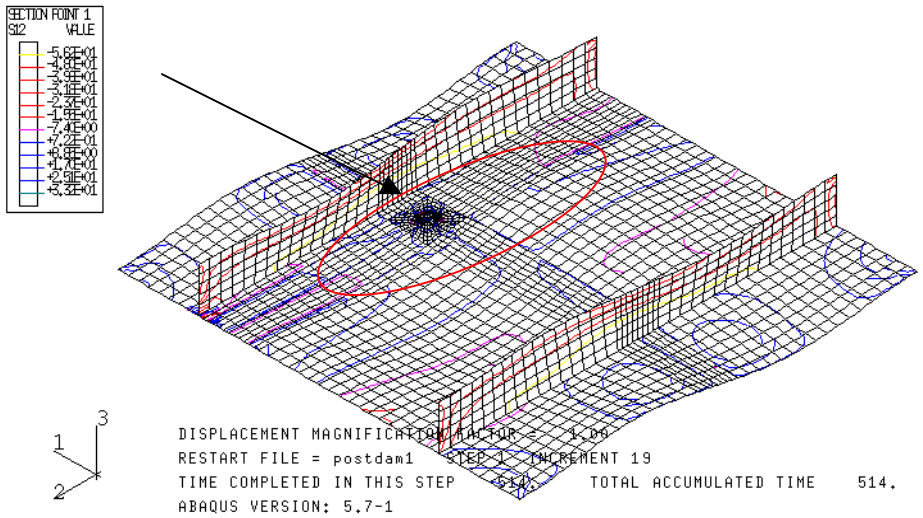


FIGURE 12. SHEAR STRESS PLOT OF CVFD PANEL AT FAILURE

5.3.3 CVSD Panel.

From figure 13, the predicted buckling and failure loads are 60 kN (56.7 MPa) and 119 kN (112 MPa), respectively. These load levels are significantly below those for the undamaged and CVFD panels. The deformed shape at failure is not symmetric because of the damaged stiffener, as shown in figure 14. The final failure occurs due to transverse failure of flange plies at the damaged location.

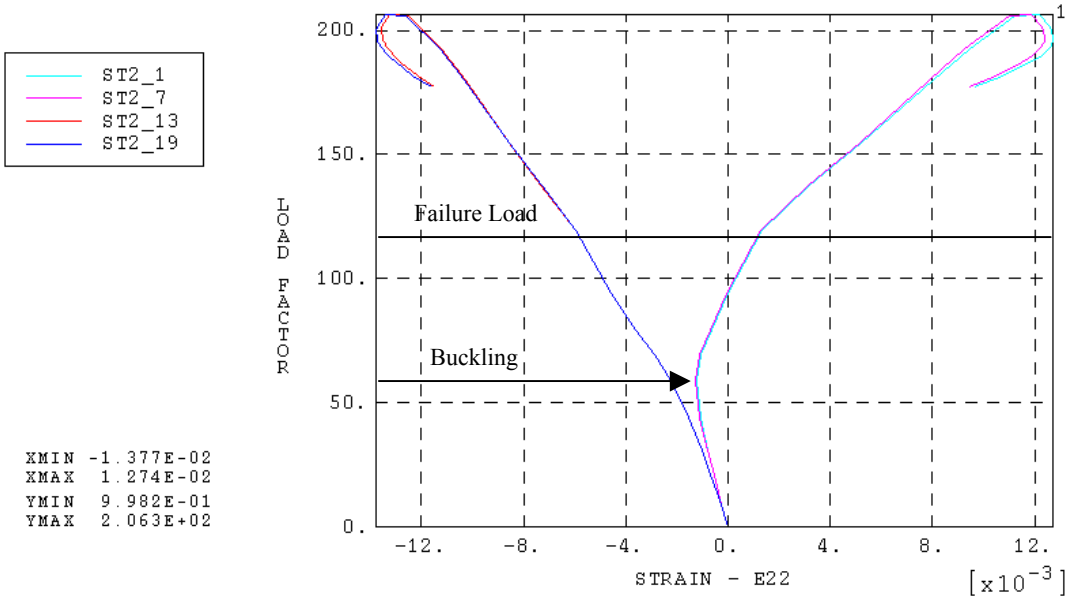


FIGURE 13. LOAD FACTOR VERSUS STRAIN OF CVSD PANEL AT CENTER ELEMENTS

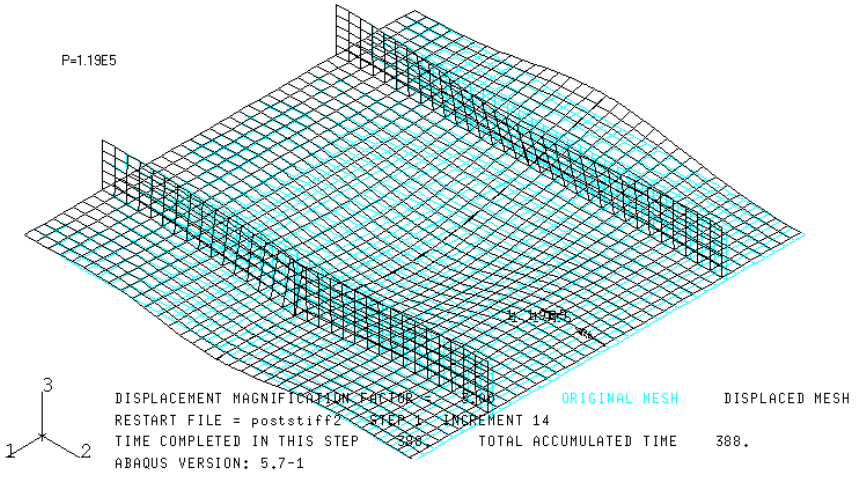


FIGURE 14. A HALF SINE WAVE DEFORMATION OF CVSD PANEL AT FAILURE

6. MANUFACTURING OF STIFFENED PANELS.

Manufacturing of stitched, stiffened panels consists of three primary steps: (1) layup and stitching of skin and stiffeners, (2) preparation of resin film, and (3) resin film infusion in an autoclave. In the case of unstitched panels, the stitching process in step 1 is replaced by stapling of skin and stiffeners to facilitate handling of the loose fabric layers, especially during the joining phase of skin and stiffeners.

6.1 STITCHING.

The quality of stitching depends on a proper control of needle thread tension, bobbin thread tension, and holder-foot pressure, as shown in figure 15. The most critical of those parameters is the needle thread tension. Applying an excessively tight tension results in knots that are embedded into the fabric, figure 16. The excess space around the knots allows resin-rich areas or dimples to form. In the present study, the following stitching conditions were found to be satisfactory after trial and error: a needle thread tension of 6.0 - 6.5 N, a bobbin thread tension of 8.0 - 9.0 N, and a holder-foot pressure of 0.2 MPa.

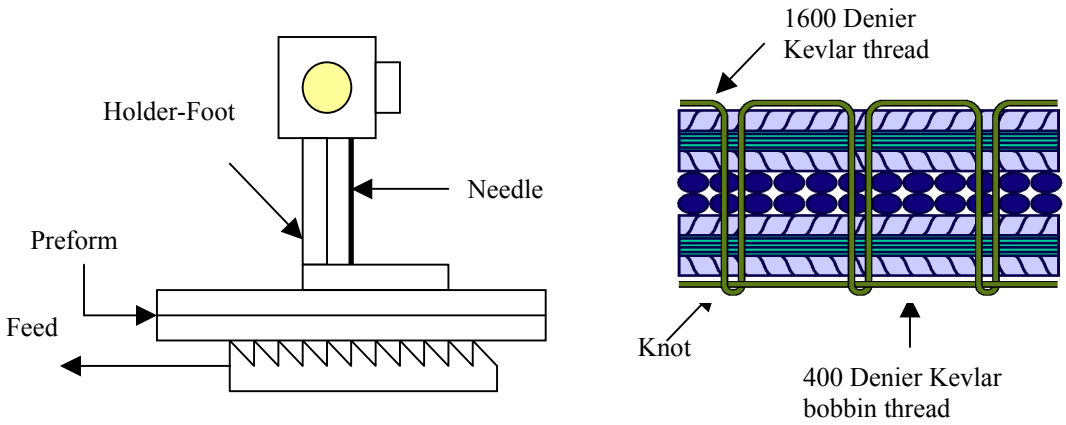


FIGURE 15. A SCHEMATIC OF STITCHING PROCESS

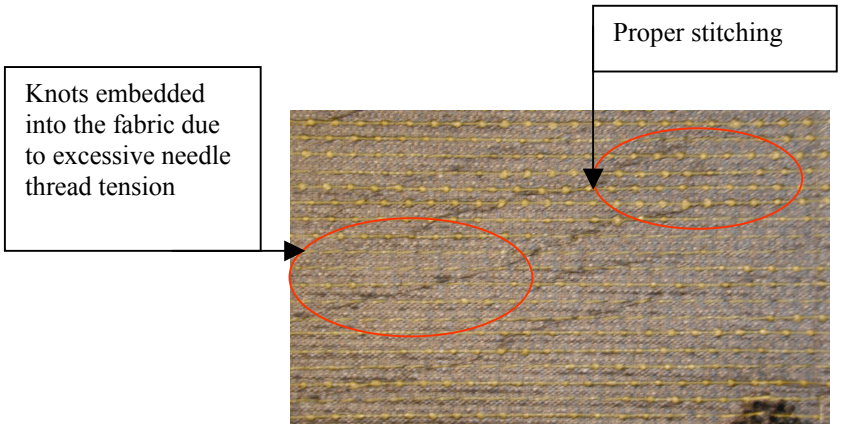


FIGURE 16. STITCHING QUALITY DEPENDENT ON VARIATION OF NEEDLE THREAD TENSION

Fabrication of dry preforms involves layup and stitching of fabric layers with Kevlar threads. A 1600-denier Kevlar thread was used for the needle and a 400-denier Kevlar thread for the bobbin. Fiber preforms for the stiffened panels were prepared as follows. First, 13 layers of skin fabric and 12 layers of stiffener fabric were stitched separately, leaving the flange areas unstitched. The unstitched portion of stiffener was divided into six layers on each side and placed over the unstitched skin. At this point, 15 tows of AS4 carbon fiber were inserted into the gap at the skin-stiffener joint to prevent the formation of groove. Both skin and stiffener were then stitched together in the flange areas. A stitched fiber preform is shown in figure 17.

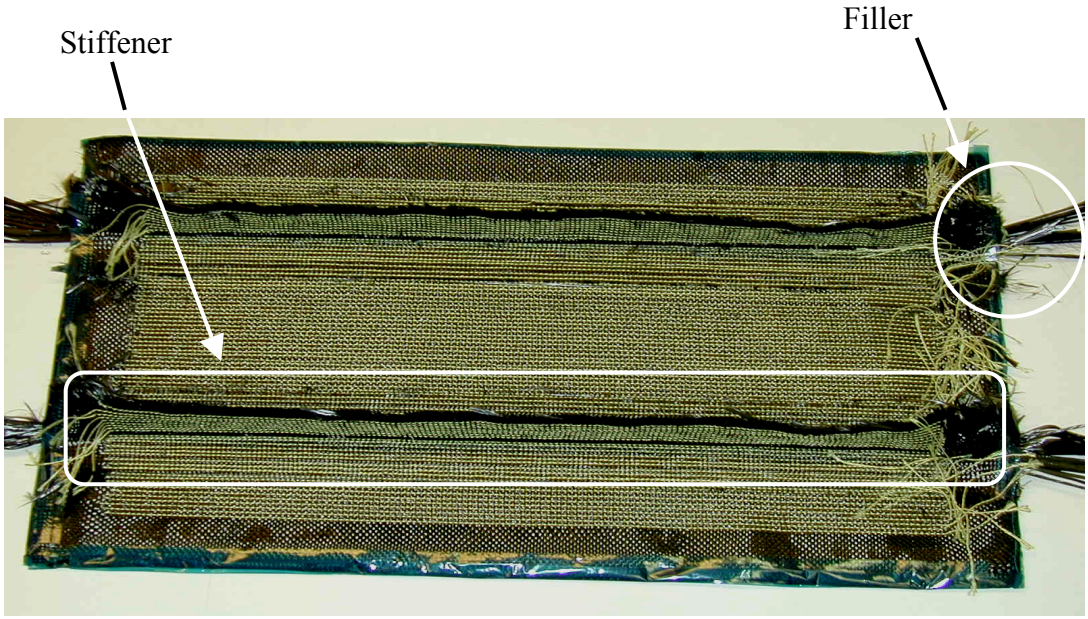


FIGURE 17. STITCHED PREFORM WITH STIFFENERS

Stitching was done on a JUKI 200 industrial sewing machine with a working platform capable of handling up to 50- × 70- × 2.5-cm preforms. The stitching speed was maintained at 18 cm/min to minimize damage to the carbon fibers near stitches [27].

6.2 RESIN FILM INFUSION.

A resin film was prepared using 500 grams of 3501-6 resin. This is slightly more than required for a 50% fiber volume content to ensure complete saturation of the dry preform. The refrigerated solid resin was crushed into fine particles smaller than 5 mm in diameter. The particles were spread evenly over the inside mold surface and heated to 60°C inside an autoclave for 20 minutes to form a flat film approximately 5 mm thick.

The mold consisted of a top and a bottom platen, four side aluminum bars, and three filleted inner aluminum bars, as shown in figure 18. The inner bars determined the location and thickness of the two stiffeners. Each of the mold parts was treated with a release agent and covered tightly with a nonporous Release Ease 234 peel ply, using a high-temperature adhesive tape.

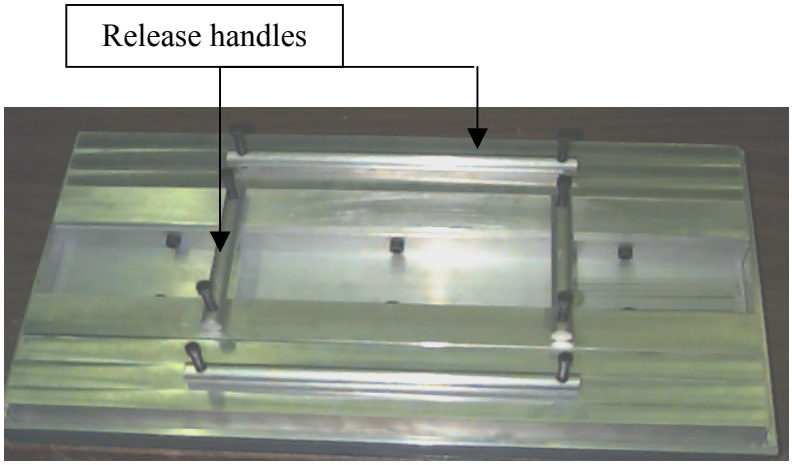


FIGURE 18. ALUMINUM MOLD ASSEMBLY

The stitched preform was placed into the mold containing the resin film, pressed down using a roller, and the inner molds were put into place. Four bleeder plies, approximately 8 by 15 cm, were placed on center where two vacuum ports were to be located. A rectangular steel frame covered with a porous ply was inserted to keep the vacuum ports and the bleeder plies apart to avoid resin flow into the vacuum ports. Two layers of Airweave breathers were used to cover the topside, and the entire assembly was vacuum bagged using IPPLON DP-1000, and sealed around the edges with a sealant tape. After attaching two vacuum lines, a leak test was performed.

The assembly was placed in an autoclave and cured using the cure cycle shown in figure 19. The cure cycle was a slight modification of the manufacturer's recommended cycle in that the first isothermal dwell was at 135°C rather than the recommended 121°C. The higher isothermal condition was necessary to ensure low-resin viscosity for maximum infiltration.

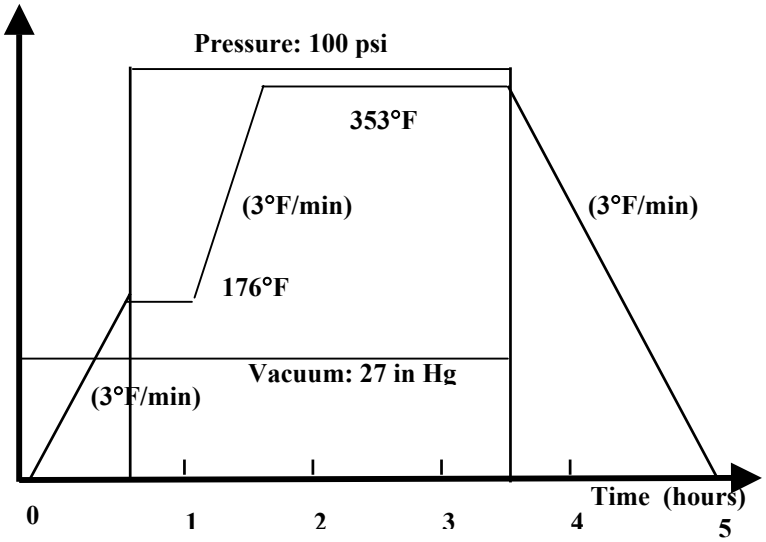


FIGURE 19. CURE CYCLE

Dimensions of the manufactured panel were 54.61 x 30.48 x 4.23 cm. Each panel was cut into two specimens using a high-pressure abrasive water-jet system[5]. Overall dimensions of each specimen were 25.4 x 25.4 cm with two 2.54-cm stiffeners. The two specimens from the same panel were then designated a and b.

Flat panels were fabricated using the same procedure. The only difference was that the inner mold pieces for stiffeners were not used.

7. QUALITY ASSURANCE.

Several techniques were used to inspect the fiber preforms before the RFI process and then the composite panels after fabrication to ensure the consistent and acceptable quality. These techniques included ultraviolet (UV) inspection of the fabrics, visual inspection of the fabricated panels, and dimensional measurements using a coordinate measuring machine (CMM) and other measurement instruments.

7.1 ULTRAVIOLET INSPECTION OF FABRICS.

ASTM D5687/D5687M 7.1.1.4 Cleanliness and Airborne Particulates [28] prescribes that the fabric exposure to particulates be minimized. In order to minimize the airborne particle contamination, fabrics were inspected under UV light, as shown in figure 20. The UV inspection was also found useful in detecting hard-to-see cracks on cured panels, as shown in figure 21.

The UV inspection reveals dust particles not visible to the naked eye. Under UV light, fabric reflects purple color, dust particles, are white color. However, the color of Kevlar thread is more or less the same, although its brightness increased in the case of insufficient resin impregnation. The damage induced by impact appears black in the midst of bluish-purple, as shown in figure 21.



FIGURE 20. ULTRAVIOLET INSPECTION OF FABRIC

[5] The condition used: water pressure of 275.6 MPa.

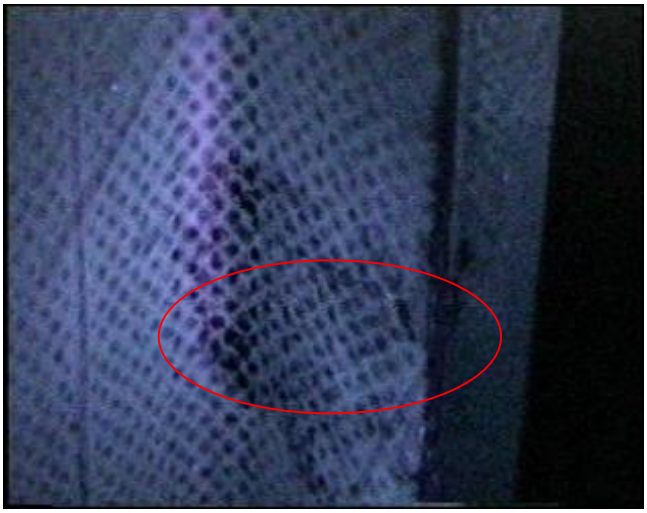


FIGURE 21. ULTRAVIOLET INSPECTION OF CRACKS IN CVSD PANEL

Dust particles detected by UV inspection were removed immediately. The UV light highlighted many features that were not readily noticeable and helped to minimize defects in the subsequent fabrication.

7.2 VISUAL INSPECTION OF PANELS.

Panels were inspected visually for their quality. The following five attributes were used in assessing the quality: stiffener grooves on skin side, stiffener alignment, skin surface resin starvation, flange edge regions, and flange alignment. Those attributes are shown in figure 22. These were typical macroscale surface defects that were observed on seemingly well-prepared panels. The stiffener groove is a groove in the skin along the stiffener where resin is starved because of skin-stiffener joining.

Five different panels from three initial batches were rated for their overall quality. For each attribute, four quality features were defined together with a numerical rating, as shown in table 12. The best quality feature was assigned a numerical rating of 4, whereas the worst was assigned a numerical rating of 1. The results are shown in table 13. Note that the same weight was given to each attribute even though the stiffener grooves may affect the panel performance more than the poor condition of flange edge regions or skin area resin starvation.

The major difference between panels 3a and 3b is the quality of the stiffener groove region. The lower quality of panel 3a is due to the stiffener groove that extended along most of the panel length. Unfortunately, only panel 2a has a very good rating from those initial batches. In subsequent panel fabrications, the initial vacuum stage was reduced in order to minimize the formation of the grooves and resin starvation areas on the skin, and the remaining panels were rated good to very good.

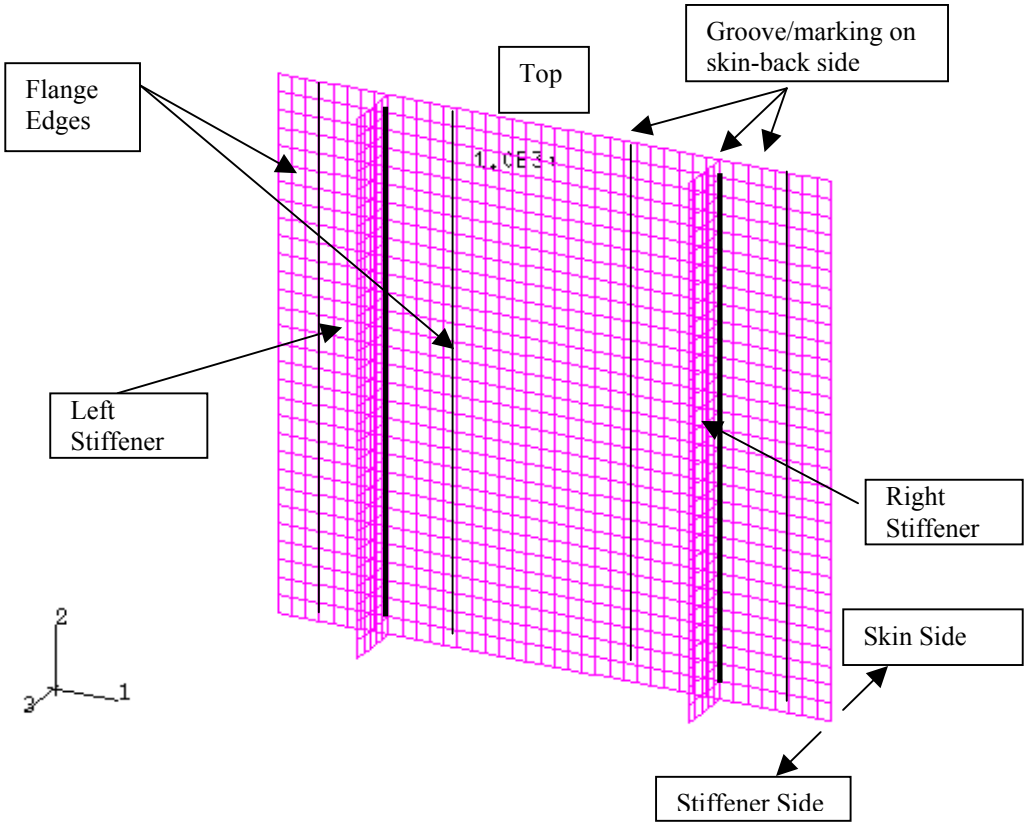


FIGURE 22. VISUAL INSPECTION AREAS

TABLE 12. QUALITY RATING SCHEME

Inspection Area	Feature	Numerical Rating
Stiffener groove areas	Severe grooves	1
	Groove	2
	Groove marking	3
	Resin-rich	4
Stiffener alignment	Misaligned, wavy	1
	Wavy	2
	Some misalignment	3
	Aligned	4
Skin surface resin starvation	Large areas	1
	Noticeable areas	2
	Few area	3
	Not apparent	4
Flange edge regions	Groove	1
	Yarn tow mess	2
	Groove marking	3
	None	4
Flange alignment	Misaligned, wavy	1
	Wavy	2
	Some misalignment	3
	Aligned	4

TABLE 13. OVERALL PANEL QUALITY

Inspection Area	P1a	P1b	P2a	P3a	P3b
Stiffener groove areas	4	3	3	1	2
Stiffener alignment	1	4	4	4	4
Skin area resin starvation	4	4	4	1	3
Flange edge regions	2	2	3	3	1
Flange alignment	1	1	4	4	4
Average	2.4	2.8	3.6	2.6	2.8
Overall Rating	Poor	Good	Very Good	Fair	Good

7.3 DIMENSIONAL VARIATIONS.

A Brown & Sharpe MicroVal PFx coordinate measuring machine (CMM) was used to measure the critical dimensions of unstitched panels, as shown in figure 23. From these CMM measurements, average thicknesses of skin, flanges, and stiffeners were calculated. Compared with their respective nominal values, as shown in figure 24, stiffeners and flanges are thinner by up to 11.4% and 2.6%, respectively. However, the skin is 5.1% thicker than nominal. The nominal dimensions are based on the manufacturer's datasheet, which states that the average ply thickness should be 0.22 mm at 50% fiber volume. The stiffeners show a much larger variation than the flanges and skin.

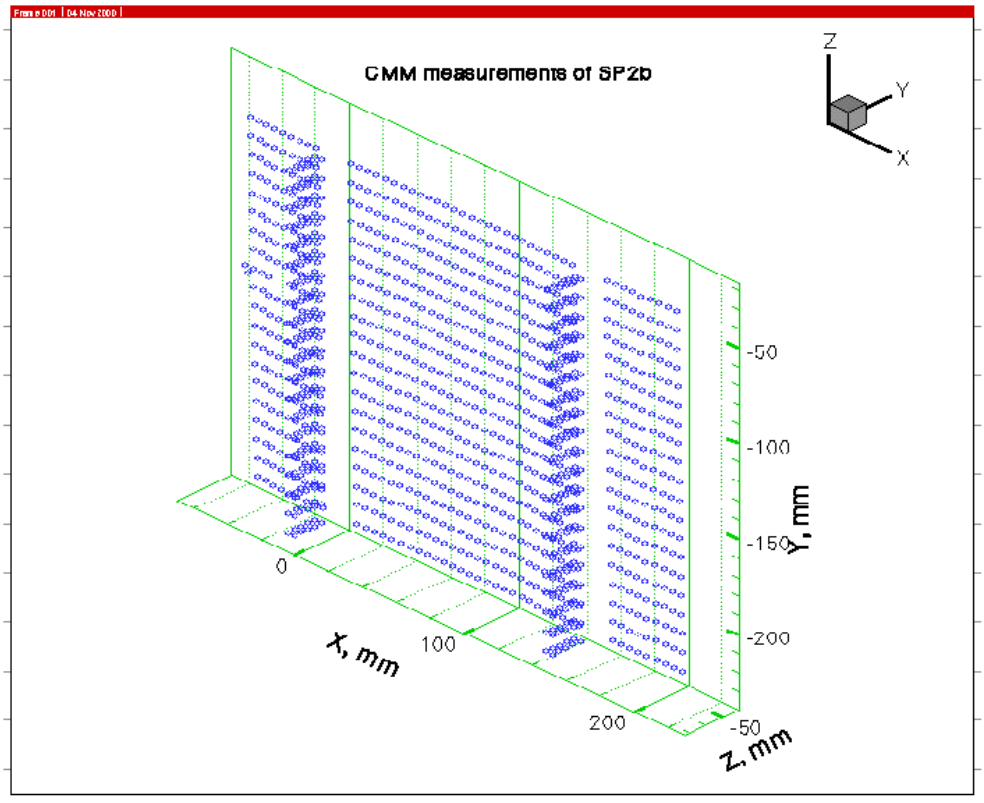


FIGURE 23. COORDINATE MEASURING MACHINE MEASUREMENT POINTS

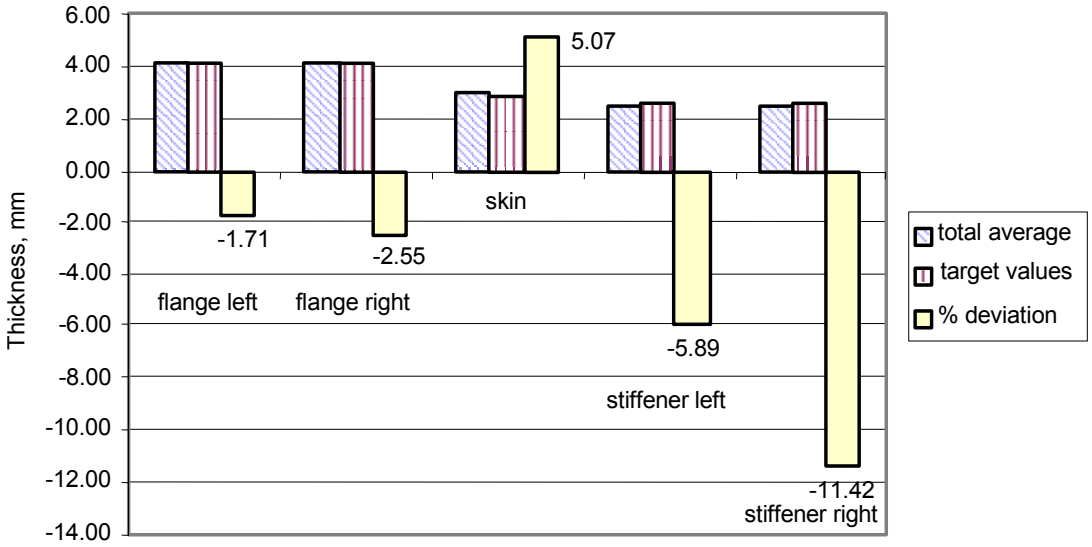


FIGURE 24. AVERAGE THICKNESSES OF UNSTITCHED PANEL VERSUS NOMINAL VALUES

As shown in figure 25, the stiffener spacing and flange widths are less than 1.25% of its nominal values. The stiffener heights and the overall dimensions are affected by the machining process rather than the manufacturing process. The maximum deviations compared to their intended values were 1.9% for stiffener heights and 3.5% for edge distances.

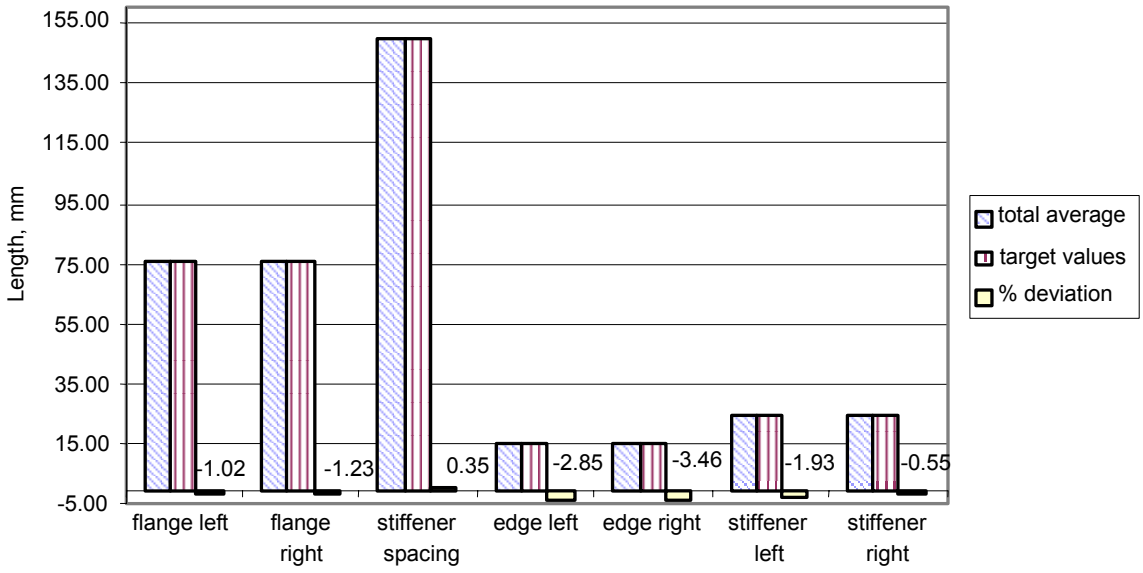
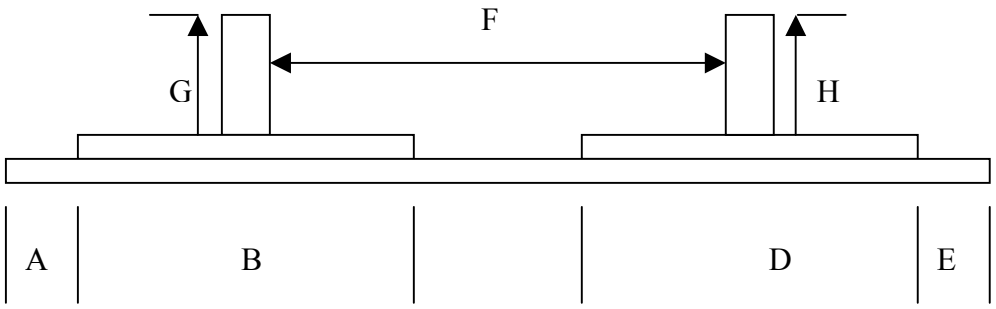
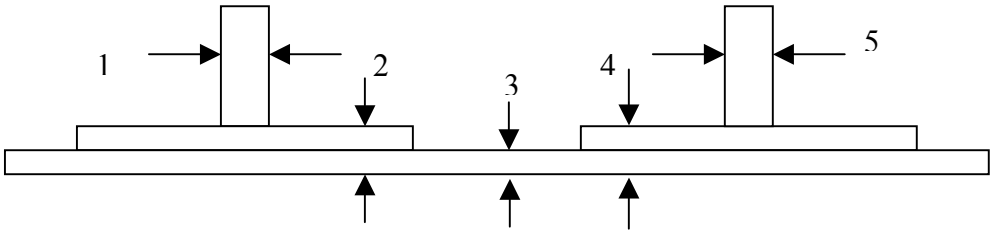


FIGURE 25. AVERAGE DIMENSIONS OF UNSTITCHED PANEL VERSUS NOMINAL VALUES

Although the CMM can provide full configurational information on each panel, it is quite time consuming. Therefore, a reduced measurement scheme was adopted for stitched panels. A digital caliper and a micrometer were used for length and thickness measurements, respectively, to take a minimum of 12 measurements to calculate the cross-sectional area of each panel, as shown in figure 26. The results of those measurements are shown in figures 27 and 28. The nominal dimensions are taken to be the same for both unstitched and stitched panels.



A – edge, left
B – flange, left
D – flange, right
E – edge, right
F – dist between stiffeners (spacing)
G – height of stiffener, left
H – height of stiffener, right



1 – stiffener thickness, left
2 – flange thickness, left
3 – skin thickness
4 – flange thickness, right
5 – stiffener thickness, right

FIGURE 26. KEY DIMENSIONS

By comparing % deviation values in figure 24 to those in figure 27, the stitched panels are shown to be thicker than the unstitched panels. Thus, stitching was shown to increase the overall thickness. However, absolute deviations from nominal values are about the same for both sets of panels. As shown in figure 28, the planar dimensions that are controlled by machining show almost the same accuracy as in the unstitched panels.

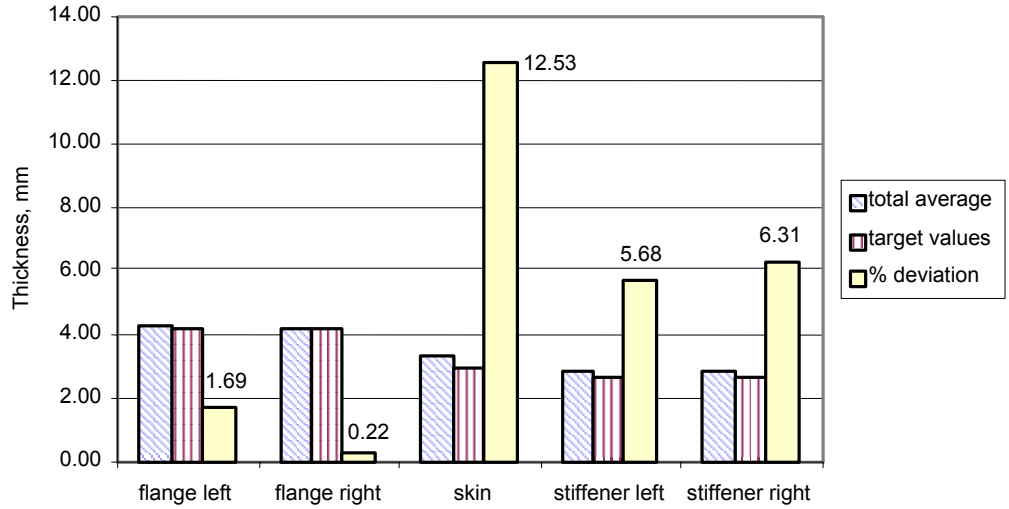


FIGURE 27. AVERAGE THICKNESSES OF STITCHED PANEL VERSUS NOMINAL VALUES

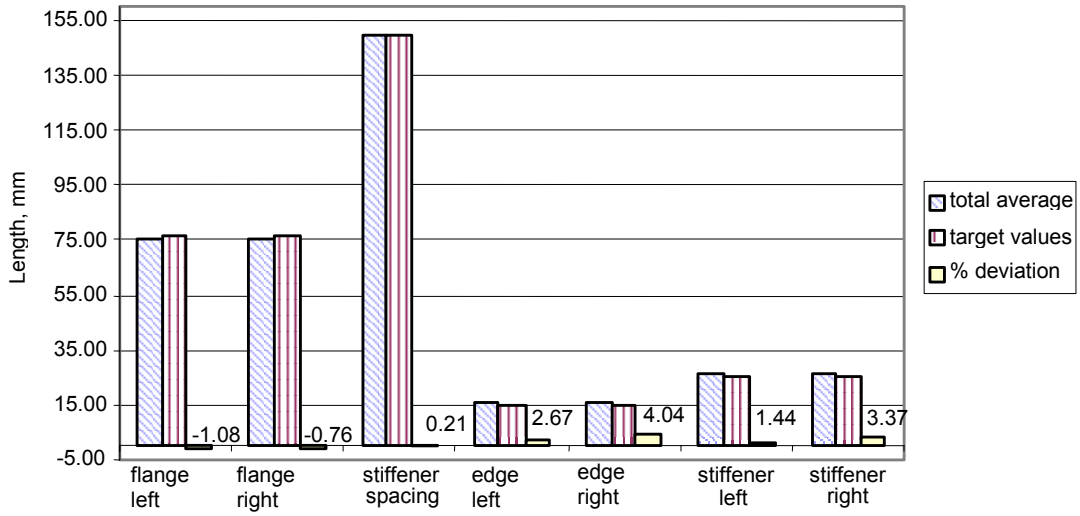


FIGURE 28. AVERAGE DIMENSIONS OF STITCHED PANEL VERSUS NOMINAL VALUES

8. PROPERTIES OF LAMINATE COUPONS.

Laminate coupons representative of the skin construction were fabricated using the manufacturing procedure described in section 6 and tested to obtain mechanical properties. Tensile modulus and strength were measured on both unstitched and stitched laminates; however, compressive modulus and strength were measured only on stitched laminates. These experiments were performed to verify the analytical predictions described in section 3 prior to the panel testing, and if necessary, to revise the analytical prediction. The stitched coupons were obtained from three flat panels, and the unstitched coupons from one flat panel.

8.1 EXPERIMENTAL PROCEDURE.

Coupons were tested in accordance with the ASTM 3039 [29 and 30] and the NASA Short-Block method [31]. For tensile tests, 5 unstitched and 15 stitched coupons were used to measure the modulus and strength. Figure 29 shows two loading directions used for tensile tests of stitched coupons: parallel and perpendicular to the stitching direction. Any difference between these two directions would indicate the effect of stitching.

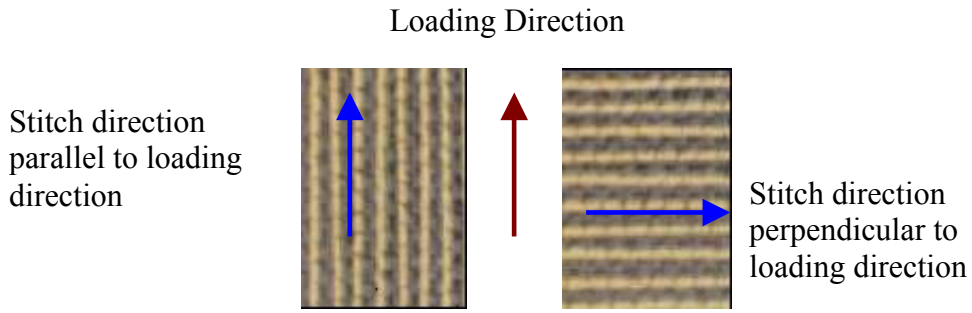


FIGURE 29. LOADING DIRECTION VERSUS STITCH DIRECTION

Coupons were machined using an abrasive waterjet machine. The width and length of a coupon were measured using a digital caliper, and the thickness was measured using a digital micrometer. For the tensile coupon, a strain gage was attached at its center, and for the compression coupon, two strain gages were used back to back at its center.

8.2 RESULTS.

Both tensile modulus and strength are slightly higher in the stitching direction; however, the difference is rather small, as shown in table 14, and considered to be within the experimental scatter. Regardless of the loading direction, coupons failed along the series of stitches, as shown in figure 30. Thus, stitches are believed to serve as weak spots.

Stitched coupons have an average tensile modulus of 40.2 GPa and an average tensile strength of 386 MPa. The modulus compares favorably with its unstitched counterpart, 40.0 GPa. However, the tensile strength of the stitched composite is higher than the unstitched composite strength of 340 MPa. This result is quite unexpected since stitches are believed to be weak spots. Also, the measured failure stains for unstitched coupons are lower than the reported values of 1.2% to 1.3% [32]. Failure near grips is suspected to be one of the reasons for lower strength of unstitched coupons. Since properties of unstitched coupons are available in the literature, no further testing was performed.

TABLE 14. TENSILE PROPERTIES OF STITCHED AND UNSTITCHED COUPONS

Stitched Coupons						
Specimen No.	Thickness (mm)	Width (mm)	Modulus (GPa)	Strength (MPa)	Failure Strain (%)	Stitch Orientation
1	2.993	25.832	39.97	372.51	0.932	Parallel
2	2.887	24.892	41.87	409.53	0.978	Parallel
3	2.761	26.340	41.61	372.86	0.896	Parallel
4	2.863	26.289	41.60	373.90	0.899	Parallel
5	2.868	25.235	39.97	372.51	0.932	Parallel
6	2.888	25.298	39.90	388.78	0.974	Parallel
7	2.863	26.911	39.12	405.07	1.04	Parallel
8	2.849	25.616	42.47	423.99	0.998	Parallel
9	2.858	25.184	41.10	407.68	0.992	Parallel
10	2.858	25.184	36.37	368.76	1.010	Perpendicular
11	2.874	25.387	39.49	387.47	0.981	Perpendicular
12	2.875	25.298	38.52	361.16	0.938	Perpendicular
13	2.880	25.375	45.43	377.69	0.831	Perpendicular
14	2.935	24.638	36.87	368.83	1.00	Perpendicular
15	2.774	25.476	39.15	398.20	1.02	Angled
Average	2.868	25.530	40.23	385.93	0.961	
Standard Deviation	0.0549	0.593	2.261	18.80	0.0557	
Unstitched Coupons						
Specimen No.	Thickness (mm)	Width (mm)	Modulus (GPa)	Strength (MPa)	Failure Strain (%)	
1	2.898	24.625	39.02	313.92	0.805	
2	2.850	24.994	38.70	325.76	0.842	
3	2.757	24.994	36.33	334.78	0.921	
4	2.799	25.362	40.47	355.04	0.877	
5	2.625	24.841	44.57	351.74	0.789	
Average	2.786	24.963	39.82	336.25	0.847	
Standard Deviation	0.104	0.269	3.042	17.35	0.0539	

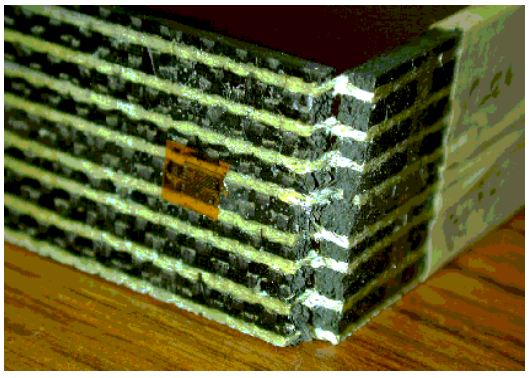


FIGURE 30. TENSILE FAILURE OF A STITCHED COUPON

As shown in table 15, the average compressive modulus and strength of stitched coupons are 36.8 GPa and 304 MPa, respectively. These results are lower than expected values due to inadvertent global buckling of the specimen as shown in figure 31. A slight imbalance in the weight distribution of the top fixture could produce a bending moment during compression loading of a thin specimen, as shown in figure 32. When the tensile modulus is used in conjunction with the compressive strain of 0.908%, the average compressive strength moves up to 365 MPa, as shown in figure 33.

TABLE 15. COMPRESSIVE PROPERTIES OF STITCHED COUPONS PARALLEL TO STITCH DIRECTION

Specimen No.	Thickness (mm)	Width (mm)	Modulus (GPa)	Strength (MPa)	Failure Strain (%)
1	2.8473	38.2524	33.82	-339.64	1.040
2	2.8893	38.2778	37.49	-302.42	0.9035
3	2.9159	39.1160	34.34	-248.80	0.9050
4	2.7877	37.8587	39.28	-369.72	0.8276
5	2.8600	39.0000	38.97	-258.96	0.8616
Average	2.8600	38.5010	36.78	-303.91	0.9075
Standard Deviation	0.0484	0.537	2.562	51.64	0.0807

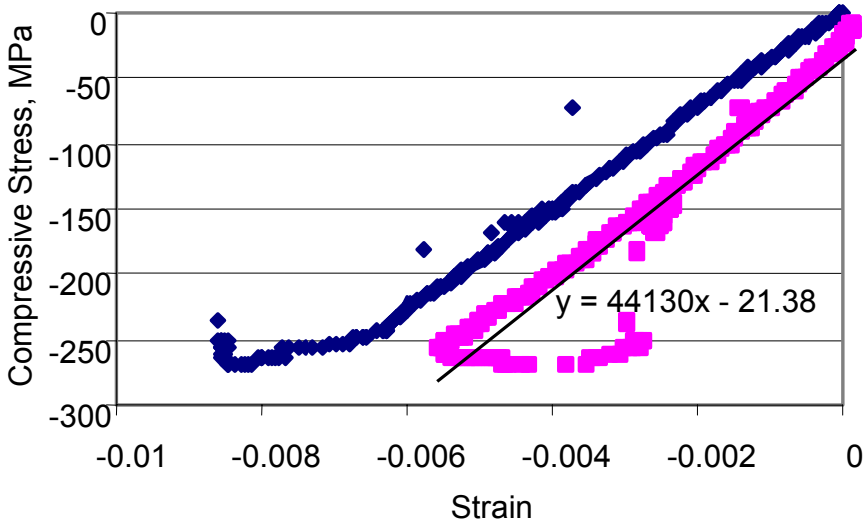


FIGURE 31. A STRESS VERSUS STRAIN PLOT FROM NASA SHORT BLOCK TEST

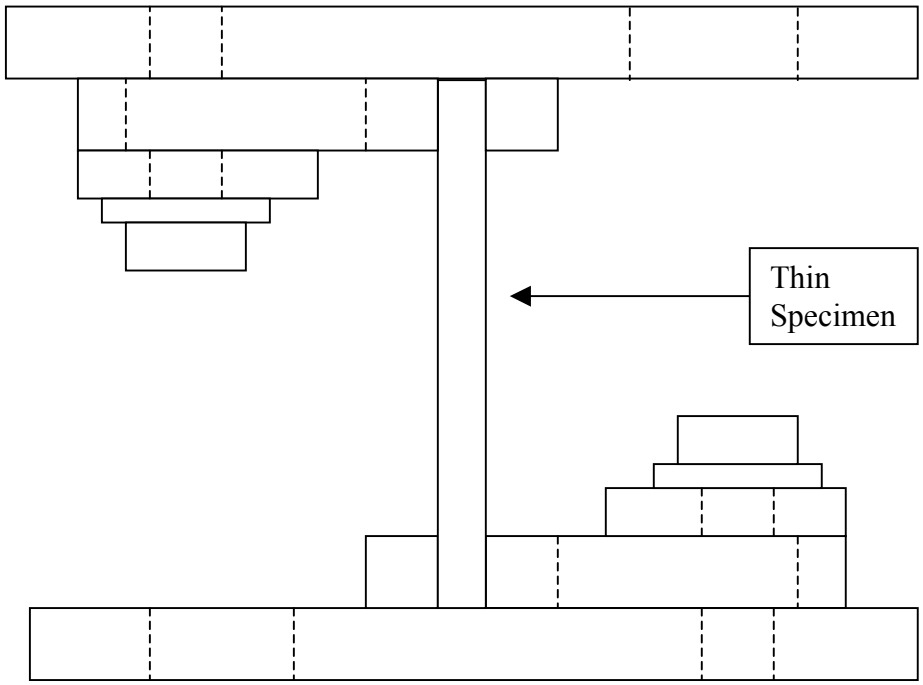


FIGURE 32. SIDE VIEW OF NASA SHORT BLOCK WITH A THIN SPECIMEN

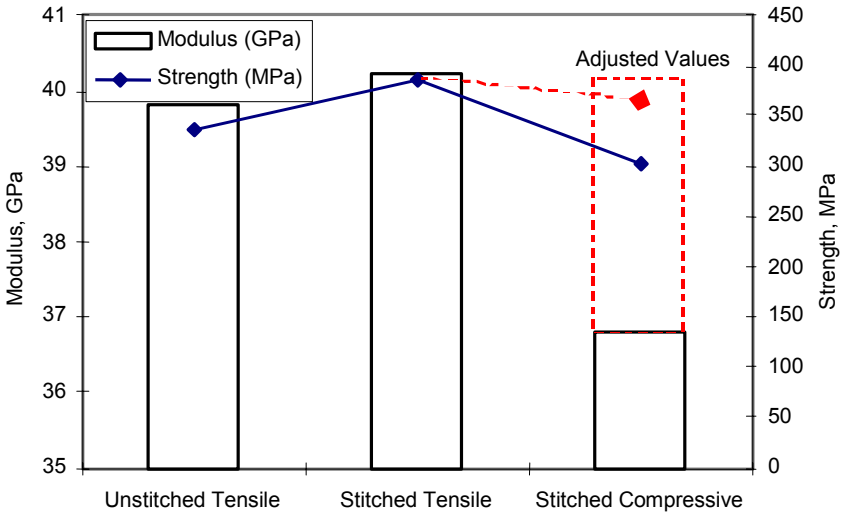


FIGURE 33. AVERAGE TENSILE STRENGTHS AND MODULI OF UNSTITCHED AND STITCHED COUPONS

The measured tensile modulus of the stitched laminate agrees fairly well with the predicted value listed in table 5. However, the measured tensile modulus of unstitched laminate is lower than predicted.

9. COMPRESSION BEHAVIOR OF STIFFENED PANELS.

The test matrix for static compression tests of unstitched and stitched panels is shown in table 16. The effects of different types of impact damage, i.e., clearly visible flange damage (CVFD) and clearly visible stiffener damage (CVSD), on the compression behavior of stiffened panels were investigated.

TABLE 16. PANEL IDENTIFICATION FOR STATIC TESTS

Stitched Panels			Unstitched Panels		
Test No.	Specimen Designation	Impact Damage	Test No.	Specimen Designation	Impact Damage
1	P1a	None	1	SP2b	None
2	P2a	None	2	SP5a	None
3	P3b	None	3	SP3a	None
4	P4a	CVFD	4	SP4a	CVFD
5	P5b	CVFD	5	SP5b	CVFD
6	P18b	CVFD	6	SP12b	CVFD
7	P1b	BVFD	7	SP3b	CVSD
8	P3a	CVSD	8	SP1a	CVSD
9	P5a	CVSD	9	SP15a	CVSD
10	P10b	CVSD	10	SP11b	CVSD

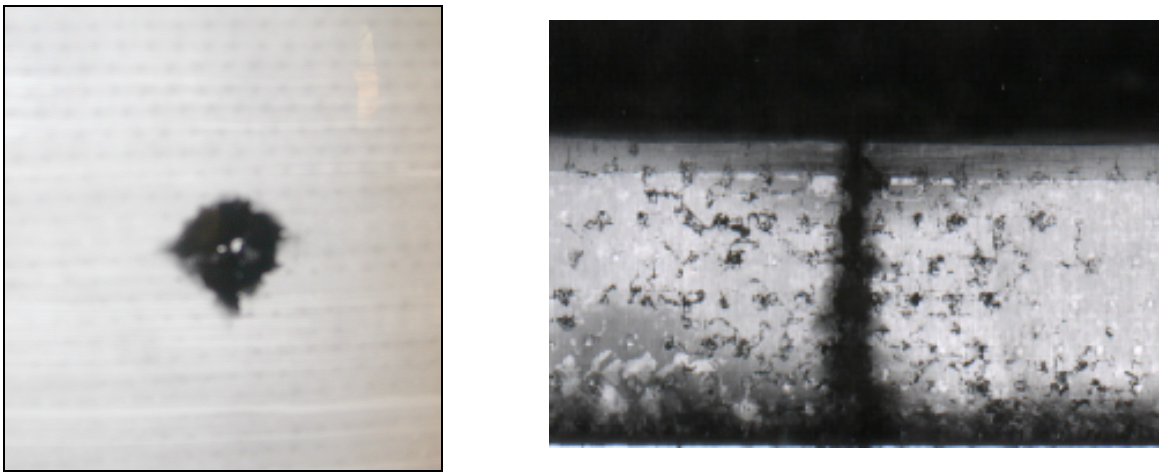
* For stitched panels BVFD, CVFD, and CVSD impact energy levels are 15, 30, and 30 J, respectively.
** For unstitched panels CVFD and CVSD impact energy levels are 15 and 30 J, respectively.

9.1 IMPACT TESTING.

Impact tests were performed according to the SACMA Recommended Test Method for Compression After Impact Properties of Oriented Fiber Resin Composites, SRM 2-88 [33]. Impact loading was applied using a drop weight on a Dynatup 8250 drop-weight impact testing machine, with a 4.3-kg indenter having a 12.7-mm-diameter tup.

For impact and subsequent compression testing, the panel was held between top and bottom end plates, which have a groove. The panel was inserted into the grooves of the end plates and secured using Cerrobend® alloy, having a melting temperature of 70°C. For each panel, 350 g of Cerrobend® was melted in a ceramic cup at 100°C for 15 min. inside an oven. The top and bottom plates were also placed inside the oven, and the molten alloy was poured into the grooves in the heated plates. The plates were then removed from the oven, placed on a Plexiglas support for better alignment, and the composite panel was slipped into the grooves. The entire assembly was then allowed to cool down in ambient conditions.

The panel assembly was placed on the base of the Dynatup for impact testing with the end plates providing support [34-37]. In both cases, the impact points were on the flat skin side of the panel. Typical x-ray radiographs of impact-damaged areas are shown in figure 34.



(a) (b)

FIGURE 34. X-RAY PHOTOGRAPHS OF DROP WEIGHT IMPACT AREA IN A STITCHED PANEL (a) CVFD DAMAGE AND (b) CVSD DAMAGE

For static compression tests, the energy of impact over a flange was 15 J, and another set was impacted at 30 J. Impact energy of 15 J was enough to achieve a clearly visible damage in the unstitched panel. However, the damage observed on one stitched panel at 15 J was barely visible. The stitched panels absorbed greater impact energy than the unstitched panel. At an impact energy of 30 J, both types of panel resulted in near penetration. Therefore, the impact energy was increased to 30 J in order to generate a clearly visible damage on the flange of the unstitched and stitched panels for fatigue tests and subsequent static tests. As for impact over the stiffener, 30 J was used for static and fatigue panels.

9.2 COMPRESSION TESTING.

Static compression tests were performed on a 500-kN Instron test frame at a displacement rate of 1.27 mm/min. The top plate of the panel assembly was secured onto a T-shaped platen with four socket cap screws. The positions of the screws ensured alignment of the centroid of the panel with the loading axis. The T-platen was held in a hydraulic grip. Securing the assembly to the top hydraulic grip prevented the upper half of the assembly from falling once the panel failed. The bottom plate of the assembly was not secured to the T platen. Rather, two aluminum guide rails were used to minimize lateral displacement between the bottom plate and the T-platen as shown in figure 35. The resulting gage length of the panel was approximately 25.0 cm.

Omega 900 series data acquisition modules were used to record strains, lateral displacement, top displacement, and applied load. Strain gages were placed back to back at the center of the panel to capture a bifurcation point during loading. Another strain gage was placed on the stiffener to monitor the stiffener strain. In addition to measuring the local strains, a shadow moiré fringe technique was implemented to observe the global deformation and mode shapes during loading as shown in figure 36. The mode shape of undamaged and CVFD panels were full-sine shape but for CVSD panels, it was half-sine shape or full-sine shape depending on the damaged stiffener to prevent buckling.

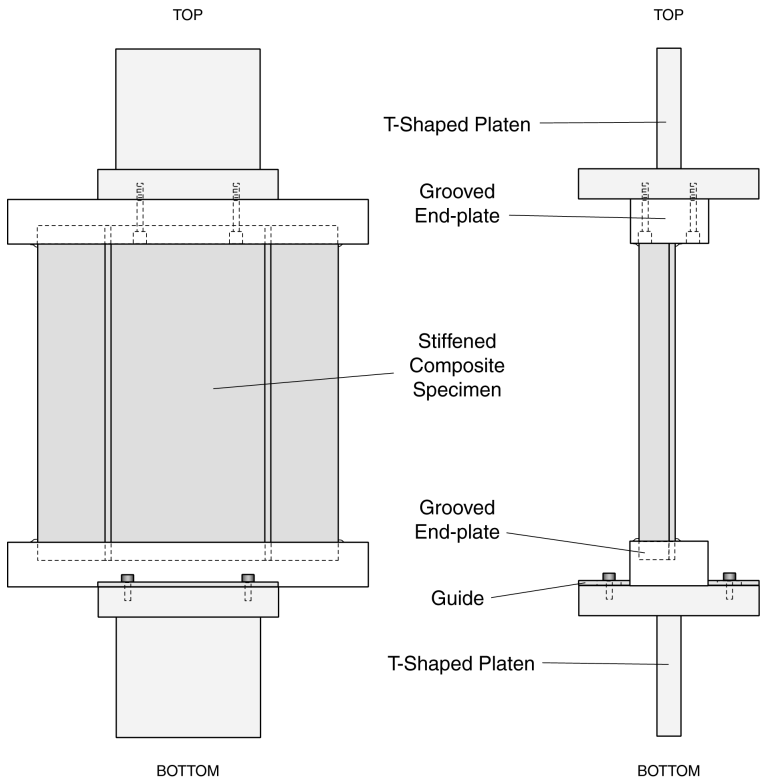


FIGURE 35. A SCHEMATIC OF TEST PANEL ASSEMBLY

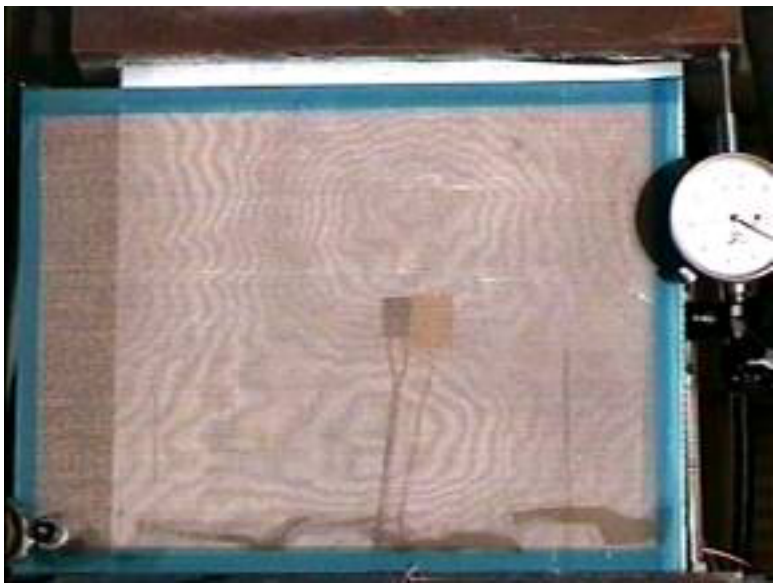


FIGURE 36. SHADOW MOIRÉ OF A STIFFENED PANEL

9.3 UNSTITCHED PANELS.

As shown in figure 37, the average buckling strengths of undamaged, CVFD, and CVSD panels are 83.7, 69.2, and 69.3 MPa, respectively. On average, undamaged panels buckled at a strain value of 2170 µstrain, whereas both the CVFD and CVSD panels buckled around 2000 µstrain. However, a wider experimental scatter was observed for CVSD panels due to differences in stiffener damages incurred on panels. Even a damaged stiffener may prevent buckling, but at higher stress levels, it fails prematurely. A monotonic decrease in failure strength was observed from undamaged to CVFD panels and from CVFD to CVSD panels, although the CVSD panels had a wider experimental scatter for failure strengths, as in buckling strengths. The reported values for the average failure strengths of undamaged, CVFD, and CVSD panels were 155.7, 136.9, and 107.2 MPa. Accordingly, the average failure strains for undamaged, CVFD, and CVSD panels were 4050, 3900, and 2850 µstrain, respectively. As expected, the initial compressive modulus remains fairly consistent with values of 36.5, 34.7, and 35.8 GPa for undamaged, CVFD, and CVSD, respectively. A slightly higher CVSD modulus versus CVFD modulus is due to two CVSD panels that had less severe damage than the other.

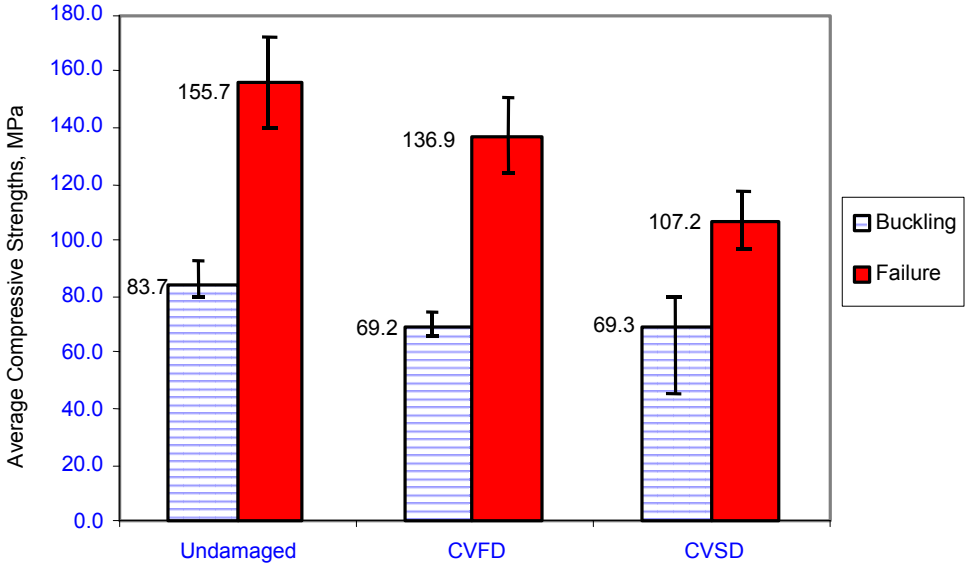


FIGURE 37. AVERAGE BUCKLING STRENGTHS OF UNSTITCHED PANELS

It is interesting that, on average, the failure-to-buckling strength ratio of 2 was maintained for both CVFD and undamaged panels, whereas the average failure-to-buckling strength ratio of CVSD panels was reduced to 1.55. Furthermore, a higher buckling strength leads to a higher failure strength value for all panels tested. This indicates that the buckling strength provides a critical indicator of the condition and performance of the panels. The exact influence of manufactured quality to buckling strength is not yet fully understood, but it does not seem to affect the buckling strength as greatly as the failure strength. As observed experimentally for both undamaged and damaged panels, a severe manufactured defect, such as a visible groove on the stiffener, lead to premature failure for both undamaged and damaged panels alike (see table 17) but the defect did not seem to influence the buckling strength.

TABLE 17. MANUFACTURING DEFECTS, IMPACT DAMAGES, AND FAILURE MODES OF UNSTITCHED PANELS

Test No.	Specimen Designation	Impact Location	Impact Damage	Manufacturing Defect	Failure Mode
1	P1a	None	None	No groove	Delamination and stiffener separation
2	P2a	None	None	No groove	Delamination
3	P3b	None	None	Groove behind left stiffener	Crack extension from grooved sided stiffener
4	P4a	Left side of right stiffener	Dent, broken fiber	Groove behind left stiffener	Crack extension from grooved sided stiffener
5	P5b	Left side of right stiffener	Dent, broken fiber	No groove	Crack extension from dented site
6	P18b	Left side of right stiffener	Dent, broken fiber	No groove	Crack extension from dented site
7	P1b	On right side stiffener	Stiffener damage	No groove	Crack extension from damaged stiffener
8	P3a	On left side of stiffener	Stiffener damage	Groove behind right stiffener	Crack extension from damaged stiffener
9	P5a	On right side of stiffener	Stiffener damage	No groove	Crack extension from both stiffener
10	P10b	On right side of stiffener	Stiffener damage	No groove	Crack extension from damaged stiffener

For those CVFD panels without defects, the crack moved perpendicular to the loading direction from the damaged location, and once the advancing crack reached the nearest stiffener, the panel failure was imminent. As observed, the complete failure occurred when the nearest stiffener fractured under compressive direct loading. For CVSD panels, the failure-mitigating cracks initiated from the damaged site toward the adjacent flange and failure occurred when the other stiffener fractured near the adjacent plane of the damaged stiffener. A factor that uniquely influences the failure strengths of undamaged panels devoid of defects is the stiffener separation and delamination that was observed experimentally. The initiation of the failure occurred at approximately one-quarter distance from the top of the panel.

9.4 STITCHED PANELS.

As shown in figure 38, the average buckling strengths of undamaged, CVFD, and CVSD panels are 87.0, 75.3, and 70.0 MPa, respectively. The results on stitched panels are more consistent than those on unstitched panels with less degree of experimental scatter for both buckling and failure strengths. A part of the reason for the consistency is due to higher quality of stitched panels. In that, all of the stitched panels received good to very good without any major manufactured defect such as a severe groove on the stiffener. On average, the undamaged panels buckled at a strain value of 2080 μstrain, whereas both the CVFD and CVSD panels buckled around 1850 and 1650 μstrain, respectively. Both buckling strengths and strains show a monotonic decrease. A monotonic decrease in failure strength is also observed from undamaged to CVFD panels and from CVFD to CVSD panels. The reported values for the average failure strengths of undamaged, CVFD, and CVSD panels are 177.4, 162.7, and 115.4 MPa.

Accordingly, the average failure strains for undamaged and CVFD panels are around 4000 μstrain, whereas the average failure strain for a CVSD panel is 3400 μstrain. As expected, the initial compressive moduli remain fairly consistent with average values of 40.0 GPa for undamaged, CVFD, and CVSD panels. Stitching is found to slightly increase both the overall panel thickness and the panel modulus. It was not clear why stitching would yield a higher modulus in stiffened panels when it was not observed in flat panels. Nevertheless, the result would be a slightly higher buckling strength for stitched panels, which is in agreement with the experimental data.

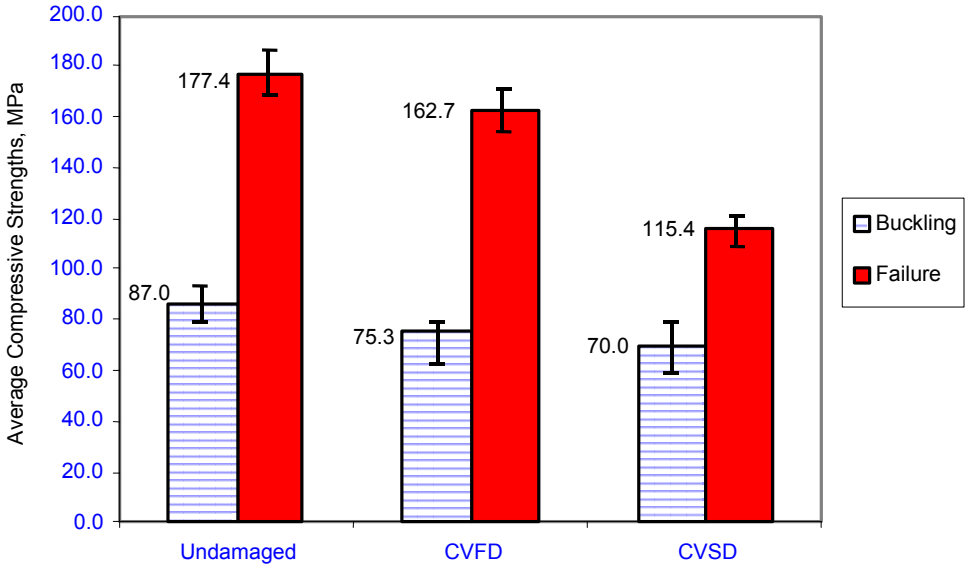


FIGURE 38. AVERAGE BUCKLING STRENGTHS OF STITCHED PANELS

As in the unstitched panels, the stitched panels' failure-to-buckling strength ratio of 2 was maintained for both CVFD and undamaged panels, whereas the average failure-to-buckling strength ratio of CVSD is reduced to 1.67. Furthermore, a similar trend of higher buckling strength leading to a higher failure strength value for all panels tested was observed. The buckling strength provides a critical indicator of the condition and performance of stitched and unstitched panels. As observed experimentally, a groove defect on one undamaged panel did not serve as a failure site, see table 18. It was inferred that stitching prevents the cracks to initiate around the defect site. However, the stitched panel buckling strengths compared to the unstitched panels are similar, as shown in figure 39.

TABLE 18. MANUFACTURING DEFECTS, IMPACT DAMAGES, AND FAILURE MODES OF STITCHED PANELS

No.	Specimen Designation	Impact Location	Impact Damage	Manufacturing Defect	Failure Mode
1	SP2b	None	None	No groove	Stiffeners broken at failure
2	SP5a	None	None	Groove behind the left stiffener	Stiffeners broken at failure (away from groove)
3	SP3a	None	None	Rough skin texture	Stiffeners broken at failure
4	SP4a	Right side of left stiffener	Dent, broken fiber	No groove	Impacted region stiffener broken
5	SP5b	Right side of left stiffener	Dent, broken fiber	No groove	Impacted region stiffener broken
6	SP12b	Right side of left stiffener	Dent, broken fiber	No groove	Impacted region stiffener broken
7	SP3b	Right side of left stiffener	Dent	No groove	Stiffeners broken at failure
8	SP1a	On right side of stiffener	Stiffener damage	No groove	Crack extended from impacted stiffener
9	SP15a	On right side of stiffener	Stiffener damage	No groove	Crack extended from impacted stiffener
10	SP11b	On right side of stiffener	Stiffener damage	No groove	Crack extended from impacted stiffener

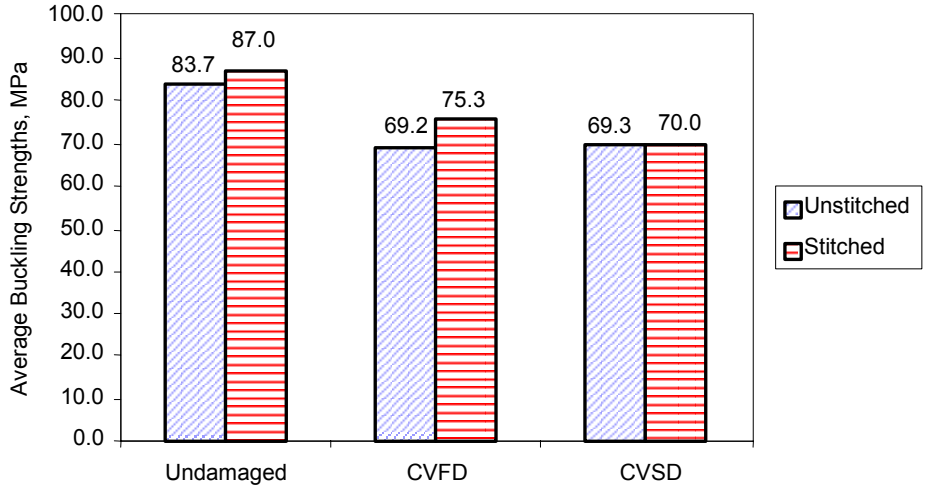


FIGURE 39. COMPARISON OF BUCKLING STRENGTHS BETWEEN UNSTITCHED AND STITCHED PANELS

For those stitched CVFD panels, the crack moved perpendicular to the loading direction from the damaged location, and once the advancing crack reached the nearest stiffener, panel failure was imminent. As observed, the complete failure occurred when the nearest stiffener fractured under compressive direct loading. However, a 4.5% increase in the failure strength was observed

compared to the unstitched CVFD panels, as shown in figure 40. For stitched CVSD panels, the failure-mitigating cracks initiated from the damaged site toward the adjacent flange and failure occurred when the other stiffener fractured near the adjacent plane of the damaged stiffener. However, little beneficial effect was observed, as a result of the stitching, for stiffener-impacted panels. The undamaged stitched panels, did not fail by stiffener separation and/or delamination as was the case for unstitched panels. As a result, an average increase of 13.9% in failure strength was experimentally determined.

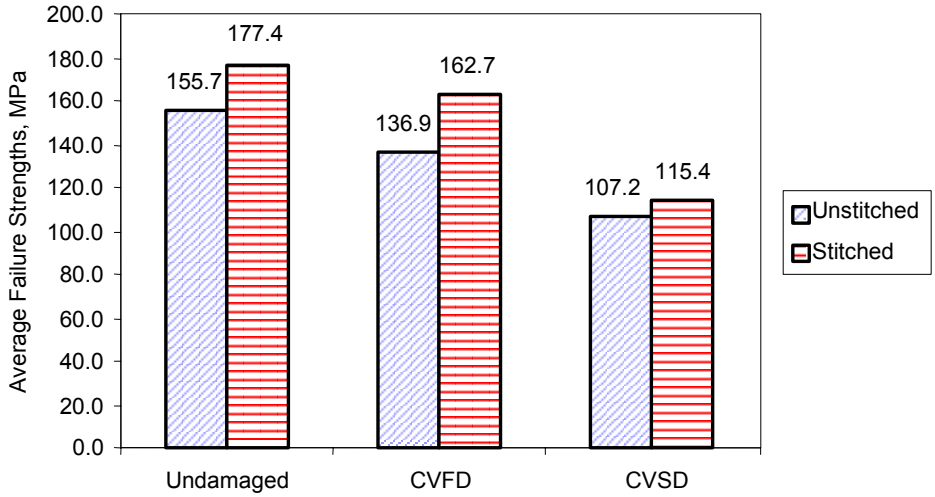


FIGURE 40. COMPARISON OF FAILURE STRENGTHS BETWEEN UNSTITCHED AND STITCHED PANELS

The benefit from stitching was significant for undamaged and CVFD panels. The prevention of flange separation by stitching was believed to be responsible for such high-damage tolerance. For the CVSD panel, the lack of difference indicates that stiffener damage is more dominant than flange separation and that stitching may even promote stiffener damage by preventing flange separation.

As a comparison, the FEM predictions and experimental results are shown in figures 41 and 42. The buckling strengths are in fair agreement with the experimental results, owing to similar moduli values and geometry for both stitched and unstitched panels tested under this investigation. However, the buckling strengths of CVSD is underestimated due to a worst-case scenario that was modeled using a finite element approach compared to the experiments where impacted stiffeners are still effective in preventing buckling. The predictions for failure strengths are shown to overestimate the experimental results except for worst-case scenario for the CVSD model.

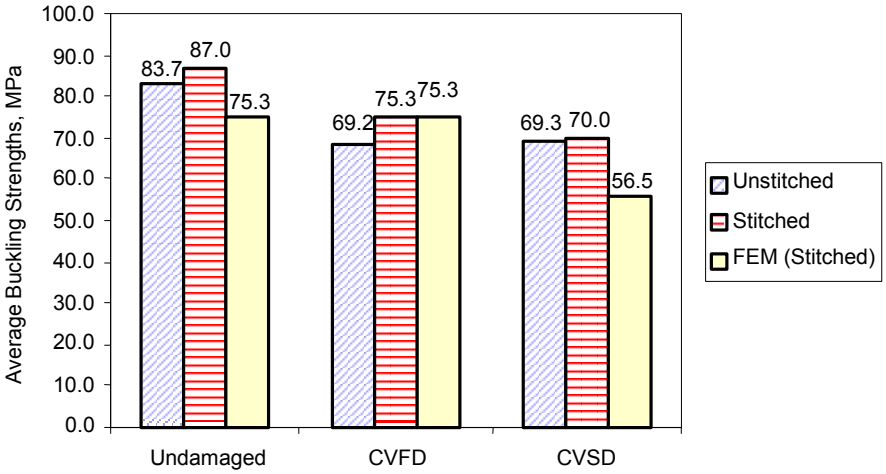


FIGURE 41. ANALYTICAL VERSUS EXPERIMENTAL BUCKLING STRENGTHS

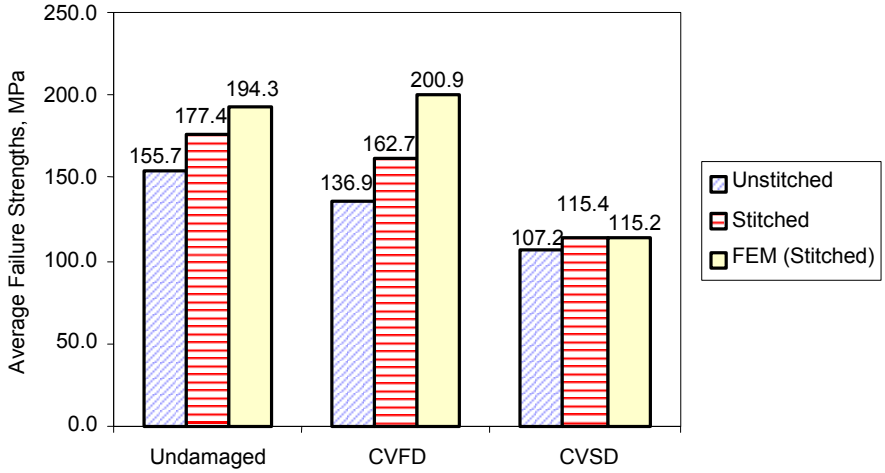


FIGURE 42. ANALYTICAL VERSUS EXPERIMENTAL FAILURE STRENGTHS

10. FATIGUE BEHAVIOR OF STIFFENED PANELS.

The effectiveness of stitching in preventing damage growth in fatigue was investigated using CVFD and CVSD panels. All damage was induced by 30-J impact and was near penetration for both unstitched and stitched panels. Both constant amplitude (C-A) and spectrum fatigue tests were conducted.

10.1 EXPERIMENTAL PROCEDURE.

Compression fatigue tests were performed on a 500-kN Instron test frame at a frequency ranging from 0.05 to 1.2 Hz depending on the load levels. The same fixtures and gripping method that were used in the static compression tests were used in the compression fatigue tests.

The modified Transport WIng Standard Test (TWIST) [38] was used for the spectrum fatigue (see table 19). Each block consists of ten alternating loads ranging from 0.222 to 1.6 times the flight mean load, representing 4,000 flights. A repetition of ten blocks represents a life cycle or 40,000 flights. It is noted that the two lowest load levels have been deleted since they were found to have negligible effect on coupon specimens in an earlier study [38]. Loading is applied in the decreasing order of magnitude. Because of the testing difficulty, any excursion into tension was truncated.

TABLE 19. MODIFIED TWIST SPECTRUM

	Alternating Load Times Flight Mean Load									
	1.6	1.5	1.3	1.1	0.99	0.84	0.68	0.53	0.37*	0.22*
No. of Cycles	1	2	5	18	52	152	800	4170	34800	358665

* These two load levels were deleted.

Constant-amplitude fatigue tests were performed at each of the five highest stress levels of the TWIST spectrum. These nominal stress levels, shown in table 20, represent flight mean stresses of 46.5 MPa and 36.4 MPa for unstitched panels with CVFD and CVSD damages, respectively, and flight mean stresses of 55.33 MPa and 39.2 MPa for stitched panels with CVFD and CVSD damages, respectively. The fatigue stress ratio R was kept at infinity.

TABLE 20. NOMINAL STRESS LEVELS FOR CONSTANT-AMPLITUDE FATIGUE TESTS

Unstitched CVFD		Stitched CVFD	
Load Level	Max. Comp. Stress (MPa)	Load Level	Max Comp. Stress (MPa)
1	120.9	1	144.1
2	116.3	2	138.5
3	107.0	3	127.4
4	97.7	4	116.3
5	92.5	5	110.2
Unstitched CVSD		Stitched CVSD	
Load Level	Max Comp. Stress (MPa)	Load Level	Max. Comp. Stress (MPa)
1	94.6	1	102.2
2	91.0	2	98.3
3	83.7	3	90.4
4	76.4	4	80.5
5	72.4	5	78.2

10.2 UNSTITCHED PANELS.

10.2.1 Constant-Amplitude Fatigue.

- CVFD Panels

  The test results are shown in table 21 and figure 43. The actual stresses are slightly different from those nominal values of table 21 because of the slight variations in the cross-sectional area. In all tests, damage emanated from the impact site and propagated toward the stiffener, ultimately leading to final failure, see figure 44.

TABLE 21. CONSTANT-AMPLITUDE FATIGUE RESULTS (Unstitched CVFD panels)

Specimen ID	Max. Comp. Stress (MPa)	Loading Frequency (Hz)	Number of Cycles to Failure	Causes of Failure
P6a	120.9	0.5	1395	Damage-induced stiffener failure
P14a	120.2	0.5	1275	Damage-induced stiffener failure
P7b	116.3	1.0	8160	Damage-induced stiffener failure
P9b	111.3	0.5	392	Damage-induced stiffener failure
P11a	107.0	1.0	843	Damage-induced stiffener failure
P11b	105.7	1.0	3064	Damage-induced stiffener failure
P4b	97.5	0.5	129	Damage-induced stiffener failure
P6b	97.7	1.0	8860	Damage-induced stiffener failure
P8a	92.4	1.0	3766	Damage-induced stiffener failure
P8b	92.3	1.0	36052	Damage-induced stiffener failure

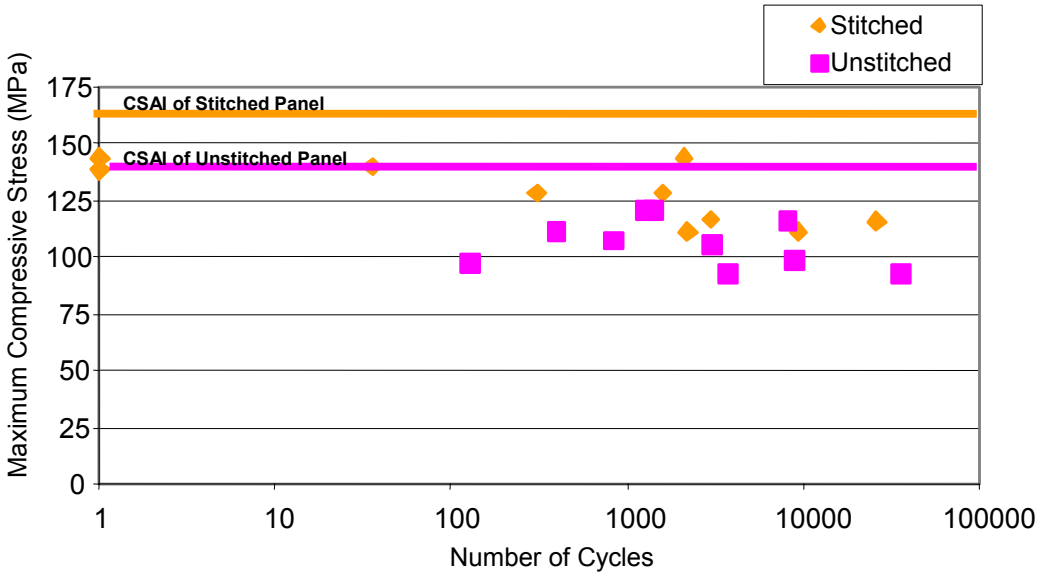


FIGURE 43. CONSTANT-AMPLITUDE FATIGUE LIVES OF STITCHED AND UNSTITCHED CVFD PANELS

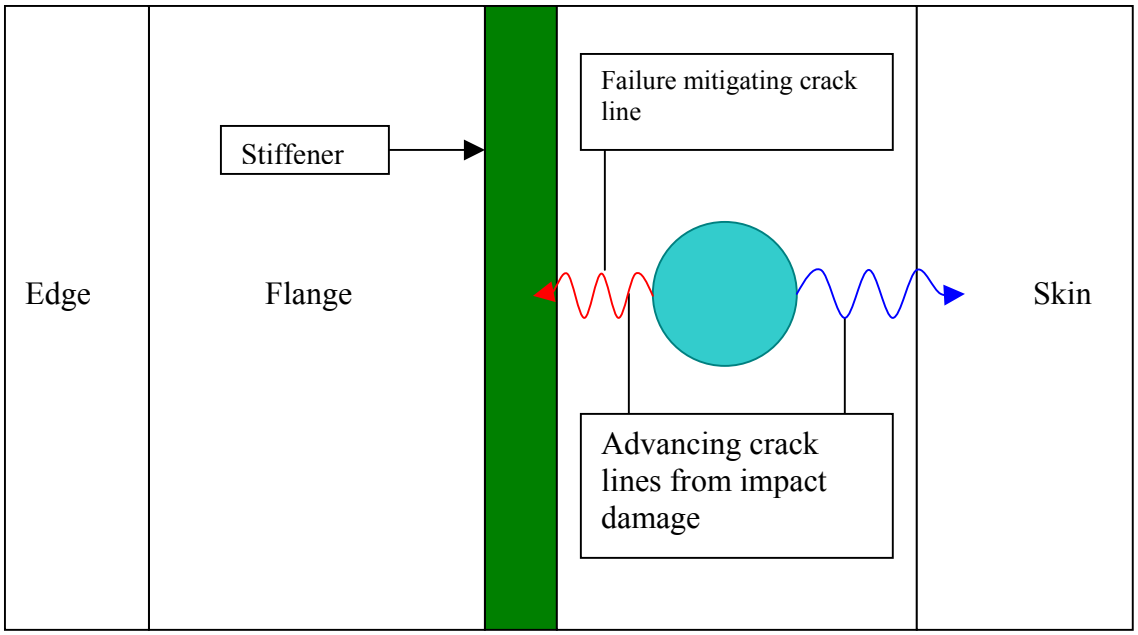


FIGURE 44. ADVANCING CRACK LINES IN CVFD PANEL

- CVSD Panels

  The test results are shown in table 22 and figure 45. Panels 9a and 10b failed rather prematurely on the first and third cycle, respectively. At higher stress levels, the combined effect of mode shape and delamination/stiffener separation may have caused premature failure of the panels.

TABLE 22. CONSTANT-AMPLITUDE FATIGUE RESULTS (Unstitched CVSD panels)

Specimen ID	Max. Comp. Stress (MPa)	Loading frequency (Hz)	Number of Cycles to Failure	Causes of Failure
P9a	94.1	0.1	1	Single half-sine mode
P10b	97.5	0.1	3	Single half-sine mode
P15b	91.7	1.0	30	Damaged stiffener failure
P12b	91.2	1.0	106	Damaged stiffener failure
P15a	84.0	1.0	5748	Damaged stiffener failure
P13b	83.7	1.0	135	Damaged stiffener failure
P7a	76.4	1.0	33113	Damaged stiffener failure
P18a	74.4	1.0	30742	Damaged stiffener failure
P12a	72.4	1.2	5505	Damaged stiffener failure
P14b	73.8	1.2	37350	Damaged stiffener failure

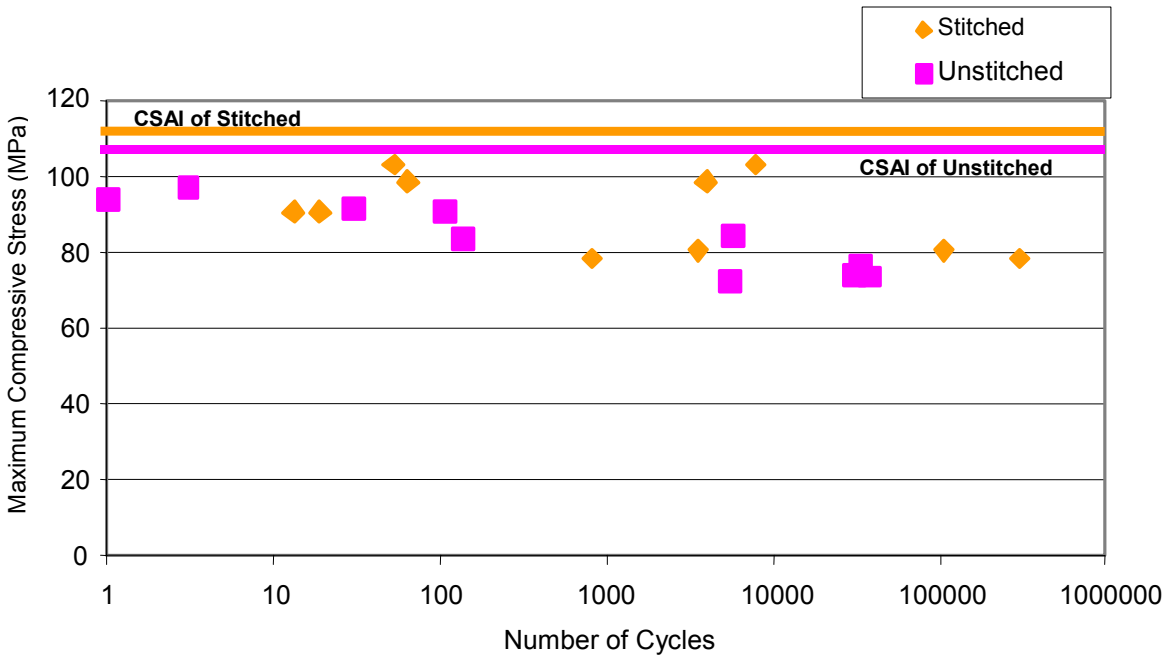


FIGURE 45. CONSTANT-AMPLITUDE FATIGUE LIVES OF STITCHED AND UNSTITCHED CVSD PANELS

10.2.2 Spectrum Fatigue.

- CVFD Panels

  All panels survived ten blocks, which represent one life cycle (see table 23). Flight mean load (FML) is 34% CSAI, which corresponds to a flight mean stress level of 46.5 MPa with maximum stress of 120.9 MPa and with tension loads truncated. Their residual strengths are fairly consistent at an average of 146.7 MPa. This residual strength is within the experimental scatter values of CSAI of CVFD panels.

TABLE 23. SPECTRUM FATIGUE RESULTS (Unstitched CVFD panels)

Specimen ID	Number of Blocks Completed	Load Level at Failure	Damage Growth	Residual Compressive Strength (MPa)
P16b	10	No failure	Damage growth into stiffener	147.3
P17a	10	No failure	Damage growth into stiffener	145.1
P17b	10	No failure	Damage growth into stiffener	147.7

- CVSD Panels

  Two panels, panels 13a and 16a, failed at the tenth and third block, respectively (see table 24). FML is 34% CSAI, which corresponds to a flight mean stress level of 36.4 MPa with maximum stress of 94.6 MPa and with tension loads truncated. The residual strength is comparable to the CSAI of CVSD panels.

TABLE 24. SPECTRUM FATIGUE RESULTS (Unstitched CVSD panels)

Specimen ID	Number of Blocks Completed	Load Level at Failure	Damage Growth	Residual Compressive Strength (MPa)
P2b	10	No Failure	Damage growth into skin	118.7
P13a	10	4th	Damage growth into skin	Failure
P16a	3	1st	Damage growth into skin	Failure

The spectrum fatigue results are consistent with constant-amplitude fatigue results. The spectrum fatigue is less damaging than constant-amplitude fatigue, however, high loads in both regimes cause failure.

10.3 STITCHED PANELS.

10.3.1 Constant-Amplitude Fatigue.

- CVFD Panels

  The test results are shown in table 25 and figure 43. Stitched panels are seen to have higher fatigue strengths compared than unstitched panels.

TABLE 25. CONSTANT-AMPLITUDE FATIGUE RESULTS (Stitched CVFD panels)

Specimen ID	Max. Comp. Stress (MPa)	Loading frequency (Hz)	Number of Cycles to Failure	Causes of Failure
SP6a	143.4	0.05	1	Premature failure
SP12a	143.4	0.05	2111	Damage-induced stiffener failure
SP7a	138.3	0.05	1	Premature failure
SP8a	139.4	0.10	35	Damage-induced stiffener failure
SP9a	127.6	0.20	306	Damage-induced stiffener failure
SP7b	127.6	0.20	1606	Impact caused stiffener damage
SP9b	116.5	0.30	3005	Damage-induced stiffener failure
SP8b	115.5	0.30	26273	Damage-induced stiffener failure
SP10a	110.9	0.30	2200	Defective panel, not fully resin infiltrated
SP11a	110.9	0.30	9474	Damage-induced stiffener failure

Panels SP6a and SP7a failed prematurely at the first cycle. In most panels, two cracks grew normal to the loading direction from the damage site. These cracks propagated intermittently such that they extended during one load cycle but then stopped for several cycles. Naturally, these cracks grew faster at higher stresses. The stiffener with the damaged flange arrested the crack from getting closer to it, and the crack on the other side seemed to stop as well. It took most of the fatigue cycles for the crack to extend into

the stiffener, and once the crack entered the stiffener, the panel failed within a few cycles. The crack growth behavior is shown quantitatively in figure 46.

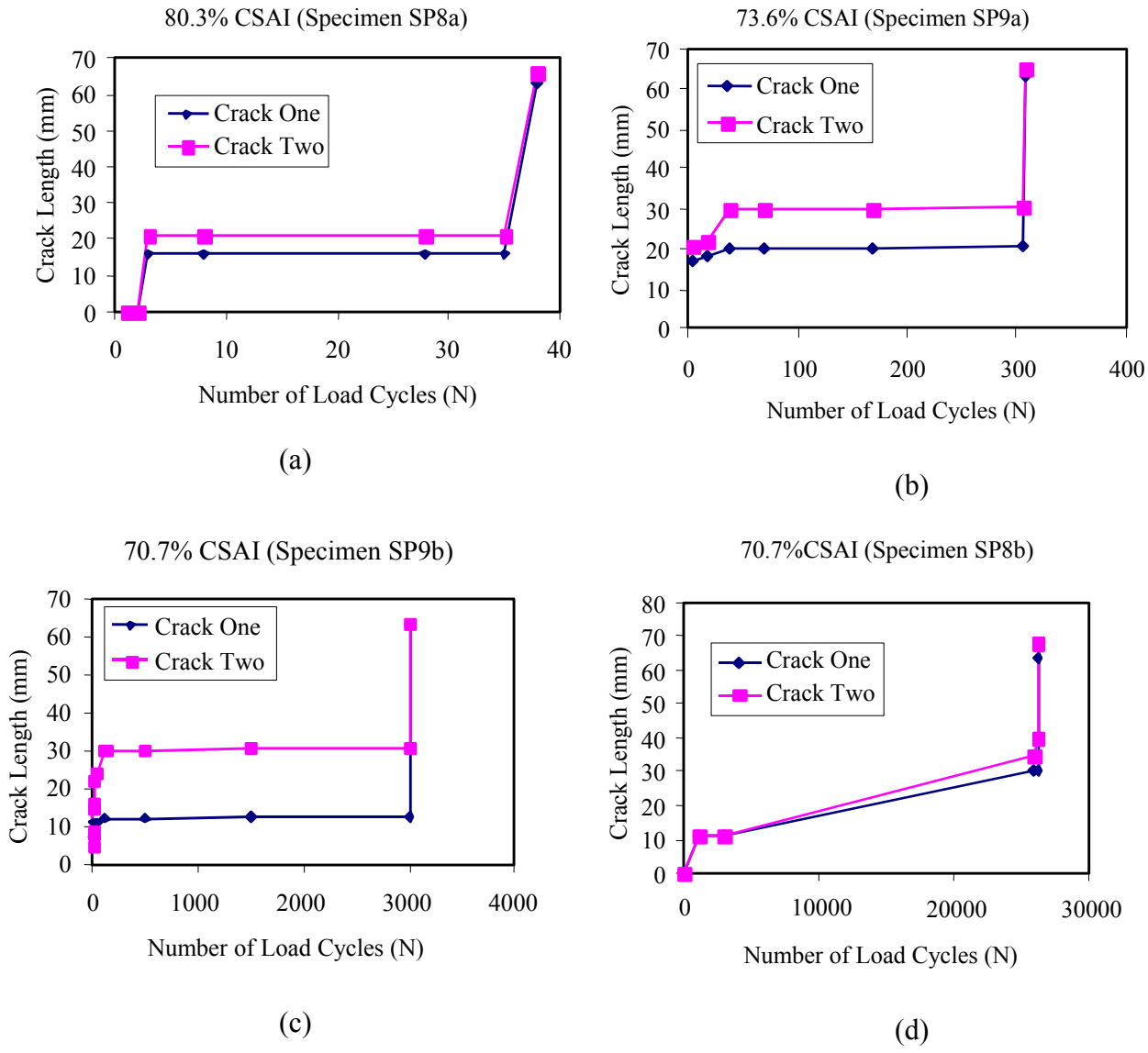


FIGURE 46. CONSTANT FATIGUE CRACK GROWTH DATA FOR CVFD PANELS

In panel SP7b, the impact did not generate a CVFD but a CVSD. Nevertheless, it did not fail prematurely. Panel SP10a was of poor quality because of vacuum leak during manufacturing. Therefore, its premature failure was not surprising.

- CVSD Panels

  X-ray radiographs of typical CVSD damage are shown in figure 47. There was little variation from panel to panel in the extent of damage. Prior to final failure, the crack in the stiffener was seen to open and close during cycling.

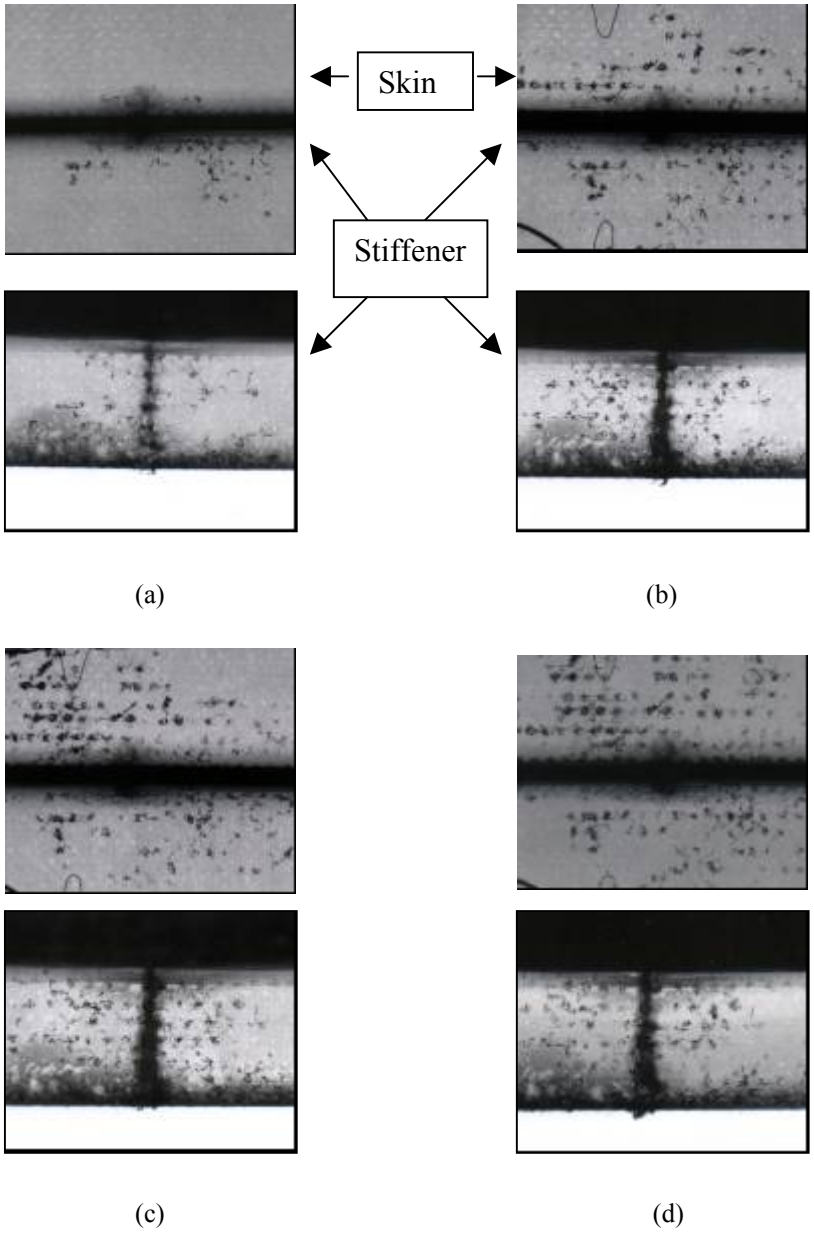


FIGURE 47. X-RAY PHOTOGRAPHS OF STIFFENER AND SKIN OF SPECIMEN SP16a (a) AFTER IMPACT, (b) AFTER TWO BLOCKS OF SPECTRUM FATIGUE, (c) AFTER FIVE BLOCKS, AND (d) AFTER TEN BLOCKS

The test results are shown table 26 and in figure 45. As in the CVFD panels, stitching improves fatigue resistance only marginally.

TABLE 26. CONSTANT-AMPLITUDE FATIGUE RESULTS (Stitched CVSD panels)

Specimen ID	Max. Comp. Stress (MPa)	Loading Frequency (Hz)	Number of Cycles to Failure	Causes of Failure
SP14A	102.9	0.8	53	Damaged stiffener broke quickly
SP17a	102.9	0.8	7900	Damaged stiffener broke slowly
SP13b	98.4	0.8	3930	Damaged stiffener broke slowly
SP14b	98.4	0.8	64	Damaged stiffener broke quickly
SP16b	90.4	1.0	13	Damaged stiffener broke quickly
SP19b	90.4	1.0	19	Damaged stiffener broke quickly
SP19a	80.5	1.0	Stopped at 105081	Damaged stiffener broke slowly
SP18a	80.5	1.0	3528	Damaged stiffener broke quickly
SP18b	78.6	1.2	814	Damaged stiffener broke quickly
SP13a	78.6	1.2	Stopped at 300300	Damaged stiffener broke slowly

10.3.2 Spectrum Fatigue.

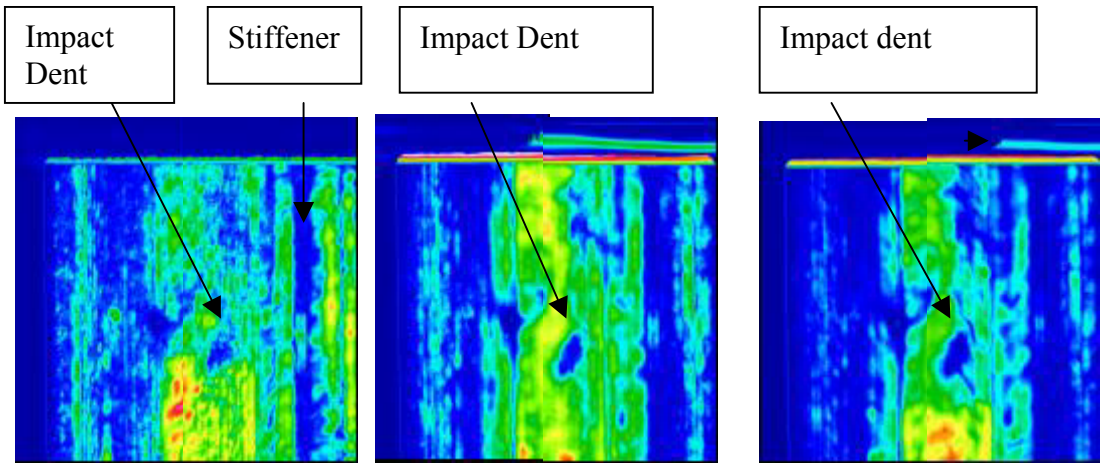
- CVFD Panels

Panel SP6b failed at the first load of the tenth block, (see table 27). FML is 34% CSAI, which corresponds to a flight mean stress level of 55.3 MPa with maximum stress of 144.1 MPa and with tension truncated. In panel SP10b, the left and right stiffeners failed one after the other at the first load of sixteenth block with a loud sound. The panel still continued to bear the load until the seventh load cycle and then failed completely. The longest surviving panel was PS11b: it survived 20 blocks, at which time testing was stopped. It should be remembered that 10 blocks constitutes one lifetime. Hence, all panels survived one lifetime.

TABLE 27. SPECTRUM FATIGUE RESULTS (Stitched CVFD panels)

Specimen ID	Number of Blocks Completed	Load Level at Failure	Damage Assessment	Residual Compressive Strength (MPa)
SP6b	10	1st	Damage growth into stiffener	Failure
SP10b	16	7th	Damage growth into stiffener	Failure
SP11b	20	No failure	Damage growth into stiffener	Residual static strength test not performed

Panel SP11b was scanned ultrasonically at the end of fifth, eighth, and thirteenth block, respectively. However, the C-scan images in figure 48 are rather difficult to interpret.



(a) Fifth Block (b) Eighth Block (c) Thirteenth Block

FIGURE 48. C-SCAN IMAGES OF SPECIMEN SP10b IN SPECTRUM FATIGUE (a) FIFTH, (b) EIGHTH, AND (c) THIRTEENTH BLOCK

- CVSD Panels

Panel SP15b failed during at the third load of the third block, (see table 28). FML is 34% CSAI, which corresponds to a flight mean stress level of 39.2 MPa with maximum stress of 102.2 MPa and with tension truncated. The damage in the stiffener opened and closed during cycling. The global deformation was a half sine wave and this type of deformation appears to lead to early failure.

TABLE 28. SPECTRUM FATIGUE RESULTS (Stitched CVSD panels)

Specimen ID	Number of Blocks Completed	Load Level at Failure	Damage Growth	Residual Compressive Strength (MPa)
SP15b	3	3rd	Damage growth into skin	Failure
SP17b	10	No failure	Damage growth into skin	164.3
SP16a	10	No failure	Damage growth into skin	135.0

Both panels SP17b and SP16a survived ten blocks of loading. These panels exhibited a full sine wave deformation characteristic of undamaged panels. Their residual strengths were measured to be 164.3 and 134.7 MPa, respectively. These residual strengths are much higher than expected and indicate that their impact damages were much less than intended.

X-ray photographs of panel SP16a show a negligible growth of the stiffener damage (see figure 47). This explains why this specimen could survive ten blocks.

As with unstitched panels, spectrum fatigue results show that spectrum fatigue is less damaging than constant-amplitude fatigue. It should be noted that the peak loads that the panels were tested to are much higher than one would expect in service.

10.4 EFFECT OF STITCHING ON CONSTANT-AMPLITUDE FATIGUE.

To quantify the effect of stitching on constant-amplitude fatigue, fatigue stresses were normalized with respect to the appropriate static strengths. The relations between the normalized fatigue stresses and cycles to failure were fit by an equation [39]:

$$S_{normalized} = \alpha N^{\beta}$$

The calculate coefficients, α and β, are listed in table 29. The stitched CVSD panels show the smallest rate of degradation while the unstitched CVSD panels show the largest. However, these numbers should be used with caution because of the large scatter in the data. Although stitching is helpful in both damage tolerance and durability, its benefits appear to be modest for the panels studied in this investigation.

TABLE 29. BEST-FIT PARAMETERS FOR UNSTITCHED AND STITCHED PANELS

	α^*	β	Fatigue Limit Stress** (MPa)
Unstitched CVF	0.8863	-0.018	102
Stitched CVF	0.8838	-0.0213	115
Unstitched CVS	0.9146	-0.0257	70.8
Stitched CVS	0.8622	-0.0149	90.8

*Normalized value using CSAI
**Fatigue limit stress using 10^7 cycles

The fatigue limit stresses of table 29 are high and indicate that fatigue of impact-damaged panels will not be problem for aircraft components in normal service usage where the fatigue loads are much lower.

11. CONCLUSIONS.

The overall objective of this work was to develop the knowledge base required for substantiation of composites structures used in air transportation systems. Specifically, the damage tolerance and durability characteristics of both stitched and unstitched, stiffened panels have been investigated analytically and experimentally. The results are summarized as follows.

- Simple micromechanics models can be used to predict the elastic properties of stitched plain weave laminates as the yarn undulation is small. This model predicts decreases of in-plane properties and increases in out-of-plane properties.

- Analyses using ABAQUS provided reasonable estimates of buckling and postbuckling failure strengths of stiffened panels.

- The first ply failure criterion and the maximum stress failure criterion can be used to estimate final failure of stiffened panels, but becomes unconservative when damage is present.

- Stitching improves impact tolerance, especially when the impact is on a flange area. Such improvement was not obvious in the case of stiffener impact. Stiffener damage competes with stiffener separation in reducing buckling and failure strengths.

- Stitching improves postimpact fatigue performance. It serves as a barrier to the damage growth. However, its benefits are modest.

- The global mode of deformation depends on the type of damage. A severe CVSD damage results in a half sine wave deformation, whereas a CVFD damage or no damage induces a full sine wave deformation. The half sine wave deformation accelerates the stiffener damage growth by opening and closing it during cyclic loading. When this occurs, the damage growth is accelerated.

12. REFERENCES.

1. Dow, M.B. and D.L. Smith, "Damage Tolerant Composite Materials Produced by Stitching Carbon Fibers," *Proceedings of 21st International SAMPE Technical Conference*, 1989, pp. 595-605.

2. Dow, M.B. and H.B. Dexter, "Development of Stitched, Braided and Woven Composite Structures in the ACT Program and at Langley Research Center (1985 to 1997); Summary and Bibliography," NASA/TP-97-206234, November 1997.

3. Dexter, H.B. and J.G. Funk, "Impact Resistance and Interlaminar Fracture Toughness of Through-The-Thickness Reinforced Graphite Epoxy," *27th Conference on Structures, Structural Mechanics and Materials*, May 1989, pp. 700-709.

4. Pelstring, R. M. and R.C. Madan, "Stitching to Improve Damage Tolerance of Composites," *34th International SAMPE Symposium*, May 1989, pp. 1519-1528.

5. Sharma, S.K. and B.V. Sankar, "Effect of Stitching on Impact and Interlaminar Properties of Graphite/Epoxy Laminates," *Journal of Thermoplastic Composite Materials*, 1997, **10**: pp. 241-253.

6. Sharma, S.K. and B.V. Sankar, "Sublaminate Buckling and Compression Strength of Stitched Uniweave Graphite/Epoxy Laminates," *Proceedings of the 10th Technical Conference of the American Society for Composites*, 1995, CA, pp. 143-151.

7. Khan, M.Z.S. and A.P. Mouritz, "Fatigue Behavior of Stitched GRP Laminates," *Composites Science and Technology*, 1996, **56**: pp. 695-701.

8. Harris H. et al., "Multiaxial Stitched Perform for RTM Fabrication," *36th International SAMPE Symposium*, April 1991, pp. 521-535.

9. Su, K.B., "Delamination Resistance of Stitched Thermoplastic Matrix Composite Laminates," In *Advances in Thermoplastic Matrix Composite Materials,* ASTM STP 1044, 1989, pp. 279-300.

10. Farley, G.L., "A Mechanism Responsible for Reducing Compression Strength of Through-the-Thickness Reinforced Composite Materials," *Journal of Composite Materials*, 1992, **26** (12): pp. 1784-1795.

11. Farley, G.L. and L.C. Dickinson, "Removal of Surface Loop From Stitched Composites Can Improve Compression and Compression-After-Impact Strengths," *Journal of Reinforced Plastics and Composites*, 1992, **11**: pp. 633-642.

12. Liu, D., "Delamination Resistance in Stitched and Unstitched Composite Plates Subjected to Impact Loading," *Journal of Reinforced Plastics and Composites*, 1990, **9**: pp. 59-69.

13. Moon, D.G., J.M. Kennedy, and M. John, "Post-Impact Fatigue Response of Stitched Composites," *Composite Materials: Fatigue and Fracture (Fifth Volume)*, ASTM STP 1230, 1995, pp. 351-367.

14. Portanova, M.A., C.C. Poe, and J.D. Whitcomb, "Open Hole and Postimpact Compressive Fatigue of Stitched and Unstitched Carbon-Epoxy Composites," *Composite Materials: Testing and Design (Tenth Volume),* ASTM STP 1120, 1992, pp. 37-53.

15. Dransfield, K., C. Baillie, and Y.-W. Mai, "Improving the Delamination Resistance of CFRP by Stitching - A Review," *Composites Science and Technology*, 1994, **50**: pp. 305-317.

16. Starnes Jr., J.H., N.F. Knight Jr., and M. Rouse, "Postbuckling Behavior of Selected Flat Stiffened Graphite-Epoxy Panels Loaded in Compression," *AIAA Journal*, 1998, **23**(8): pp. 344-352.

17. Madan, R.C., "Influence of Low-Velocity Impact on Composite Structures," Composite Materials: Fatigue and Fracture (Third Volume), ASTM STP 1110, T.K. O'Brien, ed., *American Society for Testing and Materials*, Philadelphia, PA, 1991, pp. 457-475.

18. Stevens, K.A., R. Ricci, and G.A.O. Davies, "Buckling and Postbuckling of Composite Structures," *Composites*, 1995, **26**(3): pp. 189-199.

19. Tsai, S.W. and Hahn, H.T., "Introduction to Composite Materials," Technomic Publishing Co., Inc., 1980.

20. Hahn, H.T. and R. Pandey, "A Micromechanics Model for Thermoelastic Properties of Plain Weave Fabric Composites," *Journal of Engineering Materials and Technology*, 1994, **116**: pp. 517-523.

21. Stellbrink, K.K.U, *Micromechanics of Composites*, Hanser Publishers, 1996.

22. Hull, D. and Clyne, T.W., *An Introduction to Composite Materials*, *2nd Edition*, Cambridge University Press, 1996.

23. Mal, A.K., *Deformation of Elastic Solids*, Englewood Cliffs, N.J., 1991.

24. Tsai, S.W., *Composites Design*, *3rd Edition*, Think Composites, 1987.

25. ABAQUS, Theory Manual Version 5.5. Hibbitt, Karlsson and Sorenson, Inc., Rhode Island, USA.

26. Tsai, S.W. and E.M. Wu, "A General Theory of Strength for Anisotropic Materials," *Journal of Composite Materials*, **5**: pp. 58-80.

27. Mouritz, A.P., K.H. Leong, and I. Herszberg, "A Review of the Effect of Stitching on the In-Plane Mechanical Properties of Fibre-Reinforced Polymer Composites," *Composites Part A*, 1997, **28A**: pp. 979-991.

28. Annual Book of ASTM Standards, Vol. 15.03, ASTM 3039/D3039M-95, pp. 106-118.

29. Annual Book of ASTM Standards, Vol. 15.03, ASTM D5687/D5687M-95, pp. 302-317.

30. Portanova, M.A., "Standard Methods for Unnotched Tension Testing of Textile Composites," NASA CR 198264, December 1995.

31. Stuart, M.J., "Failure Compression-Loaded Multidirectional Composite Laminates," *AIAA Journal*, 1989, **27**(9): pp. 1274-1279.

32. MIL-HDBK-17, Composite Materials Handbook.

33. SACMA Recommended Test Method for Compression After Impact Properties of Oriented Fiber-Resin Composites, SRM 2-88.

34. Choi, H.Y. and F.-K. Chang, "A Model for Predicting Damage in Graphite/Epoxy Laminated Composites Resulting from Low-Velocity Point Impact," *Journal of Composite Materials*, 1992, **26** (14): pp. 2134-2169.

35. Jackson, W.C. and M.A. Portanova, "Out of Plane Properties," Mechanics of Textile Composites Conference, NASA Conference Publication 3311 Part 2, October 1995, pp 315-348.

36. Lammerant, L. and I. Verpoest, "The Interaction Between Matrix Cracks and Delaminations During Quasi-Static Impact of Composites," *Composite Science and Technology*, 1994, **51**: pp. 505-516.

37. Portanova, M.A., "Impact Testing of Textile Composite Materials," Mechanics of Textile Composites Conference, NASA Conference Publication 3311 Part 2, October 1992, pp. 391-423.

38. Hahn, H.T. and S.W. Choi, "The Effect of Loading Parameters on Fatigue of Composite Laminates: Part V," FAA William J. Hughes Technical Center, Atlantic City International Airport, NJ, DOT/FAA/AR-01/24, June 2001.

39. Shigley, J.E. and C.R. Mischke, *Mechanical Engineering Design, 5th Edition*, McGraw-Hill, Inc., 1989.

APPENDIX A—ABAQUS INPUT

ABAQUS Input Listing [ABAQUS, User's Manual].

The input file for ABAQUS is structured in ten parts: heading, node listing, imperfection definition, nodal sets, element connectivity, element type, composite orientation, material inputs, analysis type, and output parameters. The heading section contains bookkeeping items such as number of frequency to write and whether or not the input file is to be rewritten on the output file. The nodes are defined from geometrical coordinates during pre-processing stage of the finite element modeling. After the nodal points are defined, the imperfection geometry is defined from a preceding buckling analysis output file called *name*.fil. The initial buckling analysis is listed below. Although not required, it is useful to define the nodal sets such as top, bottom and loading nodes for ease of defining boundary conditions. The *Equation* command is used to constraint the loading node to displace with the other top nodes such that it will displace equally. This is a convenient way of specifying concentrated load values instead of distributed load values.

The *Element* command provides the nodal connectivity that specifies an element type, e.g., an 8-node shell element in the present case. It includes sub-definition such as fiber orientation. Material properties of the element are specified using the *Material* command and its subcommands *Elastic* and *Fail Stress*.

Boundary conditions are imposed using the *Boundary* command. Numbers 1, 2, 3 define the translational, and 4, 5, 6 the rotational degrees of freedom in such a way that a degree of freedom is constrained if the corresponding number appears.

The nonlinear geometric RIKS algorithm is used to solve the equations, and the analysis is completed when the specified number of increments is reached. The other way to abort the program is by specifying the displacement limit, and both control commands are required. Lastly, a various outputs parameter such as strain, stress and displacements are specified to store in the output file. The parts of input file listing is shown below:

BUCKLING ANALYSIS LISTING.

```
*HEADING
*RESTART,WRITE,FREQUENCY=1
*PREPRINT,ECHO=NO,MODEL=NO,HISTORY=NO
*NODE                                          (Nodal definition)
       1,          114.3,             0.
       ***           ***               ***              ***
    5210,          -76.2,           254.,          28.26
*NSET, NSET=BOTTOM, GENERATE                   (bottom node group)
       1,        5,        1
     ***       ***         ***
    4691,    4700,        1
*NSET, NSET=TOP, GENERATE                (top node group)
     241,     245,        1
     ***       ***         ***
    5201,    5210,        1
*NSET, NSET=MASTER                       (loading location)
```

```
2072
*EQUATION                                        (displacement constraint
2                                                 of top nodes with 2072)
241,2,1.,2072,2,-1
2
242,2,1.,2072,2,-1
***
2
5209,2,1.,2072,2,-1
2
5210,2,1.,2072,2,-1
*ELEMENT, TYPE=S8R , ELSET=SKIN          (8-node shell, skin)
       1,  1,  3,  11,  9,  2,  7,
      10,  6
*ELEMENT, TYPE=S8R , ELSET=FLANGE        (8-node shell, flange)
     61,  246,  248,  268,  266,  247,  260,
     267, 259
*ELEMENT, TYPE=S8R , ELSET=STIFF         (8-node shell, stiffer)
    1201, 246, 4171, 4188,  266, 4170, 4181,
    4187, 259
*SHELL GENERAL SECTION, ELSET=SKIN, COMPOSITE
0.22, 3, PW, 0                                   (Composite lay-up definition
0.22, 3, PW, 90                                   skin section)
*SHELL GENERAL SECTION, ELSET=STIFF, COMPOSITE
0.22, 3, PW, 0                                   (Composite lay-up definition
0.22, 3, PW, 90                                   stiffener section)
*SHELL GENERAL SECTION, ELSET=FLANGE, COMPOSITE
0.22, 3, PW, 0                                   (Composite lay-up definition
0.22, 3, PW, 90                                   flange section)
*MATERIAL, NAME=PW
*ELASTIC, TYPE=LAMINA                            (Laminate properties)
4.32E+4,4.32E+4,3.0E-01,1.66E+04,4.70E+04,2.40E+03
*BOUNDARY                                        (Top and bottom boundaries)
TOP, 1,1
TOP, 3,3
BOTTOM, 1,3
*STEP
*BUCKLE
5,,60,20                                         (Specify number of modes)
*CLOAD
2072,2,-1000.                            (Initial load increment)
*EL PRINT,FREQUENCY=0
*NODE FILE, GLOBAL=YES
U
*EL FILE
S
SF
E
*END STEP
```

POSTBUCKLING ANALYSIS LISTING.

```
*HEADING
*RESTART,WRITE,FREQUENCY=1
*PREPRINT,ECHO=NO,MODEL=NO,HISTORY=NO
*NODE                                          (Nodal definition)
       1,          114.3,            0.
      ***          ***             ***           ***
    5210,          -76.2,          254.,         28.26
*IMPERFECTION,FILE=stbuck,STEP=1               (Imperfection read from
1,0.015                                         file stbuck.fil)
2,0.001
3,0.001
4,0.001
5,0.001
*NSET, NSET=BOTTOM, GENERATE                   (bottom node group)
       1,        5,        1
     ***       ***       ***
    4691,     4700,        1
*NSET, NSET=TOP, GENERATE                      (top node group)
     241,      245,        1
     ***       ***       ***
    5201,     5210,        1
*NSET, NSET=MASTER                             (loading location)
2072
*EQUATION                                      (displacement constraint
2                                               of top nodes with 2072)
241,2,1.,2072,2,-1
2
242,2,1.,2072,2,-1
***
2
5209,2,1.,2072,2,-1
2
5210,2,1.,2072,2,-1
*ELEMENT, TYPE=S8R , ELSET=SKIN                (8-node shell, skin)
       1,  1,  3,  11,  9,  2,  7,
      10,  6
*ELEMENT, TYPE=S8R , ELSET=FLANGE              (8-node shell, flange)
     61,  246,  248,  268,  266,  247,  260,
     267, 259
*ELEMENT, TYPE=S8R , ELSET=STIFF               (8-node shell, stiffer)
    1201, 246, 4171, 4188,  266, 4170, 4181,
    4187, 259
*SHELL GENERAL SECTION, ELSET=SKIN, COMPOSITE
0.22, 3, PW, 0                                 (Composite lay-up definition
0.22, 3, PW, 90                                 skin section)
*SHELL GENERAL SECTION, ELSET=STIFF, COMPOSITE
0.22, 3, PW, 0                                 (Composite lay-up definition
0.22, 3, PW, 90                                 stiffener section)
*SHELL GENERAL SECTION, ELSET=FLANGE, COMPOSITE
0.22, 3, PW, 0                                 (Composite lay-up definition
0.22, 3, PW, 90                                 flange section)
*MATERIAL, NAME=PW
*ELASTIC, TYPE=LAMINA                          (Laminate properties)
```

```
4.32E+4,4.32E+4,3.0E-01,1.66E+04,4.70E+04,2.40E+03
*FAIL STRESS
572.0,-402.0,572.0,-402,55.9              (Laminate strengths)
*BOUNDARY                                 (Top and bottom boundaries)
TOP, 1,1
TOP, 3,3
BOTTOM, 1,3
*STEP,NLGEOM,INC=30                       (Number of steps to perform
*STATIC,RIKS                               prior to aborting)
1.,1.,,,,2072,2,-2.54                     (Displacement limit)
*CLOAD
2072,2,-1000.                             (Initial load increment)
*MONITOR,NODE=2072,DOF=2
*NODE FILE                                (Write nodal displacement)
U
*NODE FILE,FREQUENCY=1,NSET=MASTER        (Write displacement and
U,CF                                       concentrated force)
*EL FILE                                  (Write element stress, force
S                                          strain)
SF
E
*END STEP
```

APPENDIX B—PREDICTION OF LAMINATE PROPERTIES

The following is performed using MathCad 2000.

Constituent Properties of AS4-3k warp&fill, 3501-6 matrix, Kevlar 29
Ref: Manufacturer's datasheet
(All dimensions except for Poisson's ratios and strains are in GPa)

$Ew1 := 228$	$Ef1 := 228$	$Em1 := 3.5$	$Es1 := 69$
$Ew2 := 40$	$Ef2 := 40$	$Em2 := 3.5$	$Es2 := 2.49$
$Ew3 := Ew2$	$Ef3 := Ef2$	$Em3 := Em2$	$Es3 := Es2$
$Gw12 := 24$	$Gf12 := 24$	$Gm12 := 1.3$	$Gs12 := 2.01$
$Gw13 := Gw12$	$Gf13 := Gf12$	$Gm13 := Gm12$	$Gs13 := Gs12$
$Gw23 := 14.3$	$Gf23 := 14.3$	$Gm23 := 1.3$	$Gs23 := 0.924$
$\nu w12 := 0.26$	$\nu f12 := 0.26$	$\nu m12 := 0.26$	$\nu s12 := 0.62$
$\nu w13 := \nu w12$	$\nu f13 := \nu f12$	$\nu m13 := \nu m12$	$\nu s13 := \nu s12$
$\nu w23 := \left(\frac{Ew2}{2 \cdot Gw23}\right) - 1$	$\nu f23 := \left(\frac{Ef2}{2 \cdot Gf23}\right) - 1$	$\nu m23 := \left(\frac{Em2}{2 \cdot Gm23}\right) - 1$	$\nu s23 := \left(\frac{Es2}{2 \cdot Gs23}\right) - 1$
$Swten := 3.93$	$Sften := 3.93$	$Smten := 0.0779$	$Ssten := 2.76$
$Swcom := -2.76$	$Sfcom := -2.76$	$Smcom := -0.158$	$Smcom := -0.517$
$\varepsilon wten := 0.0172$	$\varepsilon ften := 0.0172$	$\varepsilon mten := 0.0222$	$\varepsilon sten := 0.0222$
$\varepsilon wcom := -0.0121$	$\varepsilon fcom := -0.0121$	$\varepsilon mcom := -0.0452$	$\varepsilon scom := -0.00417$

Micromechanics: Yarn properties (AS4/3501-6, Kevlar/3501-6)

Ref: Tsai, S.W., and H.T. Hahn, "Introduction to Composite Materials", Technomic Publishing Company, 1980

Ref: Hahn, H.T., and R. Pandey, "A Micromechanics Model for Thermoelastic Properties of Plain Weave Fabric Composites", ASME *Journal of Engineering Materials and Technology*, 1994.

$\eta 1 := 1 \qquad \eta 2 := 1 \qquad \eta 3 := 1 \qquad \eta 4 := 1$

$$\eta w5 := \left[\frac{1}{4\cdot(1-\nu m23)}\right]\cdot\left(3-4\cdot\nu m23+\frac{Gm23}{Gw23}\right) \qquad \eta w5 = 0.652$$

$$\eta f5 := \left[\frac{1}{4\cdot(1-\nu m23)}\right]\cdot\left(3-4\cdot\nu m23+\frac{Gm23}{Gf23}\right) \qquad \eta f5 = 0.652$$

$$\eta s5 := \left[\frac{1}{4\cdot(1-\nu m23)}\right]\cdot\left(3-4\cdot\nu m23+\frac{Gm23}{Gs23}\right) \qquad \eta s5 = 1.156$$

$$\eta w6 := \left(\frac{1}{2}\right)\cdot\left(1+\frac{Gm12}{Gw12}\right) \qquad \eta w6 = 0.527$$

$$\eta f6 := \left(\frac{1}{2}\right)\cdot\left(1+\frac{Gm12}{Gf12}\right) \qquad \eta f6 = 0.527$$

$$\eta s6 := \left(\frac{1}{2}\right)\cdot\left(1 + \frac{Gm12}{Gs12}\right) \qquad \eta s6 = 0.823$$

$$Kwy2 := \frac{(Ew2\cdot Gw23)}{4\cdot Gw23 - Ew2 - 4\cdot Gw23\left(\frac{Ew2}{Ew1}\right)\cdot \nu w23^2} \qquad Kwy2 = 36.654$$

$$Kfy2 := \frac{(Ef2\cdot Gf23)}{4\cdot Gf23 - Ef2 - 4\cdot Gf23\left(\frac{Ef2}{Ef1}\right)\cdot \nu f23^2} \qquad Kfy2 = 36.654$$

$$Ksy2 := \frac{(Es2\cdot Gs23)}{4\cdot Gs23 - Es2 - 4\cdot Gs23\cdot\left(\frac{Es2}{Es1}\right)\cdot \nu s23^2} \qquad Ksy2 = 1.934$$

$$Km := \frac{Gm12}{1 - 2\cdot \nu m12}$$

$$\eta w8 := \left[\frac{1}{2\cdot(1 - \nu m12)}\right]\cdot\left(1 + \frac{Gm12}{Kwy2}\right) \qquad \eta w8 = 0.7$$

$$\eta f8 := \left[\frac{1}{2\cdot(1 - \nu m12)}\right]\cdot\left(1 + \frac{Gm12}{Kfy2}\right) \qquad \eta f8 = 0.7$$

$$\eta s8 := \left[\frac{1}{2\cdot(1 - \nu m12)}\right]\cdot\left(1 + \frac{Gm12}{Ksy2}\right) \qquad \eta s8 = 1.13$$

Hexcel Type 282 Fabric Parameters (12.5 yarns per inch)

$Nyarninch := 12.5$

$$Lw := \frac{25.4}{Nyarninch} \qquad Lw = 2.032$$

$Lf := Lw$

$LaminaT := 0.22$ Average Values based on Manufacturer's Datashee

Assumptions #1

$MatrixT := 0.$

$hwarp := \frac{(LaminaT - MatrixT)}{2}$ $hwarp = 0.11$

$hfill := hwarp$

$wgap := hwarp$

$fgap := hfill$

$aw := Lw - wgap$ $aw = 1.922$

$af := Lf - fgap$

$Vyarns := 0.5$ Based on Manufacturer's Datasheet for lamina thickness of 0.22 mm

$Vintervoid := 0.$

$Vintermatrix := Vyarns - Vintervoid$ $Vintermatrix = 0.5$

$$Vwy := \left(\frac{2hwarp}{\pi \cdot LaminaT}\right) \cdot \sin\left(\frac{\pi \cdot aw}{2 \cdot Lw}\right)$$ $Vwy = 0.317$

$$Vfy := \left(\frac{2hfill}{\pi \cdot LaminaT}\right) \cdot \sin\left(\frac{\pi \cdot af}{2 \cdot Lf}\right)$$ $Vfy = 0.317$

$Vy := Vwy + Vfy$ $Vy = 0.634$

$Vyf := \frac{Vyarns}{Vy}$ $Vyf = 0.788$

$Vintravoid := 0.$

$Vym := 1 - Vyf - Vintravoid$ $Vym = 0.212$

$Vim := Vintermatrix - Vy \cdot Vym$ $Vim = 0.366$

For each warp, fill and stitch components

$Vwyf := Vyf$ $Vwyf = 0.788$

$Vfyf := Vyf$ $Vfyf = 0.788$

$Vsyf := Vyf$ $Vsyf = 0.788$

$Vwym := Vym$ $Vwym = 0.212$

$Vfym := Vym$ $Vfym = 0.212$

$Vsym := Vym$ $Vsym = 0.212$

Individual Yarn Properties Calculations

$$E1warp := \left(\frac{1}{Vwyf + \eta 1 \cdot Vwym}\right) \cdot (Vwyf \cdot Ew1 + \eta 1 \cdot Vwym \cdot Em1) \qquad E1warp = 180.461$$

$$E1fill := \left(\frac{1}{Vfyf + \eta 1 \cdot Vfym}\right) \cdot (Vfyf \cdot Ef1 + \eta 1 \cdot Vfym \cdot Em1) \qquad E1fill = 180.461$$

$$E1stitch := \left(\frac{1}{Vsyf + \eta 1 \cdot Vsym}\right) \cdot (Vsyf \cdot Es1 + \eta 1 \cdot Vsym \cdot Em1) \qquad E1stitch = 55.13$$

$$\nu 12warp := \left(\frac{1}{Vwyf + \eta 2 \cdot Vwym}\right) \cdot (Vwyf \cdot \nu w12 + \eta 2 \cdot Vwym \cdot \nu m12) \qquad \nu 12warp = 0.26$$

$$\nu 12fill := \left(\frac{1}{Vfyf + \eta 2 \cdot Vfym}\right) \cdot (Vfyf \cdot \nu f12 + \eta 2 \cdot Vfym \cdot \nu m12) \qquad \nu 12fill = 0.26$$

$$\nu 12stitch := \left(\frac{1}{Vsyf + \eta 2 \cdot Vsym}\right) \cdot (Vsyf \cdot \nu s12 + \eta 2 \cdot Vsym \cdot \nu m12) \qquad \nu 12stitch = 0.544$$

$$\nu 13warp := \nu 12warp \qquad \nu 13fill := \nu 12fill \qquad \nu 13stitch := \nu 12stitch$$

$$G23warp := \frac{(Vwyf + \eta w5 \cdot Vwym)}{\frac{Vwyf}{Gw23} + \frac{(\eta w5 \cdot Vwym)}{Gm23}} \qquad G23warp = 5.74$$

$$G23fill := \frac{(Vfyf + \eta f5 \cdot Vfym)}{\frac{Vfyf}{Gf23} + \frac{(\eta f5 \cdot Vfym)}{Gm23}} \qquad G23fill = 5.74$$

$$G23stitch := \frac{(Vsyf + \eta s5 \cdot Vsym)}{\frac{Vsyf}{Gs23} + \frac{(\eta s5 \cdot Vsym)}{Gm23}} \qquad G23stitch = 0.992$$

$$G12warp := \frac{(Vwyf + \eta w6 \cdot Vwym)}{\frac{Vwyf}{Gw12} + \frac{(\eta w6 \cdot Vwym)}{Gm12}} \qquad G12warp = 7.581$$

$$G12fill := \frac{(Vfyf + \eta f6 \cdot Vfym)}{\frac{Vfyf}{Gf12} + \frac{(\eta f6 \cdot Vfym)}{Gm12}} \qquad G12fill = 7.581$$

$$G12stitch := \frac{(Vsyf + \eta s6 \cdot Vsym)}{\frac{Vsyf}{Gs12} + \frac{(\eta s6 \cdot Vsym)}{Gm12}} \qquad G12stitch = 1.829$$

$G13warp := G12warp \qquad G13fill := G12fill \qquad G13stitch := G12stitch$

$$Kwarp := \frac{(Vwyf + \eta w8 \cdot Vwym)}{\frac{Vwyf}{Kwy2} + \frac{(\eta w8 \cdot Vwym)}{Km}} \qquad Kwarp = 12.287$$

$$Kfill := \frac{(Vfyf + \eta f8 \cdot Vfym)}{\frac{Vfyf}{Kfy2} + \frac{(\eta f8 \cdot Vfym)}{Km}} \qquad Kfill = 12.287$$

$$Kstitch := \frac{(Vsyf + \eta s8 \cdot Vsym)}{\frac{Vsyf}{Ksy2} + \frac{(\eta s8 \cdot Vsym)}{Km}} \qquad Kstitch = 2.072$$

$$Mwarp := 1 + \frac{\left(4 \cdot Kwarp \cdot \nu 12warp^2\right)}{E1warp^2} \qquad Mwarp = 1$$

$$Mfill := 1 + \frac{\left(4 \cdot Kfill \cdot \nu 12fill^2\right)}{E1fill^2} \qquad Mfill = 1$$

$$Mstitch := 1 + \frac{\left(4 \cdot Kstitch \cdot \nu 12stitch^2\right)}{E1stitch^2} \qquad Mstitch = 1.001$$

$$E2warp := \frac{(4 \cdot Kwarp \cdot G23warp)}{(Kwarp + Mwarp \cdot G23warp)}$$

$E2warp = 15.649$

$E3warp := E2warp$

$$E2fill := \frac{(4 \cdot Kfill \cdot G23fil)}{(Kfill + Mfill \cdot G23fil)}$$

$E2fill = 15.649$

$E3fill := E2fill$

$$E2stitch := \frac{(4 \cdot Kstitch \cdot G23stitch)}{(Kstitch + Mstitch \cdot G23stitch)}$$

$E2stitch = 2.682$

$E3stitch := E2stitch$

$$\nu 23warp := \left(\frac{E2warp}{2 \cdot G23warp} \right) - 1$$

$\nu 23warp = 0.363$

$$\nu 23fill := \left(\frac{E2fill}{2 \cdot G23fill} \right) - 1$$

$\nu 23fill = 0.363$

$$\nu 23stitch := \left(\frac{E2stitch}{2 \cdot G23stitch} \right) - 1$$

$\nu 23stitch = 0.352$

$$\nu 21warp := \frac{(E2warp \cdot \nu 12warp)}{E1warp} \qquad \nu 21fill := \frac{(E2fill \nu 12fil)}{E1fill}$$

$$\nu 21stitch := \frac{(E2stitch \cdot \nu 12stitch)}{E1stitch} \qquad \nu m21 := \frac{(Em2 \nu m12)}{Em1}$$

$$\nu 31warp := \frac{(E3warp \cdot \nu 13warp)}{E1warp} \qquad \nu 31fill := \frac{(E3fill \nu 13fil)}{E1fill}$$

$$\nu 31stitch := \frac{(E3stitch \cdot \nu 13stitch)}{E1stitch} \qquad \nu m31 := \frac{(Em3 \nu m13)}{Em1}$$

$$\nu 32warp := \frac{(E3warp \cdot \nu 23warp)}{E2warp} \qquad \nu 32fill := \frac{(E3fill \nu 23fil)}{E2fill}$$

$$\nu 32stitch := \frac{(E3stitch \cdot \nu 23stitch)}{E2stitch} \qquad \nu m32 := \frac{(Em3 \nu m23)}{Em2}$$

$$S11w := \frac{1}{E1warp} \qquad S11w = 5.541 \times 10^{-3}$$

$$S12w := \frac{-v12warp}{E1warp} \qquad S12w = -1.441 \times 10^{-3}$$

$$S13w := \frac{-v13warp}{E1warp} \qquad S13w = -1.441 \times 10^{-3}$$

$$S22w := \frac{1}{E2warp} \qquad S22w = 0.064$$

$$S23w := \frac{-v23warp}{E2warp} \qquad S23w = -0.023$$

$$S33w := \frac{1}{E3warp} \qquad S33w = 0.064$$

$$S44w := \frac{1}{G23warp} \qquad S44w = 0.174$$

$$S55w := \frac{1}{G13warp} \qquad S55w = 0.132$$

$$S66w := \frac{1}{G12warp} \qquad S66w = 0.132$$

$$Sw := S11w \cdot S22w \cdot S33w - S11w \cdot S23w \cdot S23w - S22w \cdot S13w \cdot S13w - S33w \cdot S12w \cdot S12w + 2 \cdot S12w \cdot S23w \cdot S12w$$

$$Sw = 1.928 \times 10^{-5}$$

$$C11w := \frac{(S22w \cdot S33w - S23w \cdot S23w)}{Sw} \qquad C11w = 183.846$$

$$C12w := \frac{(S13w \cdot S23w - S12w \cdot S33w)}{Sw} \qquad C12w = 6.509$$

$$C22w := \frac{(S33w \cdot S11w - S13w \cdot S13w)}{Sw} \qquad C22w = 18.257$$

$$C13w := \frac{(S12w \cdot S23w - S13w \cdot S22w)}{Sw} \qquad C13w = 6.509$$

$$C33w := \frac{(S11w \cdot S22w - S12w \cdot S12w)}{Sw} \qquad C33w = 18.257$$

$$C23w := \frac{(S12w \cdot S13w - S23w \cdot S11w)}{Sw} \qquad C23w = 6.777$$

$$C44w := \frac{1}{S44w} \qquad C44w = 5.74$$

$$C55w := \frac{1}{S55w} \qquad C55w = 7.581$$

$$C66w := \frac{1}{S66w} \qquad C66w = 7.581$$

$$S11f := \frac{1}{E1fill} \qquad S11f = 5.541 \times 10^{-3}$$

$$S12f := \frac{-\nu 12fill}{E1fill} \qquad S12f = -1.441 \times 10^{-3}$$

$$S13f := \frac{-\nu 13fill}{E1fill} \qquad S13f = -1.441 \times 10^{-3}$$

$$S22f := \frac{1}{E2fill} \qquad S22f = 0.064$$

$$S23f := \frac{-\nu 23fill}{E2fill} \qquad S23f = -0.023$$

$$S33f := \frac{1}{E3fill} \qquad S33f = 0.064$$

$$S44f := \frac{1}{G23fill} \qquad S44f = 0.174$$

$$S55f := \frac{1}{G13fill} \qquad S55f = 0.132$$

$$S66f := \frac{1}{G12fill} \qquad S66f = 0.132$$

$$Sf := S11f \cdot S22f \cdot S33f - S11f \cdot S23f \cdot S23f - S22f \cdot S13f \cdot S13f - S33f \cdot S12f \cdot S12f + 2 \cdot S12f \cdot S23f \cdot S12f$$

$$Sf = 1.928 \times 10^{-5}$$

$$C11f := \frac{(S22f \cdot S33f - S23f \cdot S23f)}{Sf} \qquad C11f = 183.846$$

$$C12f := \frac{(S13f \cdot S23f - S12f \cdot S33f)}{Sf} \qquad C12f = 6.509$$

$$C22f := \frac{(S33f \cdot S11f - S13f \cdot S13f)}{Sf} \qquad C22f = 18.257$$

$$C13f := \frac{(S12f \cdot S23f - S13f \cdot S22f)}{Sf} \qquad C13f = 6.509$$

$$C33f := \frac{(S11f \cdot S22f - S12f \cdot S12f)}{Sf} \qquad C33f = 18.257$$

$$C23f := \frac{(S12f \cdot S13f - S23f \cdot S11f)}{Sf} \qquad C23f = 6.777$$

$$C44f := \frac{1}{S44f} \qquad C44f = 5.74$$

$$C55f := \frac{1}{S55f} \qquad C55f = 7.581$$

$$C66f := \frac{1}{S66f} \qquad C66f = 7.581$$

$$S11m := \frac{1}{Em1} \qquad S11m = 0.286$$

$$S12m := \frac{-\nu m12}{Em1} \qquad S12m = -0.074$$

$$S13m := \frac{-\nu m13}{Em1} \qquad S13m = -0.074$$

$$S22m := \frac{1}{Em2} \qquad S22m = 0.286$$

$$S23m := \frac{-\nu m23}{Em2} \qquad S23m = -0.099$$

$$S33m := \frac{1}{Em3} \qquad S33m = 0.286$$

$$S44m := \frac{1}{Gm23} \qquad S44m = 0.769$$

$$S55m := \frac{1}{Gm13} \qquad S55m = 0.769$$

$$S66m := \frac{1}{Gm12} \qquad S66m = 0.769$$

$$Sm := S11m \cdot S22m \cdot S33m - S11m \cdot S23m \cdot S23m - S22m \cdot S13m \cdot S13m - S33m \cdot S12m \cdot S12m + 2 \cdot S12m \cdot S23m \cdot S12m$$

$$Sm = 0.016$$

$$C11m := \frac{(S22m \cdot S33m - S23m \cdot S23m)}{Sm} \qquad C11m = 4.412$$

$$C12m := \frac{(S13m \cdot S23m - S12m \cdot S33m)}{Sm} \qquad C12m = 1.755$$

$$C22m := \frac{(S33m \cdot S11m - S13m \cdot S13m)}{Sm} \qquad C22m = 4.674$$

$$C13m := \frac{(S12m \cdot S23m - S13m \cdot S22m)}{Sm} \qquad C13m = 1.755$$

$$C33m := \frac{(S11m \cdot S22m - S12m \cdot S12m)}{Sm} \qquad C33m = 4.674$$

$$C23m := \frac{(S12m \cdot S13m - S23m \cdot S11m)}{Sm} \qquad C23m = 2.074$$

$$C44m := \frac{1}{S44m} \qquad C44m = 1.3$$

$$C55m := \frac{1}{S55m} \qquad C55m = 1.3$$

$$C66m := \frac{1}{S66m} \qquad C66m = 1.3$$

$$S11s := \frac{1}{E1stitch} \qquad S11s = 0.018$$

$$S12s := \frac{-\nu 12stitch}{E1stitch} \qquad S12s = -9.863 \times 10^{-3}$$

$$S13s := \frac{-\nu 13stitch}{E1stitch} \qquad S13s = -9.863 \times 10^{-3}$$

$$S22s := \frac{1}{E2stitch} \qquad S22s = 0.373$$

$$S23s := \frac{-\nu 23stitch}{E2stitch} \qquad S23s = -0.131$$

$$S33s := \frac{1}{E3stitch} \qquad S33s = 0.373$$

$$S44s := \frac{1}{G23stitch} \qquad S44s = 1.008$$

$$S55s := \frac{1}{G13stitch} \qquad S55s = 0.547$$

$$S66s := \frac{1}{G12stitch} \qquad S66s = 0.547$$

$$Ss := S11s \cdot S22s \cdot S33s - S11s \cdot S23s \cdot S23s - S22s \cdot S13s \cdot S13s - S33s \cdot S12s \cdot S12s + 2 \cdot S12s \cdot S23s \cdot S12s$$

$$Ss = 2.11 \times 10^{-3}$$

$$C11s := \frac{(S22s \cdot S33s - S23s \cdot S23s)}{Ss} \qquad C11s = 57.692$$

$$C12s := \frac{(S13s \cdot S23s - S12s \cdot S33s)}{Ss} \qquad C12s = 2.356$$

$$C22s := \frac{(S33s \cdot S11s - S13s \cdot S13s)}{Ss} \qquad C22s = 3.158$$

$$C13s := \frac{(S12s \cdot S23s - S13s \cdot S22s)}{Ss} \qquad C13s = 2.356$$

$$C33s := \frac{(S11s \cdot S22s - S12s \cdot S12s)}{Ss} \qquad C33s = 3.158$$

$$C23s := \frac{(S12s \cdot S13s - S23s \cdot S11s)}{Ss} \qquad C23s = 1.174$$

$$C44s := \frac{1}{S44s} \qquad C44s = 0.992$$

$$C55s := \frac{1}{S55s} \qquad C55s = 1.829$$

$$C66s := \frac{1}{S66s} \qquad C66s = 1.829$$

$$V1w := \frac{1\int_{0}^{Lf} \cos\left[2\cdot\left(\operatorname{atan}\left(\frac{\pi}{2}\,\frac{hfill}{Lf}\,\sin\left(\frac{\pi\cdot x}{Lf}\right)\right)\right)\right]dx}{Lf} \qquad V1w = 0.993$$

$$V1f := \frac{1\int_{0}^{Lw} \cos\left[2\cdot\left(\operatorname{atan}\left(\frac{-\pi}{2}\,\frac{hwarp}{Lw}\,\sin\left(\frac{\pi\cdot y}{Lw}\right)\right)\right)\right]dy}{Lw} \qquad V1f = 0.993$$

$$V2w := \frac{1\int_{0}^{Lf} \cos\left[4\cdot\left(\operatorname{atan}\left(\frac{\pi}{2}\,\frac{hfill}{Lf}\,\sin\left(\frac{\pi\cdot x}{Lf}\right)\right)\right)\right]dx}{Lf} \qquad V2w = 0.971$$

$$V2f := \frac{1\int_{0}^{Lw} \cos\left[4\cdot\left(\operatorname{atan}\left(\frac{-\pi}{2}\,\frac{hwarp}{Lw}\,\sin\left(\frac{\pi\cdot y}{Lw}\right)\right)\right)\right]dy}{Lw} \qquad V2f = 0.971$$

$$U1f := \left(\frac{1}{8}\right)\cdot(3\cdot C11f + 3\cdot C33f + 2\cdot C13f + 4\cdot C55f) \qquad U1f = 81.206$$

$$U2f := \left(\frac{1}{2}\right)\cdot(C11f - C33f) \qquad U2f = 82.795$$

$$U3f := \left(\frac{1}{8}\right)\cdot(C11f + C33f - 2\cdot C13f - 4\cdot C55f) \qquad U3f = 19.845$$

$$U4f := \left(\frac{1}{8}\right)\cdot(C11f + C33f + 6\cdot C13f - 4\cdot C55f) \qquad U4f = 26.354$$

$$U5f := \left(\frac{1}{8}\right)\cdot(C11f + C33f - 2\cdot C13f - 4\cdot C55f) \qquad U5f = 19.845$$

$$U6f := \left(\frac{1}{2}\right)\cdot(C12f + C23f) \qquad U6f = 6.643$$

$$U7f := \left(\frac{1}{2}\right)\cdot(C12f - C23f) \qquad U7f = -0.134$$

$$U8f := \left(\frac{1}{2}\right)\cdot(C44f + C66f) \qquad U8f = 6.661$$

$$U9f := \left(\frac{1}{2}\right)\cdot(C44f - C66f) \qquad U9f = -0.92$$

$$U1w := \left(\frac{1}{8}\right)\cdot(3\cdot C11w + 3\cdot C33w + 2\cdot C13w + 4\cdot C55w) \qquad U1w = 81.206$$

$$U2w := \left(\frac{1}{2}\right)\cdot(C11w - C33w) \qquad U2w = 82.795$$

$$U3w := \left(\frac{1}{8}\right)\cdot(C11w + C33w - 2\cdot C13w - 4\cdot C55w) \qquad U3w = 19.845$$

$$U4w := \left(\frac{1}{8}\right)\cdot(C11w + C33w + 6\cdot C13w - 4\cdot C55w) \qquad U4w = 26.354$$

$$U5w := \left(\frac{1}{8}\right)\cdot(C11w + C33w - 2\cdot C13w - 4\cdot C55w) \qquad U5w = 19.845$$

$$U6w := \left(\frac{1}{2}\right)\cdot(C12w + C23w) \qquad U6w = 6.643$$

$$U7w := \left(\frac{1}{2}\right)\cdot(C12w - C23w) \qquad U7w = -0.134$$

$$U8w := \left(\frac{1}{2}\right)\cdot(C44w + C66w) \qquad U8w = 6.661$$

$$U9w := \left(\frac{1}{2}\right)\cdot(C44w - C66w) \qquad U9w = -0.92$$

$C11mod := Vwy \cdot (U1w + V1w \cdot U2w + V2w \cdot U3w) + Vfy \cdot C22f + VimC11m$ $C11mod = 65.343$

$C22mod := Vfy \cdot (U1f + V1f \cdot U2f + V2f \cdot U3f) + Vwy \cdot C22w + VimC22m$ $C22mod = 65.439$

$C33mod := Vwy \cdot (U1w - V1w \cdot U2w + V2w \cdot U3w) + Vfy \cdot (U1f - V1f \cdot U2f + V2f \cdot U3f) + VimC33m$ $C33mod = 13.307$

$C12mod := Vwy \cdot (U6w + V1w \cdot U7w) + Vfy \cdot (U6f + V1f \cdot U7f) + VimC12m$ $C12mod = 4.771$

$C13mod := Vwy \cdot (U4w - V1w \cdot U3w) + Vfy \cdot (U6f - V2f \cdot U7f) + VimC13m$ $C13mod = 4.899$

$C23mod := Vwy \cdot (U6w - V2w \cdot U7w) + Vfy \cdot (U4f - V1f \cdot U3f) + VimC23m$ $C23mod = 5.016$

$C55mod := Vwy \cdot (U5w - V2w \cdot U3w) + Vfy \cdot (U8f + V1f \cdot U9f) + VimC55m$ $C55mod = 2.478$

$C44mod := Vwy \cdot (U8w + V1w \cdot U9w) + Vfy \cdot (U5f - V2f \cdot U3f) + VimC44m$ $C44mod = 2.478$

$C66mod := Vwy \cdot (U8w - V1w \cdot U9w) + Vfy \cdot (U8f - V1f \cdot U9f) + VimC66m$ $C66mod = 5.28$

Laminate Stiffness 1:
13 plies, 0 = on axis plain weave, 45 = angle ply plain weave
Skin = [0 45 0 45 0 45 0 45 0 45 0 45 0]

$no0 := 7$

$no45 := 6$

$$Aijlam1 := \frac{LaminaT}{1000} \cdot (no0 \cdot Qmodmatrix + no45 \cdot Qtmodmatrix)$$

$$Aijlam1 = \begin{pmatrix} 0.149 & 0.041 & -2.855 \times 10^{-6} \\ 0.041 & 0.149 & -2.855 \times 10^{-6} \\ -2.855 \times 10^{-6} & -2.855 \times 10^{-6} & 0.048 \end{pmatrix}$$

Laminate Stiffness 2:
12 plies, 0= on axis plain weave, 45 = angle ply plain weave
Stiffener = [45 0 45 0 45 0 0 45 0 45 0 45]

$no0 := 6$

$no45 := 6$

$$Aijlam2 := \frac{LaminaT}{1000} \cdot (no0 \cdot Qmodmatrix + no45 \cdot Qtmodmatrix)$$

$$Aijlam2 = \begin{pmatrix} 0.135 & 0.041 & -2.855 \times 10^{-6} \\ 0.041 & 0.135 & -2.855 \times 10^{-6} \\ -2.855 \times 10^{-6} & -2.855 \times 10^{-6} & 0.047 \end{pmatrix}$$

Laminate Stiffness 3:
19 plies, 0= on axis plain weave, 45 = angle ply plain weave
Flange = [0 45 0 45 0 45 0 45 0 45 0 45 0 45 0 45 0 45 0]

$no0 := 10$

$no45 := 9$

$$Aijlam3 := \frac{LaminaT}{1000} \cdot (no0 \cdot Qmodmatrix + no45 \cdot Qtmodmatrix)$$

$$Aijlam3 = \begin{pmatrix} 0.216 & 0.062 & -4.283 \times 10^{-6} \\ 0.062 & 0.216 & -4.283 \times 10^{-6} \\ -4.283 \times 10^{-6} & -4.283 \times 10^{-6} & 0.072 \end{pmatrix}$$

Stitch Parameters

$\phi s := 0.9652$

$Pitch := 3.175 \qquad Spacing := 3.175$

$ratiowarp := \frac{Lw}{Spacing} \qquad ratiowarp = 0.64$

$ratiofill := \frac{Lf}{Pitch} \qquad ratiofill = 0.64$

$Exstitch1 := Exlam1(1 - Vs) + E3stitch \cdot Vs \qquad Exstitch1 = 44.672$

$Eystitch1 := Exlam1(1 - Vs) + E2stitch \cdot Vs \qquad Eystitch1 = 44.672$

$Gxystitch1 := Gxylam1(1 - Vs) + G23stitch \cdot Vs \qquad Gxystitch1 = 15.683$

$\nu xystitch1 := \nu xylam1(1 - Vs) + \nu 23stitch \cdot Vs \qquad \nu xystitch1 = 0.284$

$Exstitch2 := Exlam2(1 - Vs) + E3stitch \cdot Vs \qquad Exstitch2 = 43.186$

$Eystitch2 := Exlam2(1 - Vs) + E2stitch \cdot Vs \qquad Eystitch2 = 43.186$

$Gxystitch2 := Gxylam2(1 - Vs) + G23stitch \cdot Vs \qquad Gxystitch2 = 16.575$

$\nu xystitch2 := \nu xylam2(1 - Vs) + \nu 23stitch \cdot Vs \qquad \nu xystitch2 = 0.306$

$Exstitch3 := Exlam3(1 - Vs) + E3stitch \cdot Vs \qquad Exstitch3 = 44.209$

$Eystitch3 := Exlam3(1 - Vs) + E2stitch \cdot Vs \qquad Eystitch3 = 44.209$

$Gxystitch3 := Gxylam3(1 - Vs) + G23stitch \cdot Vs \qquad Gxystitch3 = 15.964$

$\nu xystitch3 := \nu xylam3(1 - Vs) + \nu 23stitch \cdot Vs \qquad \nu xystitch3 = 0.291$